12-2018

Studies in hydrogel microfluidics and development of low cost imaging for quantitative TLC in the undergraduate teaching laboratory

Alexandra Marie Anderson
University of Tennessee

To the Graduate Council:

I am submitting herewith a thesis written by Alexandra Marie Anderson entitled "Studies in hydrogel microfluidics and development of low cost imaging for quantitative TLC in the undergraduate teaching laboratory." I have examined the final electronic copy of this thesis for form and content and recommend that it be accepted in partial fulfillment of the requirements for the degree of Master of Science, with a major in Chemistry.

Christopher Baker, Major Professor

We have read this thesis and recommend its acceptance:

Michael Best, Bhavya Sharma

Accepted for the Council:
Dixie L. Thompson

Vice Provost and Dean of the Graduate School

(Original signatures are on file with official student records.)

Studies in hydrogel microfluidics and development of low cost imaging for quantitative TLC in the undergraduate teaching laboratory

A Thesis Presented for the
Master of Science
Degree
The University of Tennessee, Knoxville

Alexandra Marie Anderson
December 2018

This work is dedicated to my mother, Lisa Anderson.

Thank you for always pushing me to venture outside my comfort zone, for believing in me more than I believed in myself, and for showing me truly unconditional love and support. I couldn’t have done it without you.

ABSTRACT

Microfluidics is the micrometer-scale manipulation of small volumes of fluids, which allows the miniaturization of benchtop biological and chemical assays. Small volume analyses provide analytical and practical advantages like high precision, temporal resolution, throughput, speed, portability, and low cost and reagent consumption. Microfluidics is particularly suited to studying microscale problems, and so has been used to model biological systems like the microvasculature. Such biomimics have been produced in many ways, including 3-D printing and self-organization through various extracellular matrices. An attempt at templating a perfusable microvessel mimic through hydrogel in a microfluidic device is described in chapter 2.

Thin-layer chromatography (TLC) is a simple microfluidic separation technique offering much lower cost, time requirement, and reagent consumption than other separation methods. These attributes make TLC attractive for use in point-of-care, preparatory, and pedagogical applications, and it is often used qualitatively in these ways. TLC can be quantitative as well, but generally requires expensive imaging instrumentation that can be cost-prohibitive. A simple and inexpensive quantitative TLC imaging experiment for the determination of counterfeit drugs was developed for undergraduates, and is described here in chapter 3. This imaging method was expanded for the quantitation of amino acids utilizing a cellphone camera as described in chapter 4, and future directions for the method are discussed in chapter 5.

TABLE OF CONTENTS

LIST OF FIGURES

CHAPTER 1. INTRODUCTION

1.1 Microfluidic vessel mimics

Microfluidics—typically defined as the micrometer-scale manipulation of corresponding small volumes of fluids—is a rapidly expanding field with unique approaches to many scientific problems. Microfluidic chips have large modifiable surface areas relative to small volumes of sample and reagent consumption; besides analytical benefits such as high precision, temporal resolution, thermal homogeneity, and throughput capabilities, microfluidic assays are generally faster, less expensive, more portable, and more environmentally friendly than macroscale approaches (1-3). These advantages have prompted the use of microfluidic chips for such varied applications as analytical separations, syntheses, point-of-care analyses, and biological assays (1,2). Miniaturization has proven particularly helpful in studying microscale systems and events, allowing analysis of single cells and molecules, *in vivo* interfacing, and *in vitro* biomimicry on physiological scales (1-20). One such system microfluidics has greatly improved understanding of is the microvasculature.

Studying the vasculature can provide crucial insights into normal biological processes, disease pathology, drug and solute transport, and endothelial response to physical and biochemical signals (1,2,4-11). Large blood vessels have been studied *in vivo* with relative ease, but the microvasculature has been much more difficult to access and observe (4). The role of small vessels in biological processes is becoming more discernible with time, but the tools to study them are still being developed. Animal models have been used to study the microvasculature, but are resource-, labor-, and time-consuming endeavors with debatable genetic relevance and ethical concerns (1,5,12). *In vivo* studies are also prone to biological crosstalk, which can be significant given the number of bodily factors that can alter endothelial barriers (12). *In vitro* models allow the isolation of barrier mimics from bodily interference and, especially with recent advances, maintain biological relevance. Early attempts to model the vasculature *in vitro* involved endothelial cells (ECs) in plastic culture dishes without integrated flow, which is inconsistent with natural cellular architecture, contact and communication with other cells, and exposure to dynamic physical conditions (1,4). Parallel-plate flow

chambers greatly improved upon previous methods by allowing the introduction of shear stress, a major determinant of endothelial barrier function (4,6,7,13-15). Transwell devices have also been used to study barrier permeability, and are acceptable mimics for larger, flatter membranes; however, cell morphology in planar barriers is vastly different than those in small, curved vessels, and the two respond differently to stimuli (7). Furthermore, these methods all lack the ability to produce the cylindrical vessel geometries seen *in vivo*.

The advent of microfluidics allowed miniaturization of these methods as well as the introduction of laminar flow to cells (4). Unfortunately, the membranes commonly used in miniature transwell devices complicate imaging; miniature flow chambers, while more precisely defined than their benchtop counterparts, still suffer from a number of shortcomings (4,6). The rectangular chambers experience different conditions (particularly relating to flow and shear stress) at different points of their cross sections, prevent EC stretching and remodeling, are limited in applications due to low liquid permeability, and are poor surfaces for cell growth (4). Microfluidic models have been enhanced by implementing natural or synthetic extracellular matrices that can be remodeled by ECs, allowing more natural cellular behavior (2,4,6,7). Such matrices—generally of collagen, gelatin, polyethylene glycol, or fibrin of sufficient concentration to resist invasion and distortion by cells and perfusate—have been used to produce vessel mimics with a few fabrication methods, including templating, self-organization, and 3-D printing (2,6,8,9,11,12,16-20).

Templating a channel in the matrix with a needle or rod is a simple and reproducible way to create a vessel with well-defined cylindrical geometry and simple perfusion (4,6,9,16,20). This method is, however, limited to straight channels to allow template removal, as well as channel diameters greater than about 50 μm due to difficulties distributing ECs and achieving appropriate cell densities; in practice, templates are generally 60 to a few hundred μm (6). Smaller and more complex vessels can be self-assembled using pressure or chemical gradients or other means to induce spontaneous vessel formation by cells in some matrix, but are less controllable, more difficult to perfuse, and take a considerable amount of time to grow—generally weeks as opposed to days (4,6). 3-D printing can also be used to build devices by depositing droplets of

cell-containing matrix. While this does open the field to many exciting possibilities, with current technology the resolution is limited to larger vessels (diameters >100 μm) and the process takes quite some time to complete (6). Furthermore, the price of a 3-D printer with sufficient resolution can negate the general cost advantage of microfluidics. In chapter 2, a novel fabrication method for templating a three-dimensional microfluidic cell culture system will be discussed.

1.2 Quantitative thin layer chromatography

Chromatography is a widely used analytical technique for the separation, identification, and determination of the components in a mixture. All chromatographic methods use pressure, gravity, or capillary action to flow a mobile phase through a stationary phase such that sample components are separated by differential partitioning between the two phases (3,21,22). The stationary phase can be prepared in columnar or planar geometries, and the many types of chromatography can be further classified by the physical states of the two phases as well as the mechanism of separation, such as affinity, ion exchange, molecular exclusion, and hydrophobic interactions (3,21). Many of these chromatographic techniques are technically demanding, time-consuming, and require expensive instrumentation, which greatly limits accessibility.

Thin-layer chromatography (TLC) is a planar liquid chromatography technique in which small amounts of sample are adsorbed to a thin layer of solid stationary phase on an inert backing plate. The plate is developed when liquid mobile phase is wicked through the plate, carrying sample components with it to varying extents and separating them based on their intermolecular interactions (22,23). Normal phase TLC uses a polar stationary phase and less polar mobile phase such that the least polar sample component has the highest affinity for and is carried furthest by the mobile phase; reverse phase TLC switches those polarities and consequent elution order. After development, component spots can be detected in a variety of ways; colored compounds can be visualized directly, but colorless compounds require alternative detection methods (23,24). Indirect fluorescence, sometimes called quenching, is a detection method that works for compounds absorbing in the UV regime, especially organic molecules (23,25,26). UV light incident on a plate coated with fluorescent indicator is absorbed by sample components, reducing excitation of the indicator and

resulting in dark spots on the plate (22,23,27). Many stains have also been used for TLC visualization, and can be universal, like permanganate and cerium molybdate, or selective for molecules or functional groups of interest (23,25,26,28,29). Amine groups, like those found in the residual amino acids of fingerprints, are commonly targeted by the chromogenic stain ninhydrin or the fluorogenic stain fluorescamine (30-34).

Like other chromatographic techniques, TLC on its own cannot enable unknown identification. It can be used qualitatively to establish the presence or absence of a small number of known species in a mixture by their characteristic retention under certain development conditions, as compared with standards of known composition (21,22). In this manner, TLC is commonly used in agricultural, pharmaceutical, biological, forensic, medical, and environmental sciences for applications like purity testing, diagnostics, and reaction monitoring (22,24,30). Compared to other chromatographic techniques, TLC sacrifices some resolution and sensitivity to consume less time, money, and reagents. There are a few ways TLC has been improved to be more suitable for quantitative use. High-performance TLC (HPTLC) plates have particle sizes around 5 μm and layer thicknesses around 200 μm compared to regular TLC plates' 10 μm and 250 μm, respectively. The smaller particles and thinner layers in HPTLC reduce the distance for mass transfer and resultant sample diffusion, so the method has increased sensitivity, speed, and resolution of analysis (35,36). Automatic spotters can reproducibly apply precise amounts of sample with high throughput. A variety of densitometers can be used to scan plates and measure the intensity of developed spots, which is proportional to the amount of analyte present in an approximation of Beer's law (24,37). These technologies can greatly improve the quantitative capabilities of TLC, but at great cost; HPTLC plates are nearly three times more expensive than otherwise equivalent TLC plates, spotters are thousands of dollars, and scanners tens of thousands (24,25,36,38).

Its greater accessibility makes TLC more suitable than other chromatographic techniques for low-resource and pedagogical applications. TLC is a simple and convenient way to expose young scientists to analytical methods in relevant and interesting ways—with samples like food products or crime scene evidence—in the short span of a laboratory period (39-42). It has long been used in introductory

undergraduate synthetic laboratories as a gauge of reaction success, but is arguably under-utilized in more advanced classes, though analogous in principle to more complex and costly techniques. Furthermore, though commonly seen in a qualitative context, quantitative TLC has largely been cost-prohibitive for high school and undergraduate laboratories (23,39-46). Some have recognized this need and developed lower-cost quantitative TLC methods using digital cameras or even flatbed scanners in lieu of densitometers (24,37,45,46). Unfortunately, technologies for improving access to quantitative TLC imaging have not kept pace with the rapid growth of high resolution, low cost imaging systems now widely available in portable electronics. In chapter 3, we will update and expand upon the approach of Hess with a quantitative TLC procedure designed for the undergraduate laboratory (45). In chapter 4, we will extend our quantitative TLC method to the analysis of amino acids utilizing smartphone imaging with a variety of illumination modalities.

CHAPTER 2. TEMPLATED MICROFLUIDIC VESSEL MIMIC

2.1 Introduction

Culturing cells in templated microfluidic channels has enabled the creation of controllable, perfusable vessel mimics *in vitro*. Early microfluidic devices used photolithography to pattern channels into inorganic materials like glass and silicon. These fabrication methods are well-established and the resulting chips can easily be sealed and integrated with other parts, but the materials are opaque, inflexible, and impermeable to liquids and gases. These physical and mechanical properties inhibit imaging and natural cell-cell and cell-surface interactions (1,2). The advancement of polymer science led to the use of plastics like polystyrene for cell culture; while biocompatible, these stiff materials are often soluble in organic solvents and lack the desired permeability of native extracellular matrices. Elastomers like polydimethylsiloxane (PDMS) greatly improve upon previously used materials, as transparency allows imaging, and greater flexibility and gas permeability are better for cell proliferation. Soft lithography techniques have also been extensively studied such that PDMS is as easily used as glass, and hybrid PDMS/glass chips are often used for cell culture today, including this work. However, PDMS is hydrophobic, which prevents extracellular transport of aqueous cellular factors and often necessitates coatings or surface modifications to encourage cell adhesion (1,3). The desire for a more realistic extracellular matrix permeable to aqueous reagents has led to the use of hydrogels as device substrates where cells meet channel surfaces. Synthetic gels like polyethylene glycol as well as natural gels like collagen, gelatin, cellulose, and alginate have been used for 3-D cell cultures with better mass transport, cell viability, and biomimetic channel geometries than seen previously (1-11).

The vessels to be mimicked in this study are capillary blood vessels, key players in bodily solute exchange with diameters around 10 μm. Agarose and alginate, both cytocompatible algae-derived hydrogels, were explored here as extracellular matrices. Agarose is thermo-reversible and hysteretic—with gelation temperature around 36°C and melting point around 90°C—which allows facile manipulation of molten agarose to produce a predictable chip once cooled and solidified; alginate solidifies with ionic

cross-linking. Our device was originally designed to mimic those constructed by Chrobak et al. in 2006 to model giant capillaries (4). This design required punching inlet and outlet holes in the gel and filling in the channel ends after fabrication, and had no way to seal the channel to flow without leaks. While materials like PDMS and glass can be sealed with commercially available adhesives, the hydrogels used in this application are 98% water and thus incompatible with such methods. Our fabrication method makes use of GelBond®, a commercially available clear polyester film intended to bond to agarose gel for electrophoresis and subsequent processing, as the interface necessary to seal the chip. One side of GelBond® has a hydrophilic coating to bond to the hydrogel agarose, while the other can be sealed to the glass microscope slide using conventional means.

Another consideration for this study that greatly affects cell viability, morphology, and behavior is the rate of channel perfusion. *In vivo*, endothelial cells are exposed to different amounts of shear stress depending on their location in the vascular system (12,13). Too much shear stress decreases the proliferation rate of cells *in vivo* and *in vitro*, while too little shear stress diminishes barrier function (10-12,14). In a straight cylindrical channel exposed to laminar flow, shear stress can be described by:

$$\tau = \frac{4Q\mu}{\pi r^3}$$

where τ is shear stress in Pa, Q is the volumetric flow rate in $m^3\ s^{-1}$, μ is the viscosity in Pa·s, and r is the radius of the channel in m. Pressures above 0.5 Pa have previously been determined to decrease cell proliferation, so it was used as the maximum shear stress here (11-13). Considering the viscosity of water to be 0.001 Pa·s, the maximum flow rate was determined to be $1.06 \cdot 10^{-11}\ m^3\ s^{-1}$ for a 60-μm channel and $3.93 \cdot 10^{-10}\ m^3\ s^{-1}$for a 200-μm channel; practically, this corresponds to volumetric flow rates of 0.64 μL min^{-1} and 23.6 μL min^{-1}, respectively. Following completion of a sealed, perfusable device, cell culture and method optimization with a well-studied biological system were to be done in collaboration with the lab of Dr. Colleen Jonsson (UTHSC). Finally, specific temporal analyte profiles would be applied to the on-chip cell culture.

2.2 Materials & methods

2.2.1 General

Agarose, 3-aminopropyltriethoxysilane (APTES), N-hydroxysulfosuccinimide sodium salt (sulfo-NHS, 97%), 1-ethyl-3-(3-dimethylaminopropyl)carbodiimide hydrochloride (EDC), hydrogen peroxide (30%), 2-(N-morpholino)ethanesulfonic acid (MES) hydrate (99%), 4-(2-hydroxyethyl)-1-piperazineethanesulfonic acid (HEPES), fluorescein disodium salt, calcium chloride, sulfuric acid (ACS grade), Nile blue A, Sylgard® 184 silicone elastomer base and curing agent, and alginic acid sodium salt were purchased from Thermo Fisher Scientific (Waltham, MA). PDMS (250-µm) was purchased from Stockwell Elastomerics (Philadelphia, PA). GelBond® film for agarose gels was from Lonza (Morristown, NJ). Confocal microscopy was performed with the Leica SP8 White Light Laser Confocal System at the University of Tennessee Advanced Microscopy and Imaging Center. Further imaging was done using the SE306R-PZ-E digital forward-mounted binocular stereo microscope and SM-4TZ-144A professional trinocular stereo zoom microscope from AmScope (Irvine, CA). ImageGrab (downloaded from http://paul.glagla.free.fr/imagegrab_en.htm) and ImageJ (National Institutes of Health, Bethesda, MA) were used for image analysis.

2.2.2 Chip 1

Chip 1.0. Soft lithography techniques were used to make a barbell-shaped PDMS mold, which was pressed to form a liquid-tight seal atop a glass microscope slide (15-16). A channel template, either 200-µm glass capillary or 60-µm optical fiber, was threaded through holes pierced in opposite ends of the PDMS mold. A 2% solution of agarose in water was prepared and poured into the mold, then allowed to cool and solidify. The template was then removed from the mold to leave a clear cylindrical channel of the template's dimensions through the gel. A representative 60 µm channel chip was soaked overnight in 10 µM fluorescein and imaged via confocal microscopy.

Chip 1.1. The same barbell-shaped PDMS mold was placed atop a glass microscope slide. Circles (arbitrarily 3 mm in diameter) were laser-cut from polyvinylidene fluoride (PVDF) film of 0.02-inch thickness and placed in the centers of the barbell ends. A 60-µm optical fiber was threaded under opposite ends of the PDMS mold and suspended

between the circular supports. Agarose was then poured into the mold and allowed to solidify before removing the fiber.

Chip 1.2. A three-layer spacer was designed: the outer layers, plain circles of 3 mm diameter; the inner layer, the same circle with a channel bisecting it. The layers were cut from 0.02-inch-thick PVDF and adhered to each other to form a squat cylinder with a channel through the middle layer. An inlet was made using a washer cut from GelBond® film epoxied to flow tubing. To fabricate the chip, the same barbell-shaped PDMS mold was placed atop a glass microscope slide. A circular face from one spacer was then adhered to the glass microscope slide in the center of each barbell end. A channel template, either 200-µm glass capillary or 60-µm optical fiber, was threaded through the middle of the supports and upward through the GelBond® inlet. Molten agarose was poured into the mold and the inlet washer pressed onto the surface until solidified. The template was then removed and the flow tubing attached to a syringe pump of Nile blue dye at 23.5 µL min^{-1}.

2.2.3 Chip 2

A PDMS substrate was fabricated and functionalized with alginate following the procedure of Cha et al. (3). Briefly, the PDMS was immersed in a 3:1 mixture of H_2SO_4:H_2O_2 for 30 minutes, rinsed three times, incubated in APTES for one hour, then rinsed three times. Finally, the PDMS was incubated in a mixture with molar ratio of 1:30:25, respectively, of 1% alginate in MES buffer, sulfo-NHS, and EDC for 24 hours with gentle shaking at 20 rpm. After functionalization, the PDMS-alginate was covered with 2% alginate in 20 mM $CaCl_2$, followed with a coverslip, and incubated for one hour at 37°C. A chip was also fabricated in the same manner as chip 1.0 but using alginate gel in place of agarose.

2.2.4 Chip 3

Chip 3.0. A barbell-shaped mold was laser-cut from a 250-µm-thick layer of PDMS and pressed to form a liquid-tight barrier on a glass microscope slide. A 60-µm optical fiber was laid across, held taut, and covered with the same thicker PDMS molds used previously. The layers were held together while agarose gel filled the mold and solidified before removal of the optical fiber.

Chip 3.1. A barbell-shaped mold was laser-cut from a 250-µm-thick layer of PDMS and pressed onto a glass microscope slide. A 200-µm glass capillary (channel template) inside cuts of 700-µm glass capillary (flow tubing) was laid across the top such that the thicker capillary pieces covered the ends of the barbells. This was covered with the same thicker PDMS molds used previously and held together while agarose was poured into the mold and allowed to solidify. The channel template was then removed, leaving the flow tubing embedded in gel connected by a clear channel. The channel was then perfused with Nile blue dye at 23.5 µL min^{-1}.

Chip 3.2. Melting point capillaries (inlet tubing) were etched in Armour Etch overnight before being thoroughly rinsed and flushed with water. A chip was then fabricated using the same method as chip 3.1, except the etched inlet and outlet tubes were embedded in the gel rather than flow tubing. The inlet and outlet were then epoxied to flow tubing hooked to a syringe pump. The channel was perfused with Nile blue dye at 23.5 µL min^{-1} and 1.41 µL min^{-1}.

Flow rate calculation. Fluorescein perfusion of chip 3.2 at 1.41 µL min^{-1} was recorded under stereoscope while illuminating the chip with white LED illumination transmitted through a 490 ± 10 nm bandpass fluorescence excitation filter. Still images were captured every five seconds via a digital microscope camera equipped with a 530 ± 15 nm emission filter, then used to measure the length from the edge of the frame to the perfusate front after fluorescein entered the channel. A pixel-to-mm conversion factor was calculated from the known width of the fabricated channel mold and used to find the distance traveled at each time point. In this manner, a linear flow rate was calculated for each time point and finally, using the channel's cross-sectional area, converted to volumetric flow rates.

2.2.5 Chip 4

Chip 4.0. Channel chip fabrication: Two holes were drilled through a microscope slide and a channel was laser-cut from a square of thin PDMS. The microscope slide and PDMS square were covalently sealed via plasma bonding to align the holes in the glass with the ends of the channel. A second piece of PDMS was sealed to the first to close the channel, and a Luer port was sealed to one hole on the microscope slide.

Gel chip fabrication: A piece of GelBond® had an access hole punched, then was placed into a mold and covered with molten agarose. A piece of glass was laid on top to produce a thin layer of gel with the same thickness as the height of the mold. After the thin layer of agarose solidified, a 200-µm glass capillary was aligned with the hole in the GelBond® and placed on top before being covered by a thick layer of agarose. After gelation, a hole was punched through the agarose from the access hole to the channel template, which was then removed. Finally, the channel chip and gel chip were sealed to align the remaining access holes. The Luer port was attached to a syringe pump of Nile blue at 1.41 µL min^{-1}.

Chip 4.1. The same method was used as for chip 4.0, except the channel of the channel chip was scored into the microscope slide rather than cut from the PDMS layer.

Electroosmotic pumping. An alternative to syringe pumping was explored by fabricating chips with no fluid ports and a 200-µm channel through a variety of 2% agarose gels. Silver or platinum electrodes were placed directly into the gel 5 mm apart in either a two- or four-electrode configuration spanning both sides of the templated channel. The chip was observed under stereoscope while a low-voltage power supply was used to apply a potential difference up to 30 V across the electrodes with either 10 mM phosphate buffered saline (PBS, pH 7.4) or 45 µM fluorescein in PBS in the channel.

2.3 Results & discussion

2.3.1 Chip 1

The templating fabrication method used for chip 1.0 (figure 2-1a) was predictable and reproducible, but the final fabrication steps requiring punching holes and filling channel ends added undesirable complexity and uncertainty to the method.

The fabricated channel could not be observed above the portion shown in figure 2-2, as the image became ill-defined and diffuse. This suggests that the channel's position extended out of the working distance for the microscope, which greatly complicates microscopic imaging and luminescent measurements across the length of the channel. This study demonstrated a need for better control of the channel's z position, especially for the less rigid 60-µm optical fiber templates. The circular supports used for chip 1.1

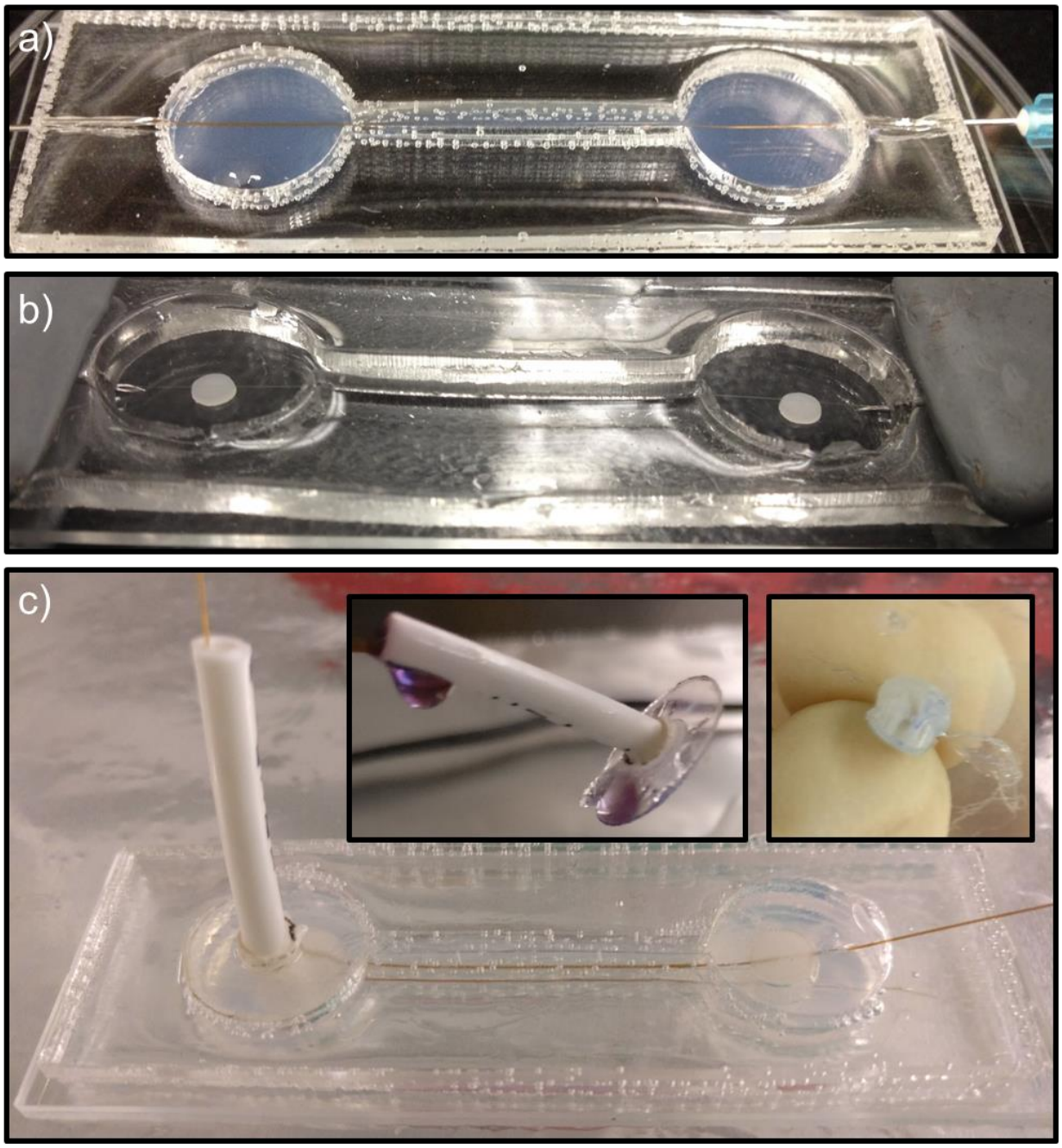

Figure 2-1. *Designs and problems of chip 1.* a) Chip 1.0 before removal of 200-µm glass capillary; b) chip 1.1 before removal of 60-µm optical fiber; c) chip 1.2 before template removal; insets show leaking, detached GelBond® inlet and melted cylindrical support.

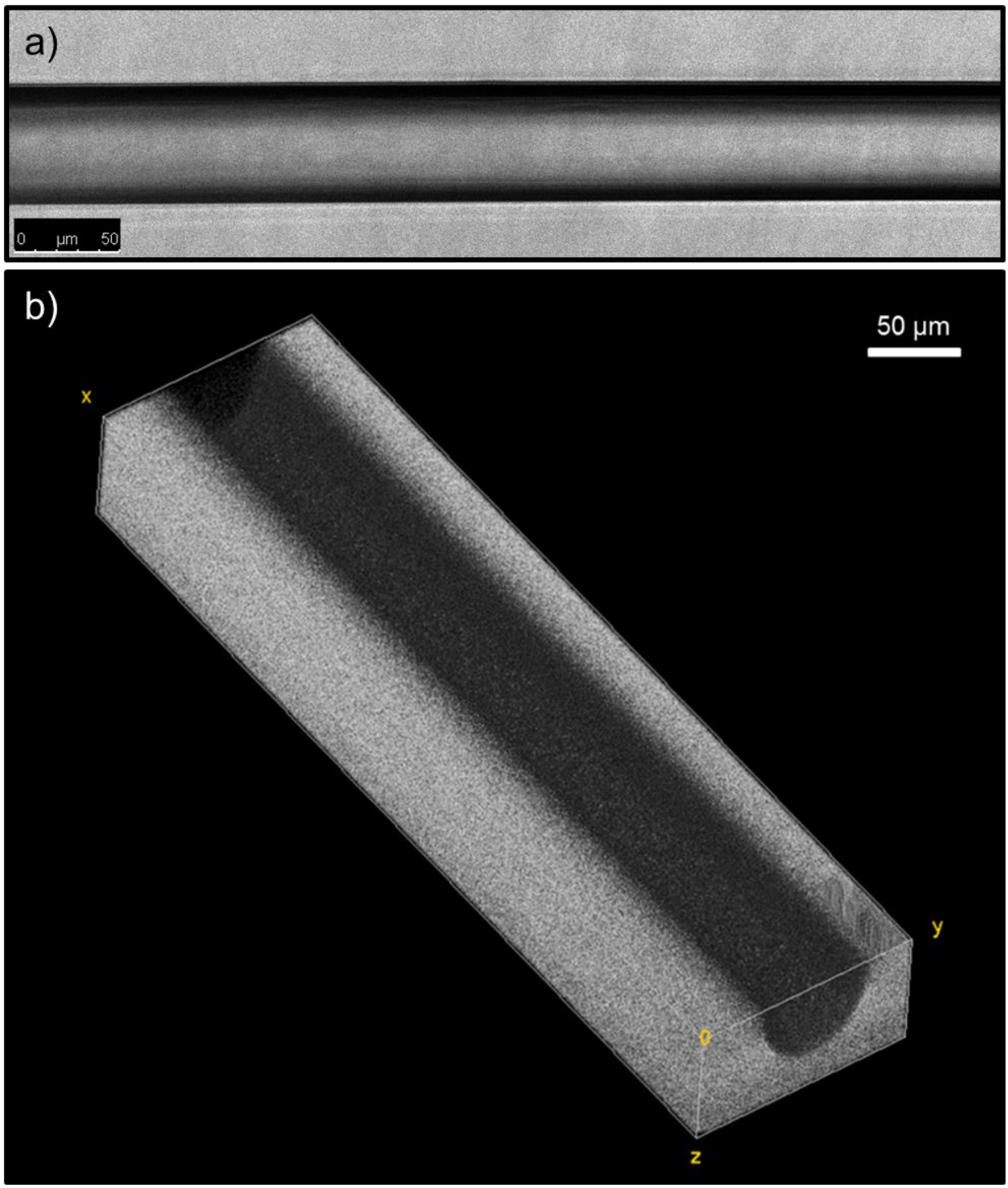

Figure 2-2. *Confocal microscopy of chip 1.* a) 60-µm templated channel in agarose gel; b) three-dimensional model of same channel reconstructed from z-stack using confocal microscopy.

(figure 2-1b) accomplished this goal, but the fabrication method still required hole-punching and end-filling.

Chip 1.2 (figure 2-1c) was an attempt to circumvent these fabrication requirements. The glass capillary was easily fed through and bent around the cylindrical supports, but the brittle optical fibers were much more difficult to work with and shattered in most chips. Once molten agarose was added to the mold, the spacers disassembled, suggesting that the adhesive used between layers cannot withstand such heat. Once attached to flow tubing, the pressure from the glass capillary overcame the inlet's bonds and the GelBond® washer detached from the agarose gel and leaked.

2.3.2 Chip 2

Increasing the hydrophilicity of PDMS should improve bonding to hydrogel, so an alternative but established fabrication method using alginate was attempted with this aim. As shown in figure 2-3a, the functionalized PDMS-alginate was no longer transparent, negating one of its most desirable qualities for cell culture studies such as this. The cross-linked alginate gel was too viscous to pipette and so was difficult to controllably distribute into chips, and contracted away from the PDMS mold upon gelation (figure 2-3b). The alginate gel also failed to solidify except at high [Ca^{2+}] that have been shown to significantly decrease cell proliferation (17). Poor optical transparency and poor materials properties made the alginate fabrication method unsuitable for optical interrogation of cell culture models.

2.3.3 Chip 3

Chip fabrication. Both the dual-layer PDMS mold and the embedded flow tubing (figure 2-4) contributed to better control of the channel's z position, but neither addressed other fabrication issues. Perfusing chip 3.1 revealed a major fabrication issue rarely addressed in the literature, as dye leaked between the agarose and flow tubing (figure 2-5a). It was hoped that etching inlet tubing with Armour Etch—a mixture of ammonium bifluoride, sodium bifluoride, sulfuric acid, and barium sulfate—would increase the surface area and roughness to improve bonding (18). Perfusion of chip 3.2 with Nile blue at the maximum flow rate calculated to apply appropriate shear stress still leaked (figure 2-5b). This flow rate would replace the volume of the channel around twenty

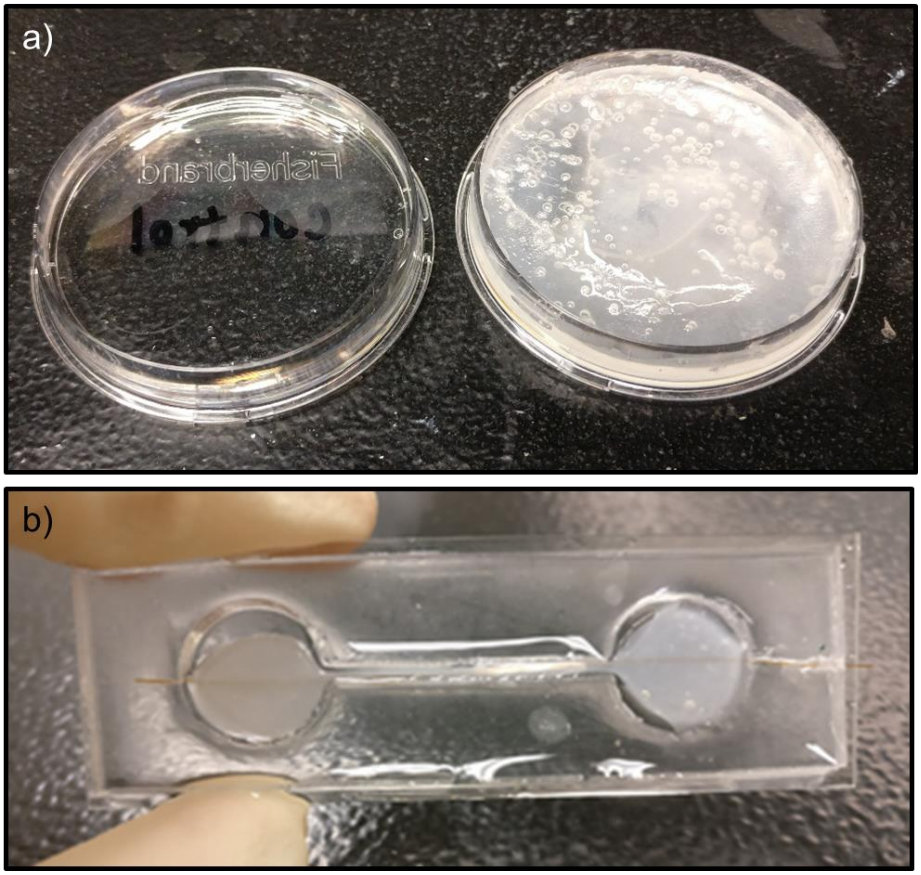

Figure 2-3. *Alginate functionalization and chip 2.* a) Unaltered PDMS (left) and functionalized PDMS-alginate (right); b) chip 2 after alginate gelation.

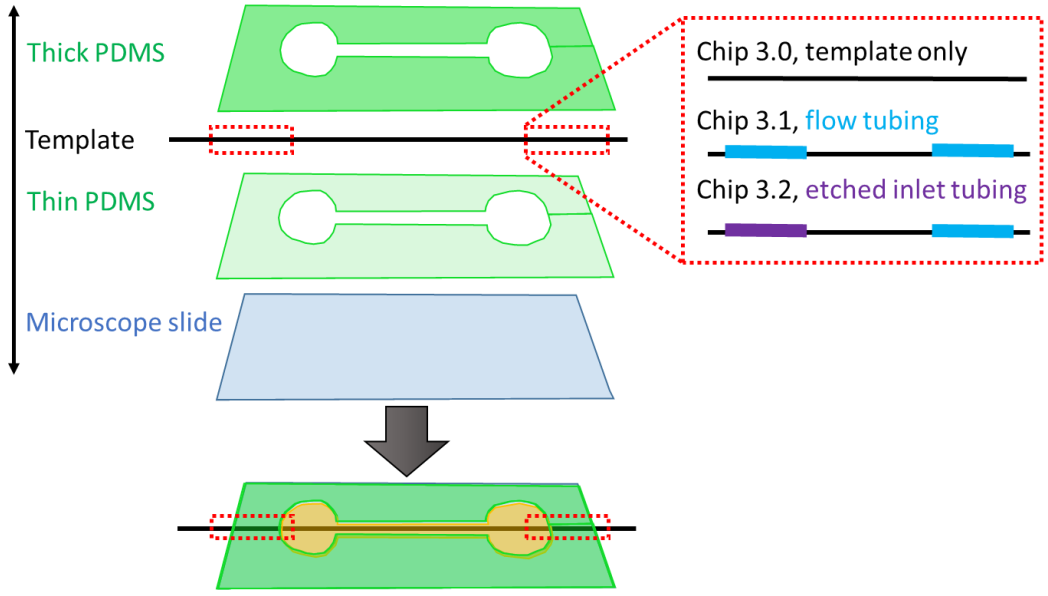

Figure 2-4. *Fabrication method of chip 3.* Channel template sandwiched between thick and thin PDMS layers; inset shows embedded tubing for chips 3.1 and 3.2.

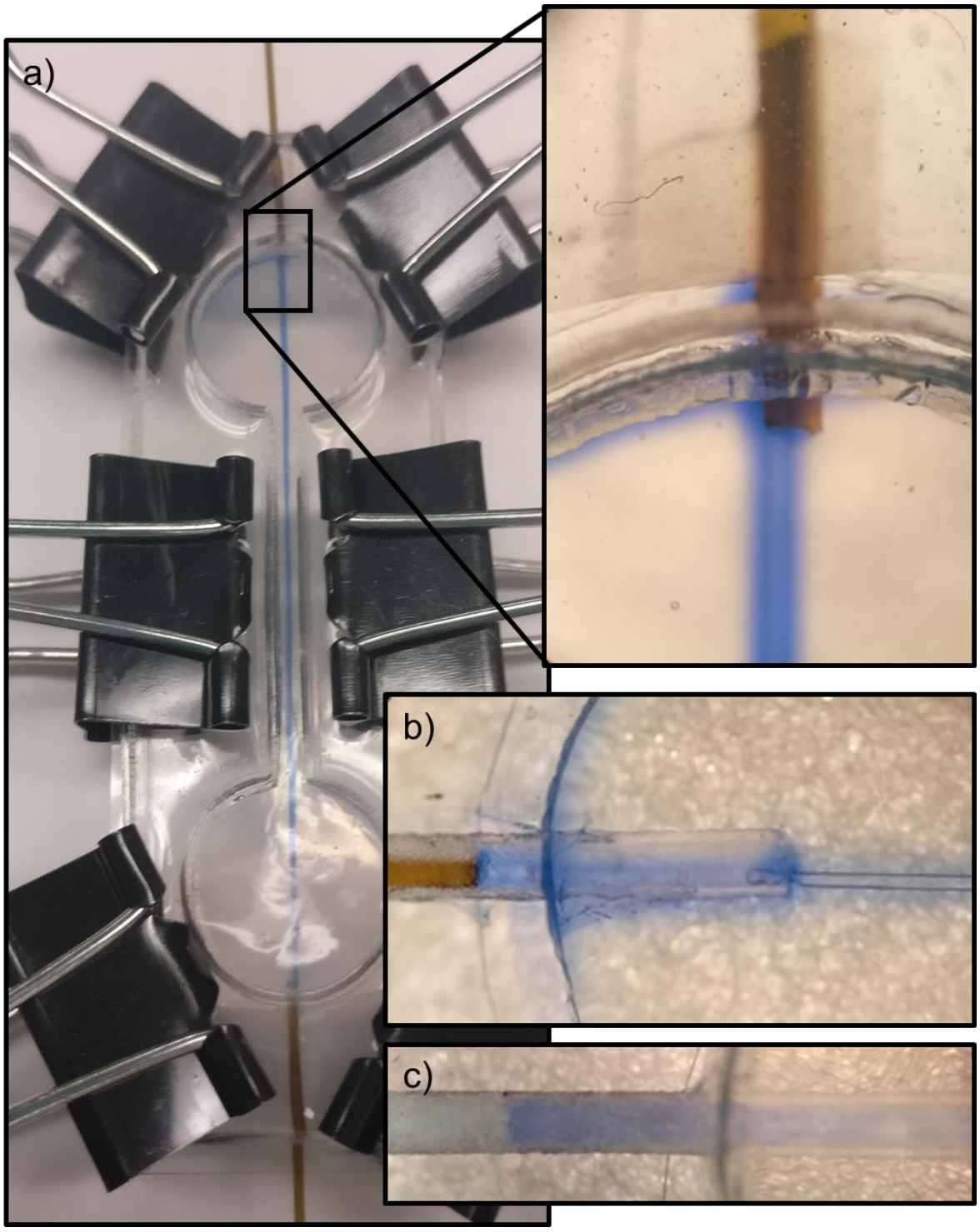

Figure 2-5. *Dye perfusion of chip 3.* a) Chip 3.1 after perfusion, inset showing leak between agarose and PDMS; b) leak between agarose and PDMS after perfusion of chip 3.2 at 23.5 µL min^{-1}; c) dye concentration after perfusion of chip 3.2 at 1.41 µL min^{-1}.

times a minute, which may be too much for the bond between the agarose and etched inlet to withstand. Lowering the flow rate of Nile blue to replace the channel volume around once a minute caused a different problem (figure 2-5c). No dye visibly leaked between the agarose and inlet, nor flowed along the length of the channel; it appeared to concentrate at the beginning of the gel and lessen with distance. The solution was possibly too dilute at the end of the channel to see, or at such a small volume that it evaporated before pooling at the outlet.

Flow rate determination. The first attempt at fluorescein perfusion was done with 10 μM solution. Nothing could be seen in the channel, which could mean no flow occurred or that the solution was too dilute for the camera to detect. For the second attempt, concentration was increased to 45 μM, and flow was observed. As shown in figure 2-6, the experimental flow rate fluctuated over the measurement period, reaching a maximum of just 0.007 μL min^{-1} compared to the set flow rate of 1.41 μL min^{-1}. Conservation of mass requires all fluorescein solution pumped into the channel to go somewhere, meaning a leak must exist even if not visible. Fluorescein was observed to diffuse laterally into the gel over time; since the gel is mostly water, this movement of fluorescein molecules does not necessitate a significant volume loss from the channel. However, evaporation had caused the gel to collapse by the end of the trial, so it is possible the perfusate was lost to the bulk of the gel and subsequent evaporation.

2.3.4 Chip 4

Chip fabrication. The two-part design of chip 4.0 leaked upon perfusion with dye (figure 2-7), prompting a few adjustments (figure 2-8). Instead of cutting the channel from the PDMS layer of the channel chip, in chip 4.1 the channel was etched directly into the microscope slide, which eliminated observed leaking at this junction. Chip 4.0 also leaked between the channel and gel chips when attached via double-sided adhesive; chip 4.1 minimized this problem with the use of epoxy. However, epoxy requires hours to cure, during which time hydrogel devices can dehydrate, and epoxy clogs channels when applied too liberally. The dye was observed pooling in the dead volumes of the chip, which would alter the concentrations and temporal profiles of stimuli delivered to

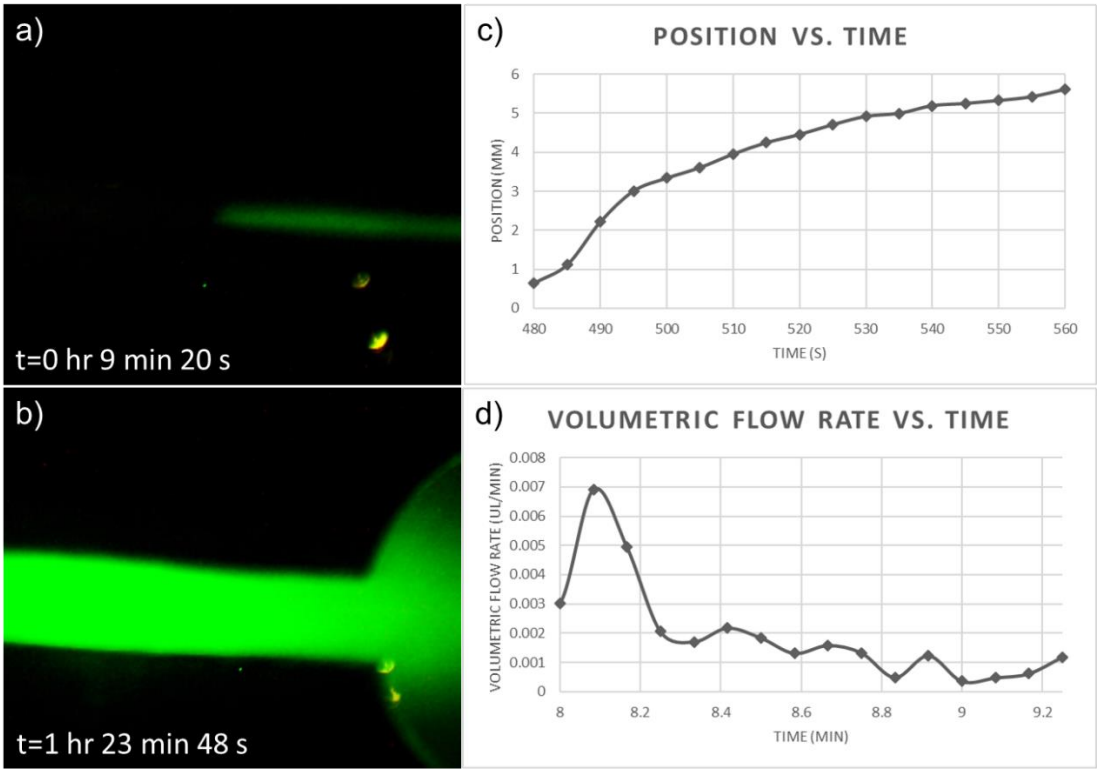

Figure 2-6. *Fluorescein perfusion of chip 3.* a) Fluorescein in channel after 9 min 20 s; b) fluorescein-saturated gel after 1 hr 23 min 48 s; c) position vs. time of fluorescein over measurement period; d) volumetric flow rate vs. time of fluorescein over measurement period.

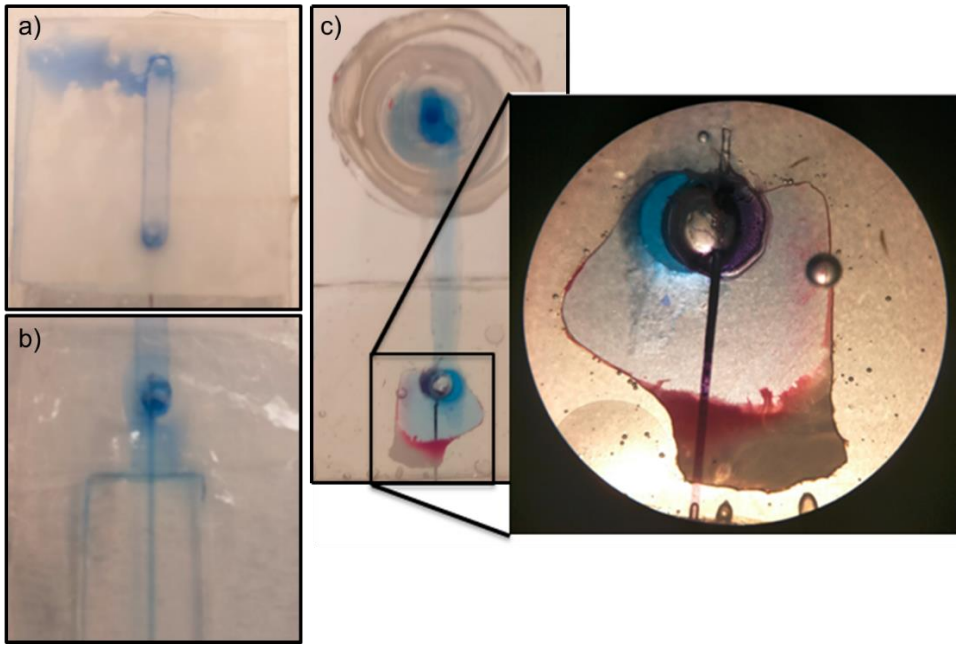

Figure 2-7. *Problems of chip 4.* a) Leak from PDMS channel in chip 4.0; b) leak between channel chip and gel chip in chip 4.0; c) dye buildup in dead volume between channel and gel chip in chip 4.1.

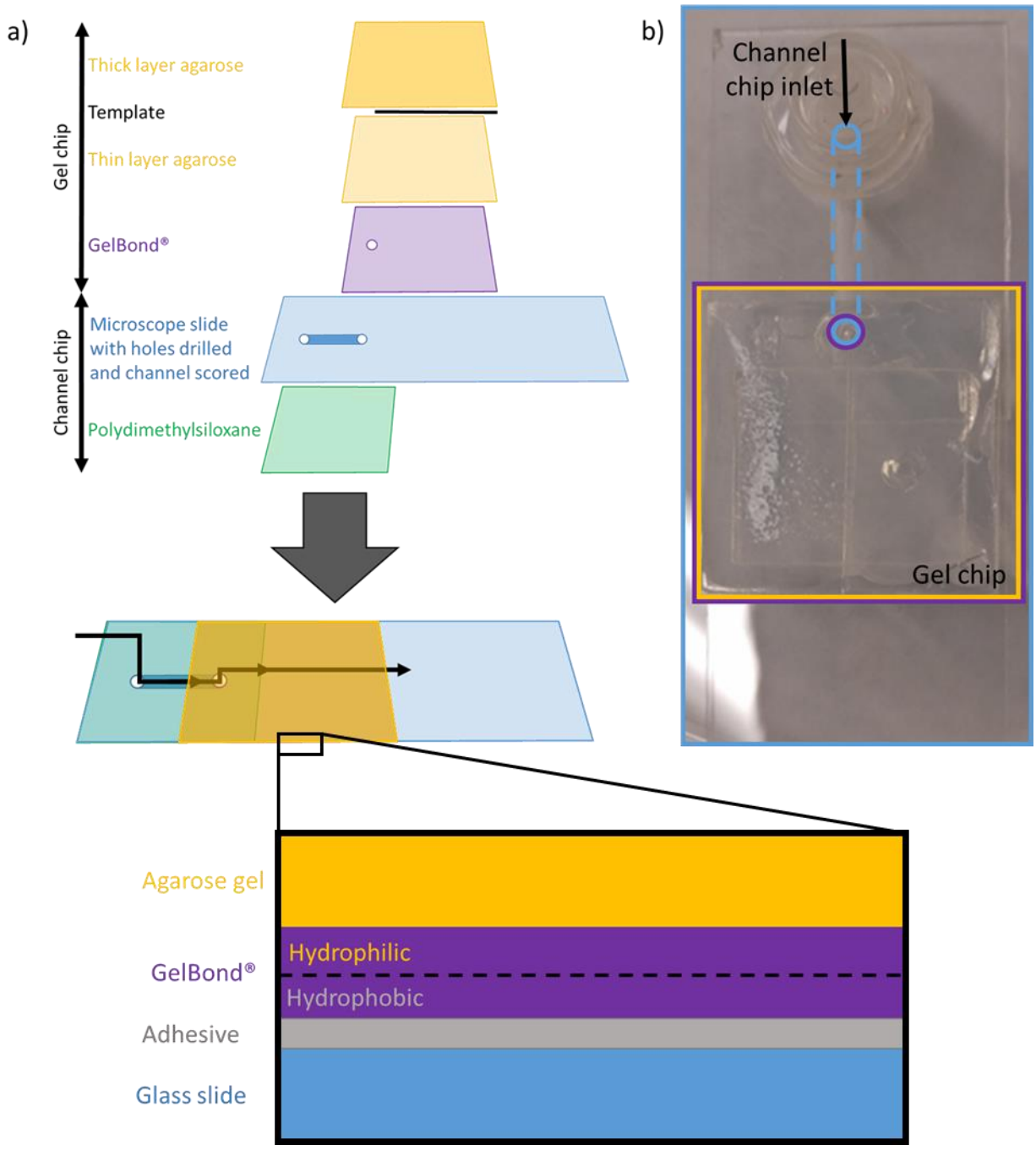

Figure 2-8. *Final fabrication method of chip 4.* a) Channel chip and gel chip are fabricated separately; b) channel and gel chips are combined into one microfluidic device. Inset shows GelBond® interface between agarose gel and glass.

cell cultures. This approach also returns to punching fluid access holes through the gel, which is undesirable.

Electroosmotic pumping. Electroosmotic pumps are attractive alternatives to syringe and other pumps because they require no moving parts and can be fully integrated on-chip, voiding the need for interfacing with the gel at all. The original chip was fabricated from low-electroendoosmosis (EEO) agarose dissolved in PBS, and no bulk movement of PBS through the channel could be observed when attempting electroosmotic pumping in these channels. 45 μM fluorescein was substituted in the channel to better visualize any possible flow than the colorless PBS solution, but no electroosmotic flow was observed, and devices were consistently dehydrated during the course of the experiment. High-EEO agarose in PBS, high-EEO agarose in 15 mM HEPES buffer, and high-EEO agarose in 15 mM HEPES with 5-μm silica spheres were used for further attempts to drive and observe electroosmotic pumping. The intent of these measures was to increase the conductivity within the channel to drive electroosmotic flow within the device, but still no flow was observed. When voltage was applied to the electrodes, bubbles formed, likely due to the electrolytic production of H_2 or O_2 or even reactions of the electrodes themselves (19). Craters also formed in the gel surrounding electrodes, which could be evidence of Joule heating of the thermo-reversible agarose. Eliminating electrical contact between the electrodes and gel could avoid these issues, but this solution may require the pump no longer be entirely on-chip. Another option would be increasing the gel concentration and subsequent strength to resist distortion, but at higher strengths the gel would be more physically restricting to cells (20). Alternatively, decreasing the voltage to levels below those necessary for electrolysis would also decrease Joule heating, but more importantly it would decrease the rate of electroosmotic flow (19). Electroosmotic pumping requires a tradeoff of these factors, and did not appear viable in the agarose gel microfluidic channel.

2.4 Conclusions

Pouring molten agarose around glass capillaries and optical fibers has proven a fast and facile way to template channels in a realistic extracellular matrix that could be remodeled by cells. This work used a 60-μm optical fiber as a channel template, which

is the lower limit of channel diameters currently feasible by templating. However, cell culture was never attempted in this device because it could not be successfully sealed to flow. The chip on which our original design was based required punching fluid access holes and filling in channel ends to introduce flow from the top. Ideally, these steps could have been eliminated to minimize variability in fabrication, but incorporating supports and inlets to facilitate top access to the channel was unsuccessful. Supports did not survive fabrication, but more importantly, they introduced additional interfaces the agarose did not bond to and more dead volumes. All physical and chemical modifications attempted to increase hydrogel bonding to the rest of the chip were unsuccessful and had additional disadvantages. Perfusion through the templated channel never reached the intended flow rate, which further proves the existence of leaks. The only leak-free interface in the final chip design was that between GelBond® and agarose. The observed dead volumes would be detrimental when applying a specific temporal profile of chemical stimuli to cell cultures in the chip. Alternative pumping methods to circumvent these issues were not successfully incorporated. Sealing the hydrogel-chip interfaces may matter less for other applications, but as temporal analysis was the goal for this system, its shortcomings made this fabrication method unviable.

CHAPTER 3. QUANTITATIVE TLC FOR THE UNDERGRADUATE TEACHING LABORATORY

3.1 Introduction

The opportunity arose to develop an experiment for a new senior-level analytical/physical chemistry course, Advanced Measurement and Spectroscopy Laboratory CHEM 459. The four-hour laboratory period is split between two experiments, leaving only two hours to complete each, compared to the three hours typical for general and organic chemistry labs. The ideal experiment was to be quantitative, fast, and inexpensive, and preferably focus on something students find interesting. TLC is an analytical method commonly used in high school and college science labs; it is a more convenient way to apply the same chemical principles as costlier chromatographic methods, such as high-performance liquid chromatography, and so remains relevant but rarely utilized in high-level college chemistry courses (1). Teaching labs take advantage of the many benefits of TLC, some increasing student interest by showing its facile application to real-life problems, while others utilize its speed, low cost, and environmental friendliness (2-6). TLC is usually presented in a strictly qualitative context, as quantitative TLC often uses costly imaging instrumentation that negates the cost advantages of TLC. The few pedagogical methods that use TLC for quantitation generally focus on decreasing costs with alternative instrumentation, but are rendered impractical by using defunct or expensive software for analysis (7-9).

For this undergraduate lab, we chose the approach of digitally-enhanced TLC (DE-TLC), which combines a digital camera with regular TLC equipment to enable quantitative analysis (10). DE-TLC was introduced in 2007 with an accompanying public domain analysis software, but the software is now obsolete and inoperable on many modern computer systems. In this work, the DE-TLC method was revisited using free public domain software (*i.e.* NIH ImageJ) for quantitative TLC analysis using indirect fluorescence detection. To interest students, counterfeiting of the anti-malarial drug chloroquine was chosen as the proposed application. The two-hour time constraint was motivation for as much work as possible to be done outside of the lab period. Since data analysis requires only a computer and free software, it can be done anywhere, but in

our experience, solution preparation also takes students a considerable amount of time. Consequently, a prelab procedure was added for students to complete before the lab period. It lists every solution to be made along with blank tables to fill in necessary volumes of each component. Plate development is another time-consuming step that was minimized here with concurrent calibration curves, effectively halving the time devoted to separations. The final prelab and lab documents that were distributed to students in advance are included in section 3.2 below. We had the opportunity to teach the first section of students who attempted this lab exercise, and observations as well as student results will be discussed.

3.2 Materials & methods

3.2.1 General

Chloroquine diphosphate salt (98%), acetylsalicylic acid (99%), absolute ethanol, methanol (ACS grade), and silica gel 60 F254 coated plastic-backed TLC plates were purchased from Thermo Fisher Scientific (Waltham, MA). Caffeine (anhydrous), dichloromethane (99.9%), and hexanes (anhydrous) were from Millipore Sigma (Burlington, MA). Polyamide TLC plates with UV254 were from Analtech (Newark, DE). Acetaminophen (98%) was borrowed from the analytical teaching lab in Buehler 331. Handheld 254-nm UV fluorescent lamps were from UltraViolet-Tools (Round Rock, TX). Imaging was done with the SM-4TZ-144A professional trinocular stereo zoom microscope and the MU1000 10-megapixel digital camera from AmScope (Irvine, CA). All image processing was done with ImageJ from the National Institutes of Health (Bethesda, MA).

3.2.2 Method development

Concentration optimization. Solutions of chloroquine, acetylsalicylic acid, acetaminophen, and caffeine were made from 0.5-20 mg mL^{-1} in ethanol (EtOH), water, and a 1:1 mixture of the two. Using glass capillaries, each solution was spotted onto a TLC plate and allowed to dry. The plate was digitally imaged via stereoscope under UV illumination. ImageJ was used to measure the intensity of the spots, which was plotted against concentration and used to identify a sensitive linear range for each analyte. A calibration curve was then remade in the chosen range with added concentration points.

Separation conditions. Solutions of chloroquine, acetylsalicylic acid, acetaminophen, and caffeine were spotted on TLC plates and allowed to dry. The plates were developed in EtOH, water, 10% methanol (MeOH) in dichloromethane (DCM), hexane, 1:1 hexane/DCM, and various ratios of EtOH and water. The developed plates were then allowed to dry before being imaged under UV illumination.

Illumination system design. Two UV lamps were positioned within a home built acrylic illumination box such that a uniform field of illumination approximately 10 cm x 10 cm was achieved on the bottom interior face of the illumination box. The top face of the box was constructed of 1.5-mm thick clear acrylic, which was transparent to green fluorescence but did not transmit 254-nm excitation light. All other faces of the illumination box were constructed from 3-mm thick black acrylic to prevent operators from inadvertent UV exposure.

Image processing. Images of the TLC plates were analyzed with color and after conversion to grayscale, and with and without rolling ball background subtraction. After concentration optimization, images were also inverted. Intensity measurements were evaluated by three methods: ImageJ was used to measure the maximum and mean intensity of an elliptical region covering each spot, and a line profile going through the most intense region of each spot was also plotted and the peak height measured manually.

3.2.2 Prelab procedure

To expedite the solution-making process, fill out the following tables before you come to lab. For stock solutions, you should dissolve appropriate amounts of each compound in 1:1 ethanol/DI water to the desired concentration:

Table 3-1. *Stock solution preparation.*

Solution	Volume	Concentration	Mass needed
Acetaminophen	5 mL	5 mg mL^{-1}	
Chloroquine	5 mL	3 mg mL^{-1}	
Caffeine	5 mL	10 mg mL^{-1}	

For calibration mixtures, you will combine your stock solutions of acetaminophen, chloroquine, and caffeine and dilute with 1:1 ethanol/DI water to a 1 mL solution of the desired concentration:

Table 3-2. *Calibration mixture preparation.*

Mixture	Acetaminophen		Chloroquine		Caffeine		Ethanol/DI
	Conc	Volume	Conc	Volume	Conc	Volume	Volume
A	1.0 mg mL^{-1}		1.5 mg mL^{-1}		2.5 mg mL^{-1}		
B	1.5 mg mL^{-1}		1.0 mg mL^{-1}		2.5 mg mL^{-1}		
C	2.0 mg mL^{-1}		0.75 mg mL^{-1}		2.5 mg mL^{-1}		
D	2.5 mg mL^{-1}		0.5 mg mL^{-1}		2.5 mg mL^{-1}		

3.2.3 Lab procedure

The text of this section shows the laboratory procedure as provided to students. No amendments have been made to accommodate the narrative of this thesis document.

Quantitative Thin-Layer Chromatography for Identification of Counterfeit Drugs

Thin-layer chromatography (TLC) is a fast and inexpensive separation technique used by many laboratories to optimize chromatographic conditions and determine product purity. TLC can be used qualitatively to identify the components of a sample by their retention factor, R_f:

$$R_f = \frac{distance\ traveled\ by\ sample}{distance\ traveled\ by\ solvent\ front} \quad (1)$$

As with other chromatographic techniques, the performance of the separation can be determined by its resolution, R_s, where ΔZ is the difference between the centers of two peaks, and W_A and W_B are the widths of the bases of those same peaks:

$$R_s = \frac{2\Delta Z}{W_A + W_B} \quad (2)$$

Although less common, TLC can also be used quantitatively. For example, samples spotted on a fluorescent TLC plate will quench fluorescence proportional to the amount of sample present. Calibration curves can be developed and used to quantify unknown concentrations of a known analyte.

TLC generally offers lower resolution and sensitivity than instrumental separation methods like HPLC, but in exchange for inferior analytical performance TLC offers extremely simple operation that is low cost and consumes relatively few resources. These properties make TLC an excellent choice for field deployable analyses in resource-limited settings like the developing world.

According to the World Health Organization, there are more than 200 million cases of malaria annually, with more than 90% of all cases occurring in sub-Saharan Africa. UNICEF reports that over 1 million people die each year from malaria, the majority of whom are children under the age of five. Malaria prevention and treatment is complicated by a significant challenge of the developing world: drug counterfeiting. Often, counterfeiters will cut therapeutic drugs with less expensive active ingredients, like fever reducers, to help hide the fact that the counterfeit product is not effective for its intended use. For example, the anti-malarial drug chloroquine may be cut with, or replaced entirely by, acetaminophen so as to give the impression that the counterfeit drug is effective when patients' fevers are temporarily reduced upon taking the counterfeit drug. Of course, these counterfeits are not effective at treating malaria, and the counterfeiter has made significant profit selling acetaminophen in place of chloroquine. This is complicated further by the possibility that a legitimate therapeutic dose of chloroquine may be accompanied by fever reducing medications in some drug formulations. Thus, simply identifying the presence of acetaminophen is not sufficient to identify a counterfeit malaria drug; instead, a quantitative analysis is needed to determine the relative quantities of chloroquine and acetaminophen to determine if the drug is authentic.

In this lab procedure, you will develop a quantitative TLC assay, suitable for deployment to resource-limited settings, to determine if a compounded malaria drug contains a therapeutic dose of chloroquine (≥ 1 mg mL^{-1}) or if it has been adulterated by the addition of acetaminophen ([acetaminophen]/[chloroquine] > 3). To improve quantitative accuracy, caffeine will be used in this TLC separation as an internal standard.

Materials

Ruler	Digital camera
Pencil	Acetaminophen
10 cm x 10 cm TLC plates	Caffeine
Micropipettor or glass capillaries	Chloroquine diphosphate salt
254-nm UV lamp	Ethanol

All image processing is accomplished using the cross-platform open source software application ImageJ, available for free download at https://imagej.nih.gov/ij/ .

Procedure

Sample Preparation

Make 24 mL of 1:1 ethanol/DI water to serve as the solvent for all solutions. Three stock solutions (5 mL each) of 5 mg mL^{-1} acetaminophen, 3 mg mL^{-1} chloroquine, and 10 mg mL^{-1} caffeine should be made, and then used to make 1 mL of the following mixtures:

Table 3-3. *Calibration mixture concentrations.*

Mixture	[Acetaminophen]	[Chloroquine]	[Caffeine]
A	1.0 mg mL^{-1}	1.5 mg mL^{-1}	2.5 mg mL^{-1}
B	1.5 mg mL^{-1}	1.0 mg mL^{-1}	2.5 mg mL^{-1}
C	2.0 mg mL^{-1}	0.75 mg mL^{-1}	2.5 mg mL^{-1}
D	2.5 mg mL^{-1}	0.5 mg mL^{-1}	2.5 mg mL^{-1}

Notice that [acetaminophen] increases from A→D while [chloroquine] increases from D→A. This will allow for two calibration curves to be made simultaneously, after these mixture components have been separated by TLC. The unknown drug samples have already been put into solutions that include caffeine at a concentration of 2.5 mg mL^{-1}.

TLC Procedure

Prepare two 10 cm X 10 cm TLC plates. Use a pencil to draw a line, called the origin, 2 cm from the bottom edge of each TLC plate. Sample solutions will be applied as spots

directly on the origin line either by micropipettor or using a glass capillary tube. If using a micropipettor, produce a sample spot by drawing up 1 µL of sample into the pipette tip, then dispense the entire volume on the origin line to produce a single spot of approximately 1-2 mm diameter. If using a glass capillary, dip the capillary in sample solution, then touch the capillary to the origin line, being careful not to dispense a sample spot larger than 1-2 mm in diameter. Plate 1 should be spotted three times for each of the three stock solutions and once with each unknown. Plate 2 should be spotted three times with each of the mixtures, A-D, prepared in the previous step. Figure 3-1a illustrates the spots that should be made on plates 1 and 2. Use a pencil to label the identity of each spot below the origin, and allow all spots to dry completely. Meanwhile, fill an appropriate container about 1 cm deep with 1:2 ethanol/DI water, cover with a watch glass, and allow the covered container to sit for at least 5 minutes. This is your development chamber.

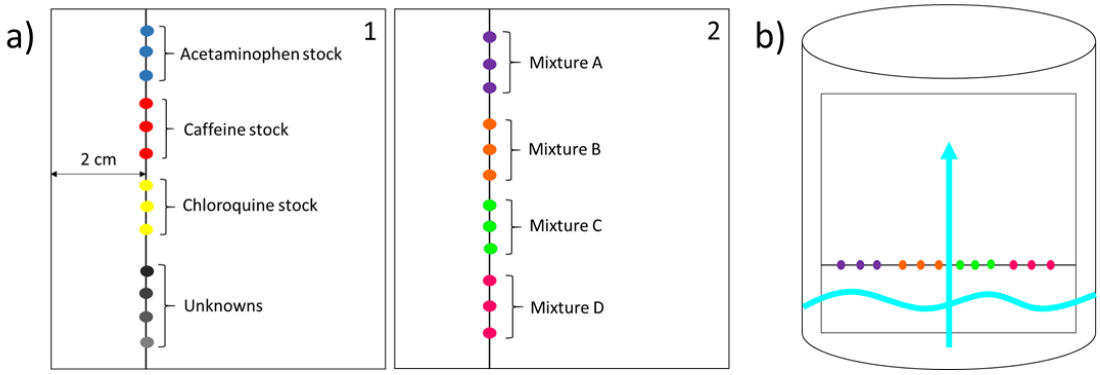

Figure 3-1. *TLC plate spotting and development.* a) TLC plate layouts; b) TLC plate development process.

To perform the TLC separation, stand a TLC plate in the development chamber with the origin towards the bottom of the chamber (see figure 3-1b), being sure not to submerge the origin, then cover the chamber again. The solvent will slowly advance up the TLC plate, and the advancing solvent front should be visible as the line where the plate goes from being wet to remaining dry. Develop each plate until the solvent front is about 2-3 cm front the top of the plate, remove from the chamber, trace the final position of the solvent front lightly with a pencil, then allow the plate to dry completely. Position each plate in the center of the UV light box, switch both UV lamps to the “Fluor” position, then cover the entire imaging setup with a drape. In the imaging software make sure that

“Auto exposure” is checked in the left-hand column, then slide the auto exposure target slider until your image shows good contrast between the green TLC plate and the darker sample spots. Figure 3-2 shows an example image of a developed TLC plate, plate 2 in this case. When you have adjusted the auto exposure target to give similar or better contrast as that of figure 3-2, capture the image for quantitative analysis. Repeat this for both TLC plates.

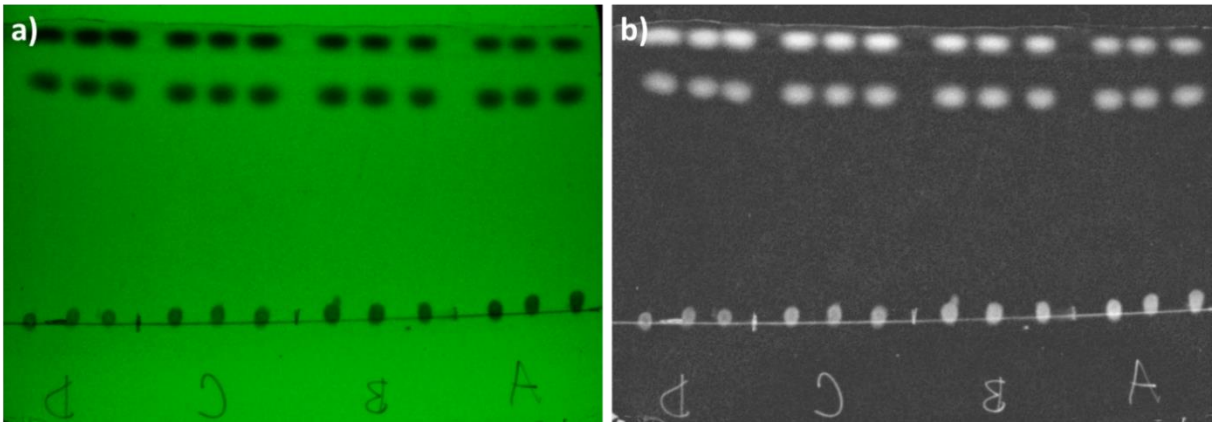

Figure 3-2. *TLC plate 2 sample images.* a) Plate 2 before processing; b) plate 2 after processing.

Image Analysis

Image Processing

The analyte quenches fluorescence of the TLC plate, meaning darker spots correspond to greater analyte amounts. If intensity was measured directly this would give negative chromatographic peaks, which complicates our calibration. Therefore, to simplify interpretation, both images must be processed before quantitative analysis. All processing and quantitative analysis below will be performed using ImageJ software. Start with your image of plate 1:

1. File → Open → Choose image file
2. *Rectangular selection tool* → highlight fluorescent plate but not dark background → Image → Crop (or Ctrl + shift + X)
3. Image → Type → 32-bit: this will convert your image to 32-bit black and white, which simplifies intensity measurements

4. Edit → Invert (or Ctrl + shift + I): this will convert dark spots on a bright background to bright spots on a dark background, which will give positive intensity values that correlate with analyte amount
5. Process → Subtract background → uncheck “light background” box → OK
6. File → Save As → Jpeg… → give your processed image a unique name

NOTE: All of the following quantitative analysis procedures must be carried out on images processed by the procedure given above. Analyses will not work using unprocessed images!

Rf Determination

Next, calculate retention factor for each spot, using the processed plate 1 image:

1. *Straight selection tool* → draw line from origin to solvent front that passes through the sample spot → record “length” from toolbar
2. *Straight selection tool* → draw line from the origin to most intense point of sample spot → record “length” from toolbar
3. Repeat steps 1 and 2 for every spot on TLC plate 1

Retention factor is then calculated for each spot using equation 1. The three calculated R_f values for each replicate of a single standard compound should be averaged. Average retention factors for each of the three standards, acetaminophen, caffeine, and chloroquine, can now be used to identify individual components found in mixtures A-D and the unknowns.

Rs Determination

Now, you’ll quantitatively investigate the separation performance of TLC by measuring resolution in our standard mixtures. First, process your plate 2 image by the “Image Processing” procedure given above. Next, follow the resolution determination procedure given below *for each of the twelve* separations performed on TLC plate 2:

1. *Straight selection tool* → draw a line from origin to solvent front passing directly through the middle of chloroquine, caffeine, and acetaminophen spots (example in figure 3-3a)

2. Analyze → Plot profile (or Ctrl + K)

   HINT: this should give a plot that looks like the chromatograms you may be used to seeing in HPLC or GC, with Gaussian peaks representing the separated components (compare to figure 3-3b).
3. Working in the window containing your plotted intensity profile: *Straight selection tool* → draw a horizontal line from the center of the chloroquine peak to the center of the caffeine peak → record "length" from toolbar
4. *Straight selection tool* → draw a horizontal that measures the width of the chloroquine peak at its base → record "length" from toolbar
5. Repeat step 4 to determine the width at the base of the caffeine peak

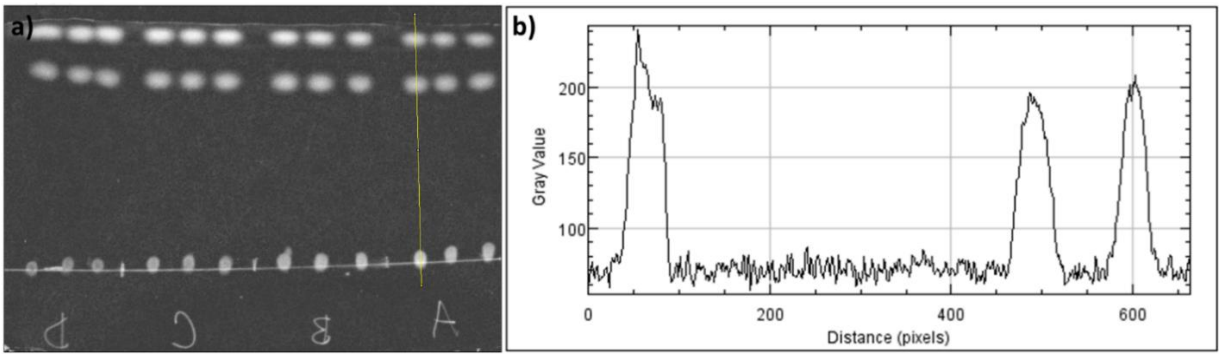

Figure 3-3. *Thin-layer chromatograms.* a) Plate 2 with line through a sample; b) resulting chromatogram.

With the values determined in steps 3-5, calculate the chloroquine-caffeine resolution using equation 2 for each separation performed on TLC plate 2. Determine the average and standard deviation for this resolution value for each set of three replicates. This should give you a single average and standard deviation value for each mixture A-D.

Calibration and Quantitation

Quantifying the components in your unknown samples will require calibration curves for both chloroquine and acetaminophen. To produce calibration curves, you'll need to measure the intensity of every spot on TLC plate 2 by the following procedure:

1. *Oval selection tool* → draw oval that encompasses most of a single component spot and no background
2. *Analyze* → *Measure* (or Ctrl + M)

Repeat process for each spot, keeping track of which measurements correspond to which spot. Compile the average intensities of all peaks on TLC plate 2 into a spreadsheet (e.g. using Microsoft Excel), being careful to keep the intensity values of the three peaks from each separation organized together. Divide the intensity of each acetaminophen peak by the intensity of the caffeine peak *from the same separation* to get the normalized acetaminophen intensity for each separation. Do the same procedure with each chloroquine peak intensity to get the normalized chloroquine intensity for each separation. Each mixture, A-D, should now have three replicate values for normalized acetaminophen intensity and three replicate values for normalized chloroquine intensity. Replicate values can be used to determine an average and standard deviation for normalized acetaminophen intensity, and an average and standard deviation for normalized chloroquine intensity for each mixture, A-D. Construct two calibration curves, one for acetaminophen and one for chloroquine, by plotting the average normalized intensity vs. concentration. Add vertical error bars to illustrate ± 1 standard deviation at each of the data points. Using Excel's built in function, add a trend line to each calibration curve, and show the equation and R^2 value.

Finally, you can quantify the chloroquine and acetaminophen present in each of the unknown samples separated on plate 1. Follow the procedures described above for the calibration curves to determine the normalized acetaminophen intensity and the normalized chloroquine intensity for each unknown. Using the trendline equations from the calibration curves, calculate the concentrations of acetaminophen and chloroquine in each unknown.

Hazards

Be careful not to breathe in any chemicals, and promptly rinse any skin that comes in contact. Be sure to wear goggles and gloves to protect eyes and skin from UV light.

Discussion

At minimum, the following data should appear in your lab writeup:

- Processed images of TLC plates 1 and 2

- A representative chromatogram showing all three peaks (see "R_s determination," step 2)
- Table(s) showing average and standard deviations for calculated R_f and R_s values
- Calibration curves for acetaminophen and chloroquine

The following questions, given in no specific order, may help to guide the discussion of your results in your lab writeup:

1. Assuming that a therapeutic dose of chloroquine is at least 1 mg mL^{-1}, which of the unknown samples are counterfeit, and which are genuine?
2. What is the stationary phase and what is the mobile phase used in these separations? Based on your answer, what retention mechanism (i.e. reversed phase, size exclusion, ion exchange, normal phase, etc.) is occurring in these separations?
3. What phenomenon causes mobile phase to flow in TLC? How is this different from HPLC?
4. Why is caffeine included in these separations? What sources of error or inaccuracy might be increased if caffeine was omitted from this experiment?
5. What do the error bars in your calibration curve communicate to the readers of your lab report? Why are they included?
6. In the R_f and R_s determinations, what are the units of the measured lengths? Would calculated R_f and R_s values differ if the lengths were measured using different units?
7. Do your multiple chloroquine-caffeine R_s values for mixtures A-D differ with statistical significance? Based on your answer, does analyte concentration influence resolution?
8. When we specifically consider the analysis of counterfeit drugs in sub-Saharan Africa, what are the key advantages of TLC over HPLC?
9. Why do the TLC plates used in this experiment fluoresce? By what mechanism does the presence of analyte reduce the intensity of TLC plate fluorescence?

References

- World Health Organization Malaria Fact Sheet. http://www.who.int/mediacentre/factsheets/fs094/en/ (accessed January 1, 2018).
- UNICEF – The Reality of Malaria. http://www.unicef.org/health/files/health_africamalaria.pdf (accessed March 16, 2018).
- Skoog, D.A.; Holler, F.J.; Nieman, T.A. Principles of Instrumental Analysis, Fifth Edition; Thomson Learning: Boston, 1998; pp. 761-765.
- Hess, A.V.I. Digitally Enhanced Thin-Layer Chromatography: An Inexpensive, New Technique for Qualitative and Quantitative Analysis. J. Chem. Ed. 2007 84 (5), 842-847.

3.3 Results & discussion

3.3.1 Method development

Concentration optimization. Solutions of the drug chloroquine, the adulterant acetylsalicylic acid, and the internal standard caffeine were initially made. Chloroquine and caffeine were soluble in water up to the maximum concentration of 20 mg mL^{-1} observed here, but acetylsalicylic acid was soluble only at concentrations so dilute that spots were not visible. All three solutions were remade using ethanol instead, but chloroquine and caffeine were not fully soluble even as low as 5 mg mL^{-1}, so a compromise of 1:1 ethanol/water was chosen as the solvent for all solutions. The final concentration ranges were chosen to enable effective visualization and linear calibration, and these were 0.5-1.5 mg mL^{-1} for chloroquine, 0.5-2.5 mg mL^{-1} for caffeine, and 1-10 mg mL^{-1} for acetylsalicylic acid; caffeine is shown as an example in figure 3-4. Due to low sensitivity and poor separation, acetaminophen later replaced acetylsalicylic acid, so the same process was repeated with it to find an appropriate concentration range of 1-2.5 mg mL^{-1}.

Separation conditions. After determining the appropriate concentration range, focus was shifted to finding appropriate conditions for separation. All three components are

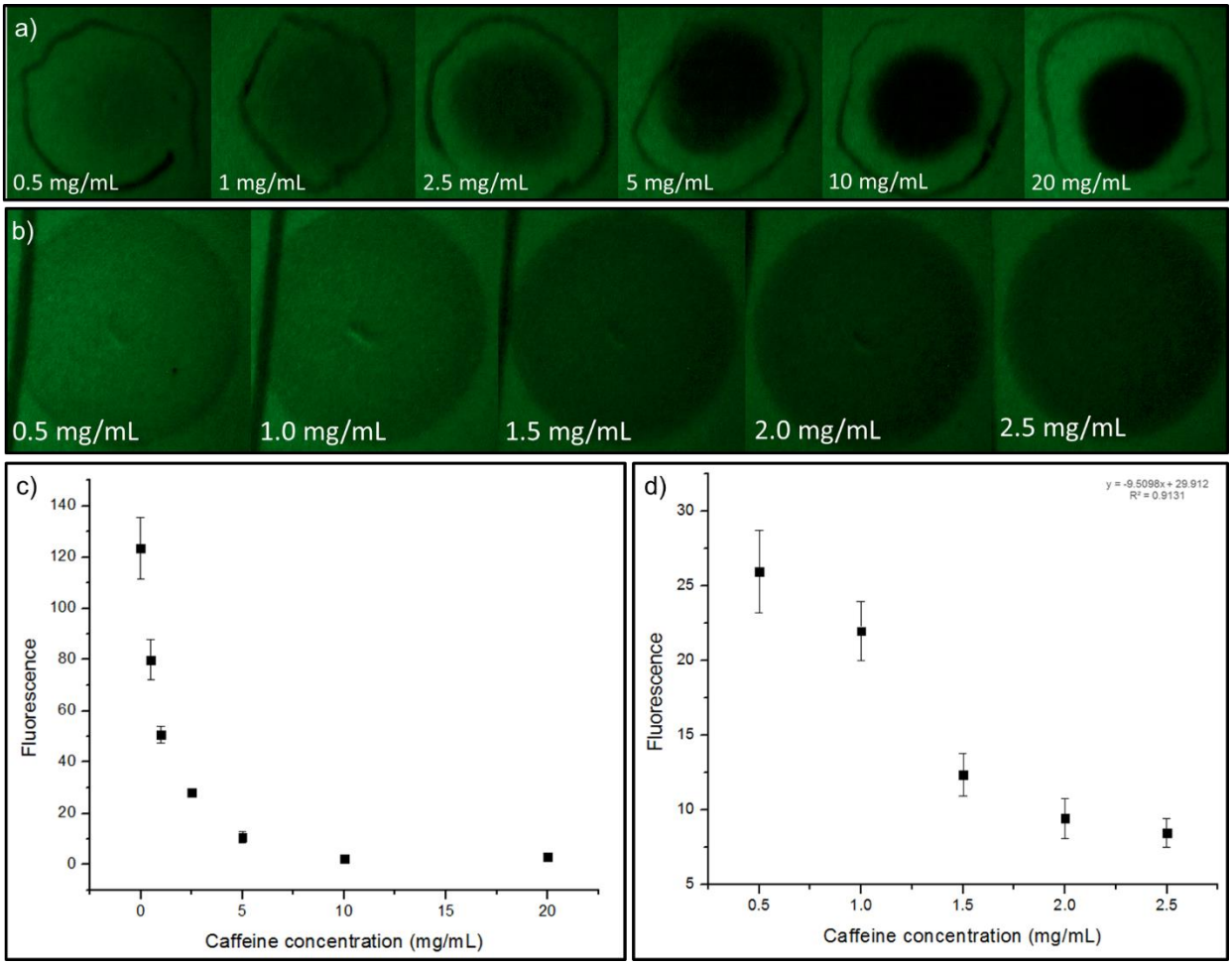

Figure 3-4. *Caffeine concentration optimization.* a) Initial wide concentration range; b) narrower linear concentration range; c) wide-range calibration curve; d) narrowed calibration curve.

relatively polar, as the less polar solvents like hexane did not achieve analyte migration (figure 3-5). Of all solvent systems tested, the best separations came from mixtures of ethanol and water. Various ratios were tested to find the combination which effected the best separation of solution components, which was identified as 1:2 EtOH:water, the developer included in the lab procedure. Many conditions included a considerable amount of quenching at the solvent front, as shown in figure 3-5. This could be evidence of analyte concentrated there, or may be contaminants from the old plates being used, which were yellow-tinted and later discovered to be a mixture of polyamide- and silica-coated plates. Once new silica plates were used, this was no longer an issue. In even the best conditions, acetylsalicylic acid was difficult to resolve from either the other components or the solvent front, so it was replaced with acetaminophen for better component resolution.

Image processing. Grayscale and color images did not give significantly different results in terms of sensitivity or calibration linearity, so grayscale was chosen for simplification. Rolling ball background subtraction improved uniformity across the plate. As shown in figure 3-4, fluorescence intensity of the plate decreases with increasing analyte concentration, which is expected with indirect detection. However, plotting the profile of a line through dark spots on a light background produces a chromatogram with negative peaks. For this reason, images were inverted to minimize confusion and help students visually equate quantitative TLC separations with more familiar HPLC separations. Among the methods of quantitation, mean spot intensity consistently provided the greatest calibration sensitivity for all analytes; it also offered the most accurate calibration linearity for acetaminophen. The maximum spot intensity method was the most linear for chloroquine. The subjectivity introduced by manually measuring peak height made it the least appropriate method for undergraduate students, and was also the most labor-intensive. For these reasons, mean intensity was chosen as students' quantitation method.

3.3.2 Prelab procedure

The purpose of the prelab was to save students time since only two hours were allotted to complete the entire procedure, but only two out of four groups completed it before

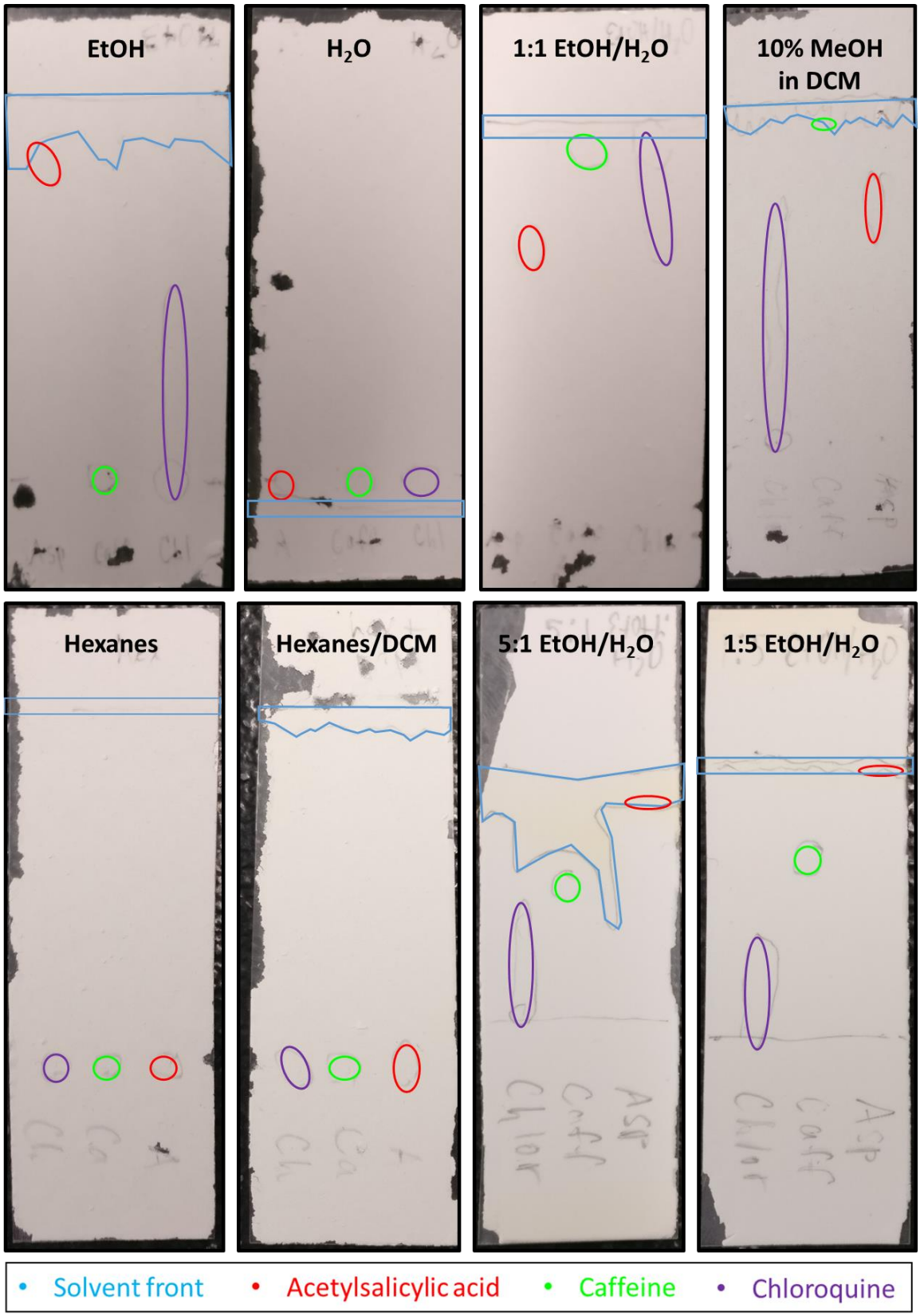

Figure 3-5. *Separation conditions.* Solvent systems labeled in black at the top of each plate, and solvent front and spots colored as shown in key.

coming to lab. One group did not print the prelab or lab procedure, and had to be reminded how to dilute solutions before completing the prelab. The teaching assistant who graded lab reports did not penalize the groups with incomplete prelabs, but we viewed the prelab as essential for lab success and therefore recommend that it is included as part of the students' assessment. This is often the case with general chemistry labs, and in our experience very few students fail to complete graded prelabs.

3.3.3 Lab procedure

Of the four groups to participate in the lab, only one finished within two hours, and they had completed the prelab. Two of the other groups finished within two and a half hours, and the last group left during plate development and returned for a final time of three and a half hours. Students asked very few questions during the lab, and most concerned the prelab calculations. There was also some confusion about the developer being a different ratio of EtOH:water than the solutions were made in, which could be avoided by including a specific procedural step to make that solution. Although it is clearly stated and illustrated in the lab procedure not to do so, some groups also submerged the origins of their plates in the developing chamber. Some students stopped their development prematurely due to time pressures, and some did not allow their plates to dry completely before imaging. The teaching assistant for the class awarded an 85, a 90, and two 95s on lab reports, and admitted to being generous as it was a new experience; the results from one of the reports that received a 95 will be discussed below. All solutions were prepared, spotted, and developed and the resulting images processed and analyzed following the procedure; these are referred to below as sample results.

Sample results for plate 1 are shown in figure 3-6a and b, and samples results for plate 2 are shown in figure 3-2 of the lab procedure. The student lab report only included plate images before processing (figure 3-6c and d), so it is unclear if images were processed correctly. Captured images are also flipped from the actual orientation of the plate, so if students do not label their spots, all their results may be reversed. Although nitrogen gas was used to speed plate drying, the student plates below still appear wet around the edges. The sample chromatogram in figure 3-3 of the procedure had a

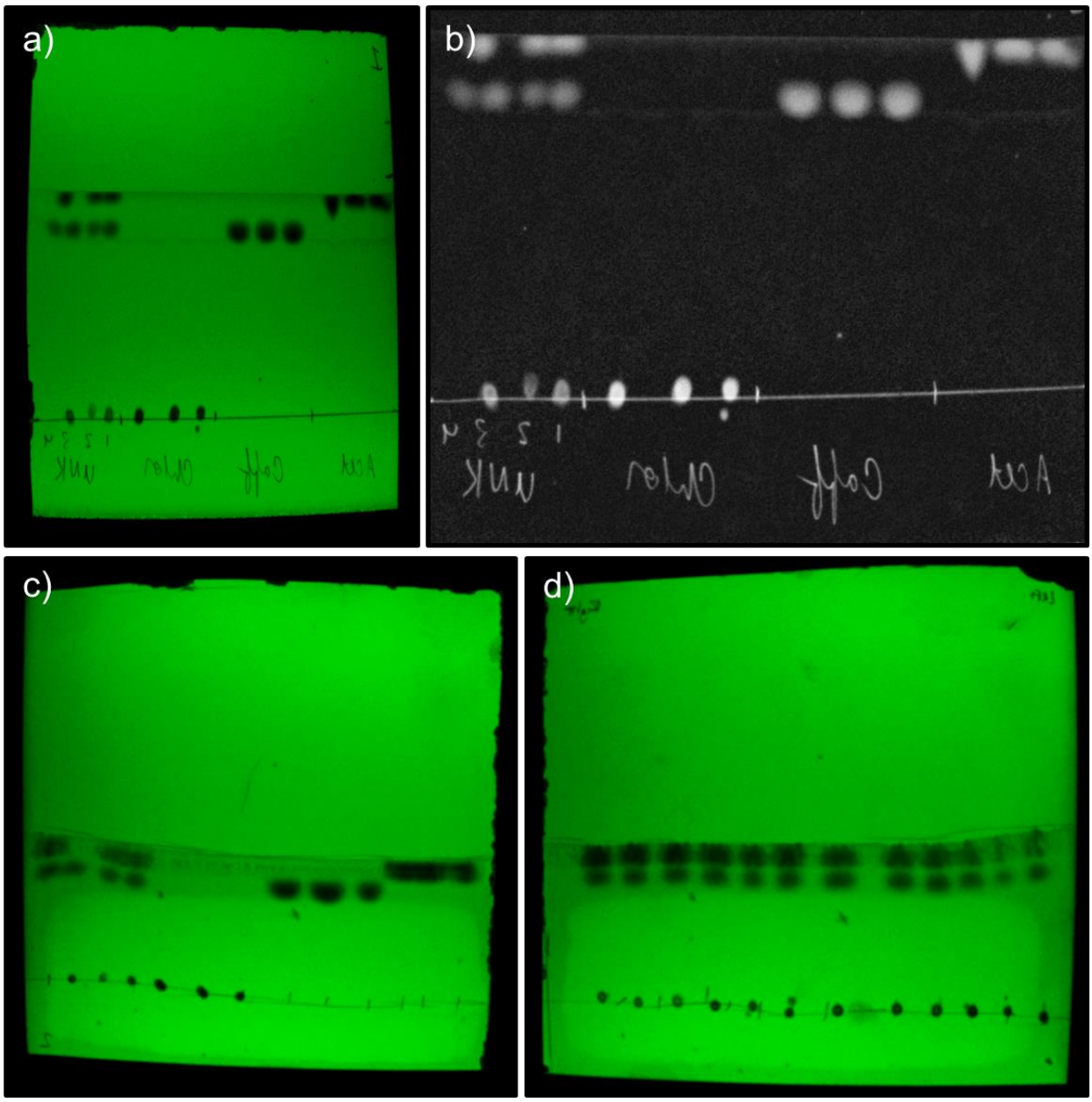

Figure 3-6. *TLC plate images.* a) Sample image of plate 1 before processing; b) sample image of plate 1 after processing; c) student image of plate 1; d) student image of plate 2.

calculated resolution between caffeine and chloroquine spots of 8.84. The student lab report did not include a chromatogram, but had an average resolution of 5.57. It is clear from the plate images that less development time contributed to this lower resolution. Student and sample retention factors agreed quite well (figure 3-7), but the students misidentified the TLC mode used here and thus reversed the identification of compound polarities in their report. The calibration curves were also surprisingly problematic for students. Figure 3-8 shows sample plots, student plots, and plots made from provided student data, and the latter two are quite different. The students set the intercept to zero, and the error bars are not the standard deviation of the measurement, both of which contributed to poor linearity. The procedure does not instruct students to set the intercept to zero, but this illustrated a need to amend it to instruct students not to do so. It does already specify that the error bars should correspond to standard deviation.

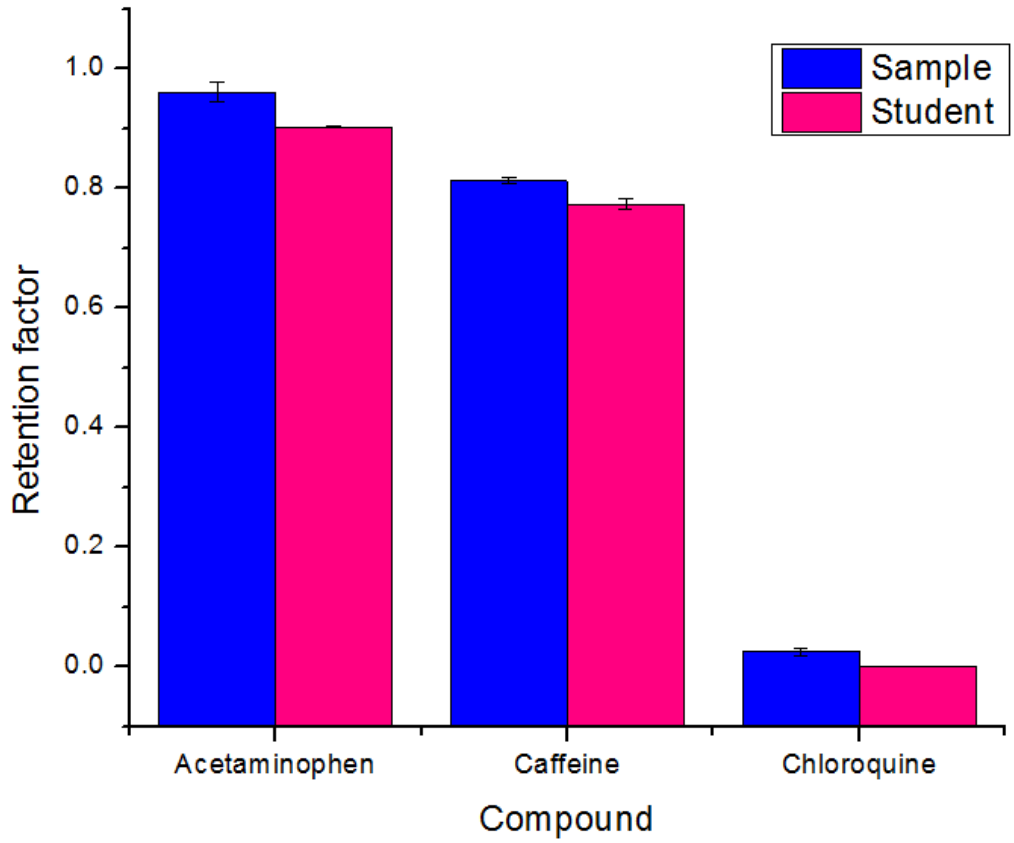

Figure 3-7. *Retention factors.* Sample retention factors compared to student results.

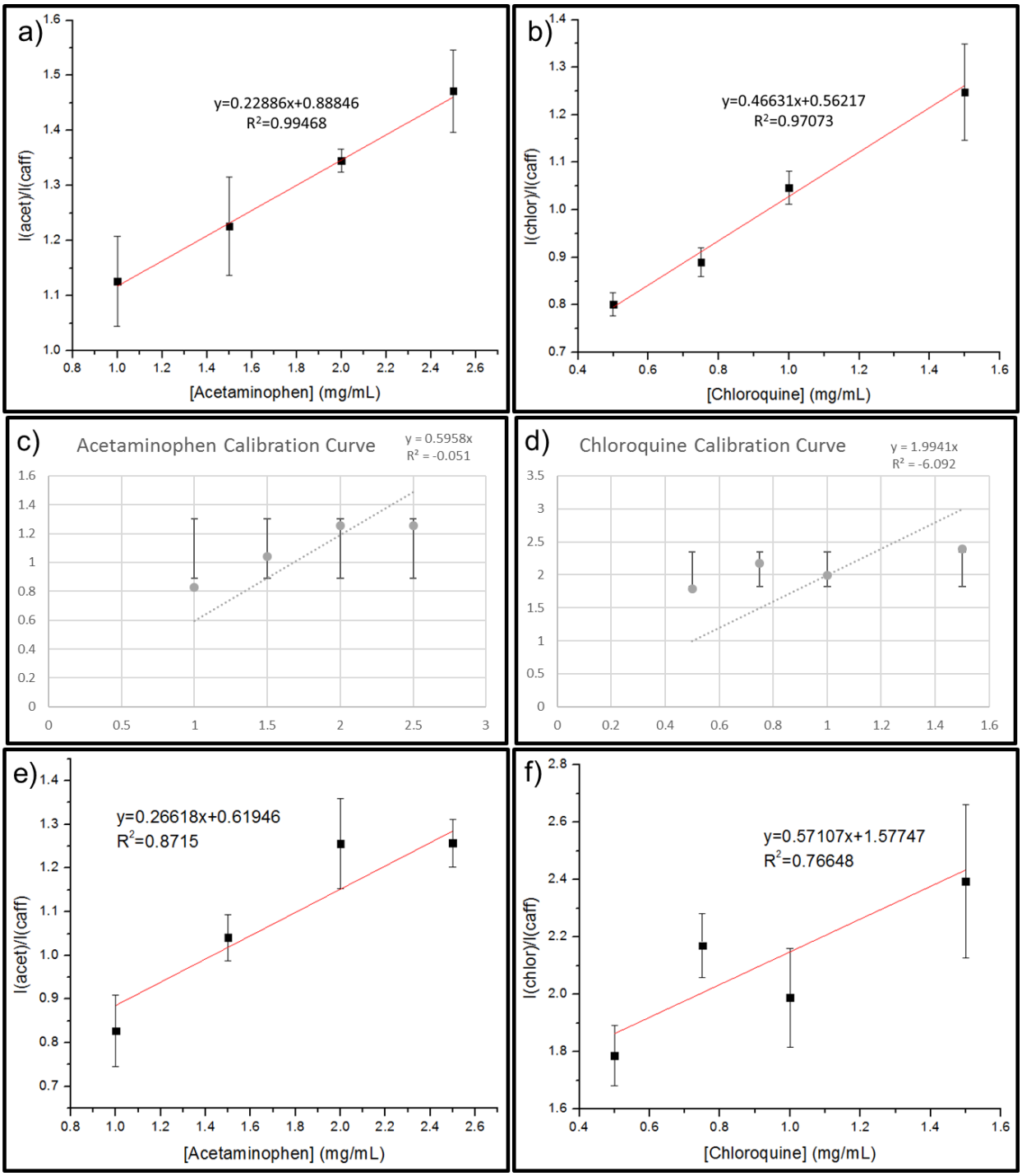

Figure 3-8. *Acetaminophen and chloroquine calibration curves.* a), b) Sample plots; c), d) calibration curves turned in by students; e), f) plots constructed from student data.

Figure 3-9 shows sample chromatograms for the unknowns. Unknown 1 is a therapeutic dose of chloroquine with a small amount of acetaminophen; unknown 2 is counterfeit with a small amount of chloroquine and more acetaminophen; unknown 3 is therapeutic with only chloroquine; and unknown 4 is counterfeit with only acetaminophen. The sample calibration curves were used to successfully classify all four unknowns as therapeutic or counterfeit based on both chloroquine concentration and [acetaminophen]/[chloroquine] (table 3-4). The students were correct for three of four unknowns, but misidentified unknown 2 as therapeutic based on chloroquine concentration. They did not list the concentration of each component in each mixture, but instead gave a range of 0-3.6 mg mL^{-1} for chloroquine concentrations in the unknowns and 0.23-0.5 mg mL^{-1} for acetaminophen concentrations, although unknown 3 contained no acetaminophen. Student error was due at least in part to incorrect calibration curves, but there are other possibilities as well. If students take measurements for acetaminophen in unknown 3 and chloroquine in unknown 4, they will most likely calculate negative concentration values as there are no spots for those components. Their [acetaminophen]/[chloroquine] ratio would then be negative, which they could misinterpret. If they instead consider those concentrations to be zero, their concentration ratio for unknown 4 would technically be divided by zero, which may also confuse them. Overall, student accuracy was good considering the other issues they experienced.

Table 3-4. *Unknown drug determination.* Actual and experimentally determined values for acetaminophen and chloroquine concentrations (in mg/mL), concentration ratios, and therapeutic/counterfeit determination of unknown drug samples.

UNK	[Acetaminophen]		[Chloroquine]		[Acet]/[Chlor]		Therapeutic/counterfeit?		
	Actual	Sample	Actual	Sample	Actual	Sample	Actual	Sample	Student
1	1.5	2.3	1.0	1.5	1.5	1.6	T	T	T
2	1.5	3.4	0.5	0.9	3.0	3.8	C	C	T
3	0.0	---	1.0	1.6	0.0	0.0	T	T	T
4	2.0	4.9	0.0	---	>3	>3	C	C	C

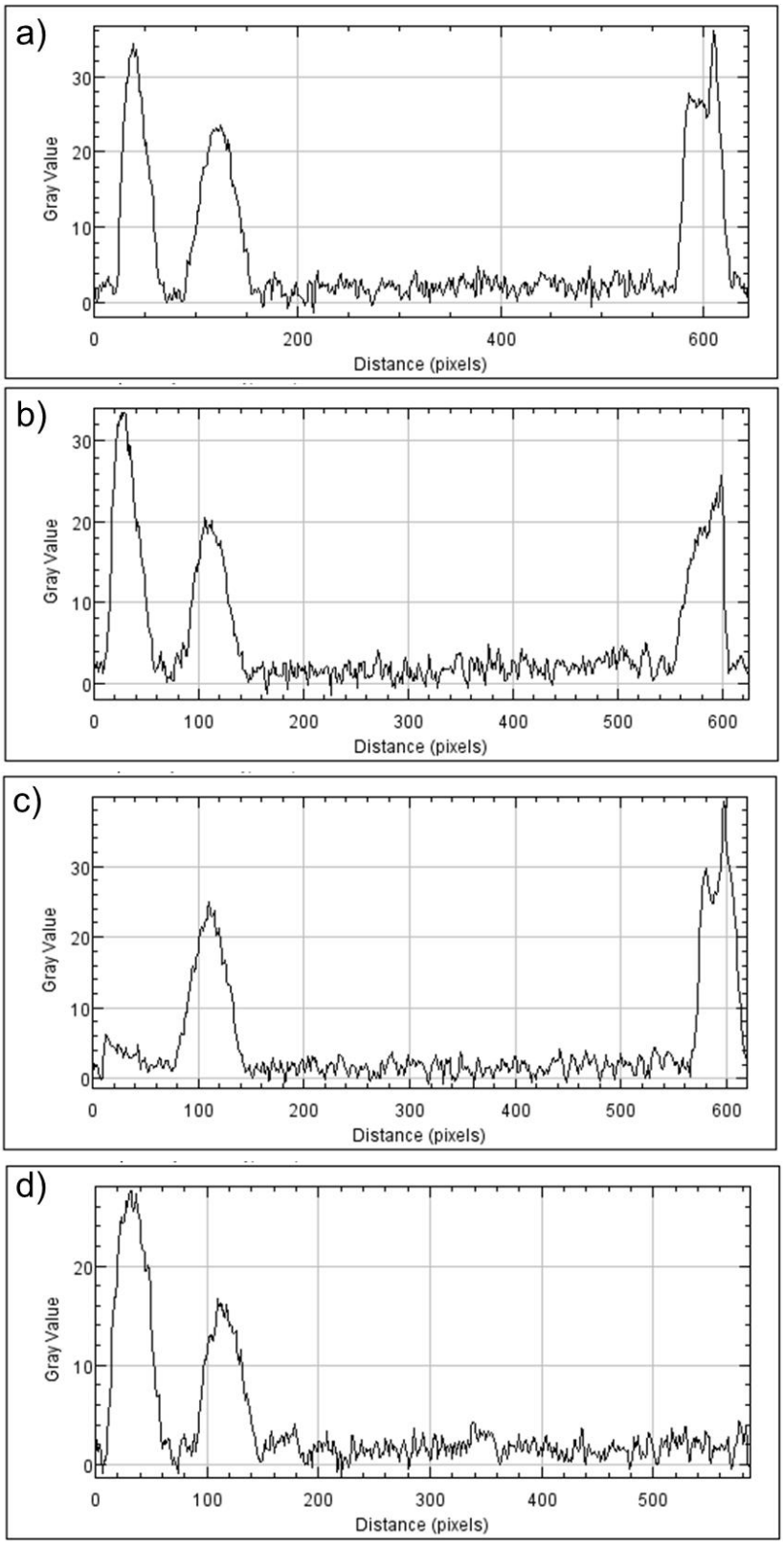

Figure 3-9. *Sample unknown drug chromatograms.* Peaks, left to right, correspond to acetaminophen, caffeine, and chloroquine. Images a-d are chromatograms for unknowns 1-4, respectively.

3.4 Conclusions

The simple, fast, inexpensive, and quantitative DE-TLC procedure developed here enabled us to successfully separate the components of and correctly identify four unknown drug samples as therapeutic or counterfeit. Teaching the inaugural lab was very informative about sources of student confusion and errors that can be amended. A three-hour period would have helped students, as here the biggest issue was time. When every step had to be completed within two hours, plate development and drying time and thus student results suffered. One way to help this could be providing an external source of motivation to ensure the prelab calculations are completed ahead of time. Stock solutions of chloroquine, acetaminophen, and caffeine could also be made by lab personnel ahead of time to shorten the process. Some additional experimental steps should be specified, like making the mobile phase when other solutions are prepared. Some important details students missed should also be emphasized more, including labeling the spots on their plate and being sure not to submerge the origins of their plates. Data analysis seems to have even more room for error, but without watching students step-by-step, it is difficult to identify all possible missteps. The method performed well, and with a few adjustments the procedure can improve an already successful experiment for future classes.

CHAPTER 4. DEVELOPMENT OF LOW-COST QUANTITATIVE TLC DETECTION FOR AMINO ACID ANALYSIS

4.1 Introduction

TLC has been used quantitatively with a variety of detection modes, which could be useful in expanding the previously developed quantitative TLC method for future pedagogical applications. Colorimetric detection, where the color of a spot is directly proportional to the amount of analyte present, can be used for naturally colored compounds or colorless compounds dipped in or sprayed with chromogenic stains. Some stains, like permanganate, cerium molybdate, and phosphomolybdic acid, are advantageous in being able to detect almost any analyte. These universal stains also have some disadvantages, such as often requiring strong heating which can evaporate volatile analytes and discolor TLC plates. Some of these stains are also expensive, and many change the background color of the plate itself (1). Other stains are specific for a functional group of interest; ninhydrin, a sensitive stain frequently used to label amine groups like those in amino acids, only requires gentle warming and exhibits little to no background labeling. Ninhydrin-labeled spots are various shades of purple-blue, except for secondary amino acids like proline which turn a yellow color and so are less sensitively detected (2,3). Fluorometric detection, useful for fluorescent or fluorescently-labeled compounds, is another option that is usually more sensitive but also higher in cost (4). Fluorescamine is a fluorogenic stain that has been shown as a more sensitive method for amino acid detection, but must be viewed quickly as signal decays over time (5,6). Some compounds can also be detected without labeling via indirect fluorescence. When spotted on a plate coated in fluorescent indicator, analytes absorb incident UV light to lessen the plate's fluorescence in that spot proportional to the amount present (1).

In this study, three different detection modes will be explored for the quantitative detection of amino acids via DE-TLC: colorimetric detection with ninhydrin labeling, fluorometric detection with fluorescamine labeling, and indirect fluorescence detection with no labeling. The twenty standard amino acids will be detected in all three modes with regular TLC equipment and digital photography to find optimal conditions for

quantitation. A novel aspect of this work is that images are captured with a cellphone rather than a digital camera. This reduces experimental costs by eliminating the need to purchase a camera, which is especially useful for potential pedagogical applications. Recent data shows that 95% of American teens thirteen to seventeen years old and 94% of eighteen to twenty-nine-year-olds have a smartphone, which makes it likely that at least one member per group in a high school or college science class would have a camera suitable for this experiment (7,8). Furthermore, many current cell phone cameras are higher resolution than digital cameras within budget. The inexpensive digital camera used for the undergraduate experiment described in chapter 3 had a 10-megapixel sensor, while many manufacturers no longer sell smartphones with less than 12-megapixel cameras, and the cellphone camera used here was 16 megapixels (9,10). An added benefit to using a cellphone is complete portability. Here, the camera was operated with a manual camera application, Camera FV-5 Lite, while the previously used digital camera required a computer connection to be software-controlled (11). The main camera setting that was varied here was ISO speed, a measure of a camera's sensitivity to light. Sensitivity increases with increasing ISO, but image quality is generally reduced due to noise at higher ISO (12). Light sources were also varied here in light color and intensity. Fluorogenic and indirect fluorescence detection are limited to the use of 385- and 254-nm light, respectively, but the subtle variations in spot color of ninhydrin-labeled amino acids motivated the investigation of light sources other than the typical white. Detection mode, illumination, imaging, and processing conditions were investigated to identify the most sensitive quantitation method for all twenty amino acids.

4.2 Materials & methods

4.2.1 General

L-alanine (99%), D-L-cysteine (99%), L-(+)-aspartic acid (98+%), L-(+)-glutamic acid (99%), L-phenylalanine (98.5+%), glycine, L-histidine (98%), L-isoleucine (99%), 😟+)-lysine monohydrate (99%), D-L-leucine (99+%), L-methionine (98+%), D-L-asparagine monohydrate (98%), L-proline, L-(+)-glutamine (99%), L-(+)-arginine hydrochloride (98+%), L-serine (99%), L-threonine (98%), L-valine (99%), L-(-)-tryptophan (99%), and

L-tyrosine disodium salt (98%), fluorescamine (pure), acetone (ACS grade), glacial acetic acid, absolute ethanol, 1-butanol (ACS grade), and silica gel 60 F254 coated plastic-backed TLC plates were purchased from Thermo Fisher Scientific (Waltham, MA). Ninhydrin (>98%) was from Honeywell Fluka (Morris Plains, NJ). White light sources were LED-144A white bulb ring light with intensity control and 50W LED fiber optic gooseneck light microscope illuminator from AmScope (Irvine, CA). The monochromatic light source was the four-wavelength high-power LED (385/470/565/625-nm) from ThorLabs (Newton, NJ). 254-nm UV lamps were from UltraViolet-Tools (Round Rock, TX). Images were captured with a manually focused 16-megapixel cell phone camera from OnePlus (Shenzhen, China). Camera settings were controlled through the free application Camera FV-5 Lite (Stuttgart, Germany). All image processing was done with ImageJ from the National Institutes of Health (Bethesda, MA).

4.2.2 Characterization of illumination uniformity

A blank TLC plate was photographed while illuminated by white, 254-nm UV, 385-nm, 470-nm, 565-nm, or 625-nm light. Light intensity was varied for monochromatic sources, elevation was varied for UV light, and camera ISO was varied with all sources. Images were cropped, converted to 32-bit, inverted for detection modes that create dark spots on light backgrounds, and rolling ball background subtracted using ImageJ. A histogram was then constructed to find the standard deviation across the surface of the plate under each set of conditions.

4.2.3 Calibration curve development

Colorimetric detection & ninhydrin labeling. Solutions of all twenty amino acids were made from 0.1-1 mg mL^{-1} in water. A micropipette was used to spot 1 µL of each solution in triplicate on a TLC plate. Once the spots were dry, the plate was sprayed with 2 mg mL^{-1} ninhydrin in ethanol and allowed to dry before heating at 110°C until spots appeared. The plate was imaged under illumination by white and monochromatic light sources at varying intensities and ISO.

Fluorometric detection & fluorescamine labeling. Solutions of all twenty amino acids were made from 0.1-1 mg mL^{-1} in water. A micropipette was used to spot 1 µL of each solution in triplicate on a TLC plate. Once dry, the plates were sprayed with 0.05%

fluorescamine in acetone, allowed to dry, and imaged under 385-nm illumination while varying intensities and ISO.

Indirect fluorescence detection. Solutions of all twenty amino acids were made from 0.1-1 mg mL^{-1} in water. A micropipette was used to spot 1 µL of each solution in triplicate on a TLC plate. After drying, spots were imaged under 254-nm UV illumination. The process was repeated with 1.75-10 mg mL^{-1} solutions in water while elevating the UV light to various distances from the plate.

Image analysis. Images from all three detection modes were processed in the same manner as the blank plates. The elliptical selection tool was used to cover the area of each spot, and the maximum and mean intensities measured to serve as the signal for each spot. The same was done for ten blank areas on the plate with each image, and the standard deviation was found and used as the noise for each image. The signal to noise ratio (S/N) was then found for each spot, and triplicate measurements of each concentration were averaged and plotted against corresponding concentrations.

4.2.4 Detection optimization

The slope of each calibration curve was determined, and these sensitivities were used to determine the optimal conditions for each detection method. The optimal conditions for each method were then compared to determine the optimal conditions overall for each amino acid.

4.2.5 Amino acid separation

Solutions of all twenty amino acids were made at 5 mg mL^{-1} in water, as well as mixtures of three to four amino acids at 5 mg mL^{-1} each. A micropipette was used to spot 1 µL of each pure solution in triplicate on TLC plates, while mixtures were only spotted once each. The plates were developed in 3:1:1 butanol/acetic acid/water and allowed to dry. Once dry, the plates were sprayed with 2 mg mL^{-1} ninhydrin in ethanol and allowed to dry before heating at 110°C until spots appeared. Imaging under optimal conditions was followed by using ImageJ to process the images as before. The line tool was used to measure the distance from the origin to the most intense region of each spot and to the solvent front. These values were used to calculate the retention factor for each pure amino acid, and then to identify the spots in each mixture.

4.2.6 Amino acid quantitation

The same combinations of amino acids previously separated were combined from 0.1-1 mg mL^{-1} in water. A micropipette was used to spot 1 µL of each solution in triplicate on TLC plates. The plates were developed in 3:1:1 butanol/acetic acid/water and allowed to dry. Once dry, the plates were sprayed with 2 mg mL^{-1} ninhydrin in ethanol and allowed to dry before heating at 110°C until spots appeared. Imaging under optimal conditions was followed by using ImageJ to process the images as before to produce a calibration curve for each amino acid. The process was repeated for mixtures with all amino acids at 0.45 mg mL^{-1}, and the calibration curves used to quantify each.

4.3 Results & discussion

4.3.1 Characterization of illumination uniformity

As standard deviation across a plate increases, the uniformity of illumination decreases. As shown in figure 4-1, the gooseneck white light was more uniform overall than the ring white light, and so was used for further white light illumination. At any ISO 400 or above, overexposure caused both white lights to plateau at a maximum uniformity. The UV light exhibited a less clear trend with ISO at a single elevation, but uniformity appears to increase with distance from the light source. In general, the monochromatic sources' uniformity decreases with increasing ISO. Typically between 400 and 800 ISO, standard deviation plateaus at some maximum value. This suggests that at that point, camera sensitivity can be increased to improve contrast with no great loss to uniformity. White light was by far the most uniform source, followed by UV. The monochromatic sources were relatively uniform at low ISO. These results agree well with literature evaluations that cite nonuniform illumination, especially with monochromatic sources, as one of the greatest limitations of quantitative TLC (13-17).

4.3.2 Calibration curve development

Colorimetric detection & ninhydrin labeling. Some spots began to appear upon contact with ninhydrin even before applying heat, and all were visible after heating. Most spots were some shade of purple, but proline spots were much lighter and more difficult to see, as expected. As shown in figure 4-2, most spots were visible with all illumination sources. Figures 4-3 and 4-4 show calibration curves for histidine as a sample.

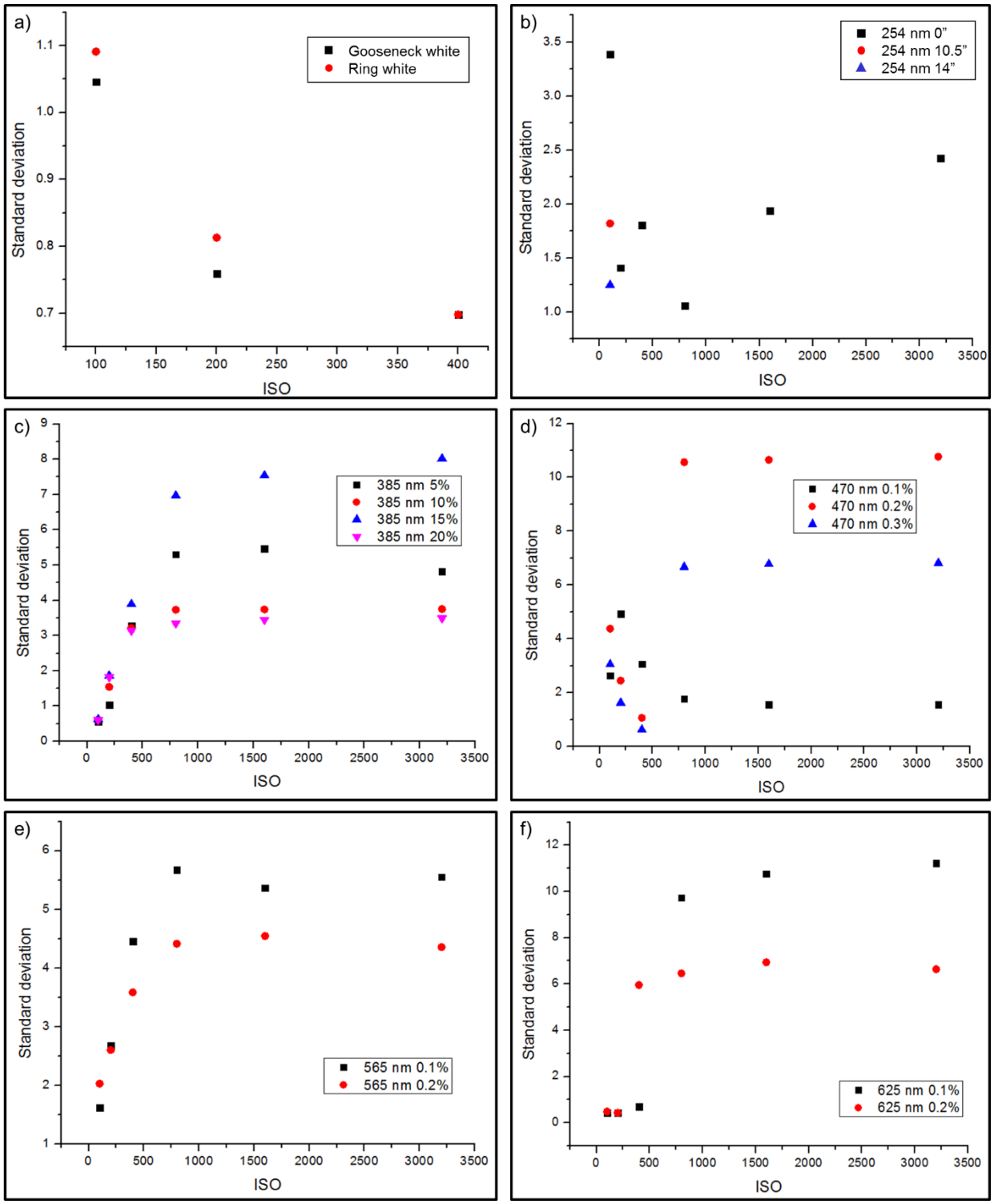

Figure 4-1. *Illumination uniformity.* Standard deviation vs. ISO for a) white lights; b) 254-nm UV lights by elevation; c) 385 nm lights by intensity; d) 470 nm light by intensity; e) 565 nm light by intensity; and f) 625 nm light by intensity.

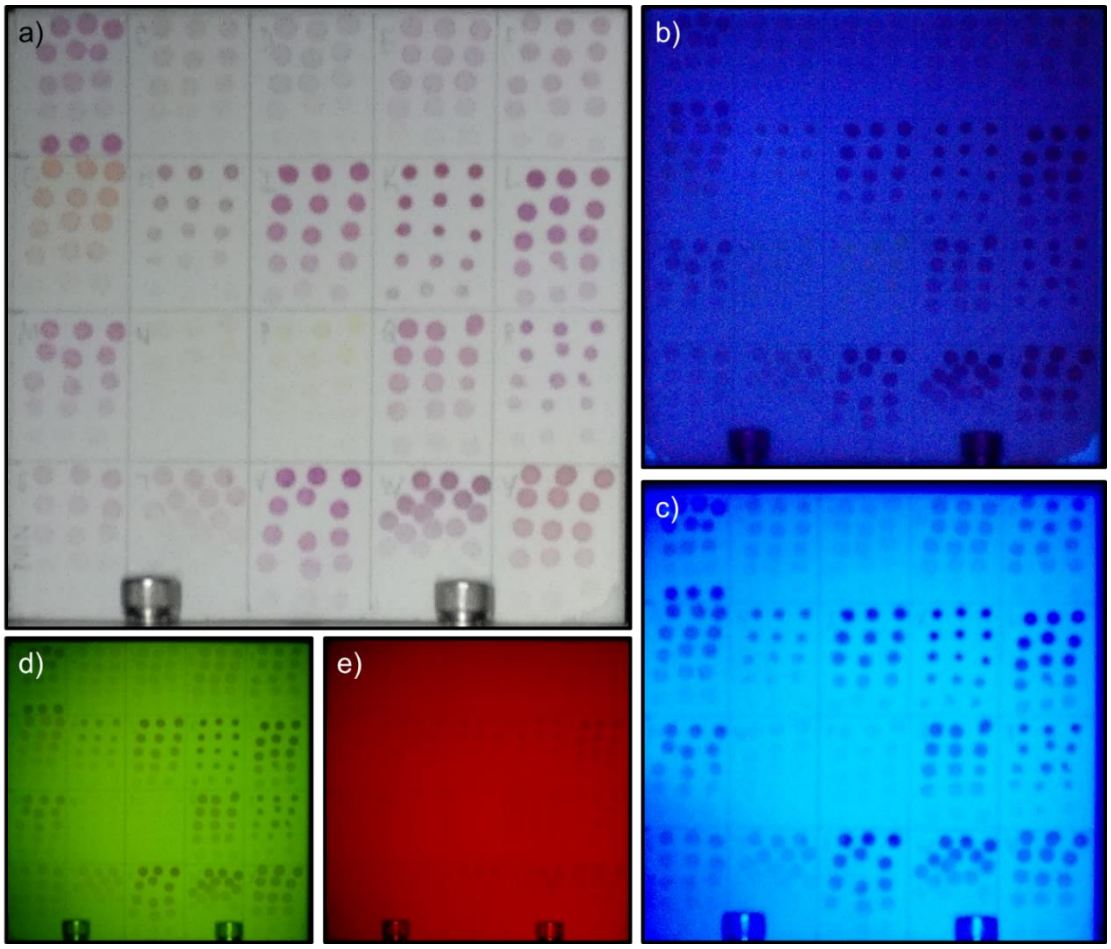

Figure 4-2. *Colorimetric amino acid detection.* Ninhydrin-labeled amino acids illuminated with a) white; b) 385-nm; c) 470-nm; d) 565-nm; and e) 625-nm light.

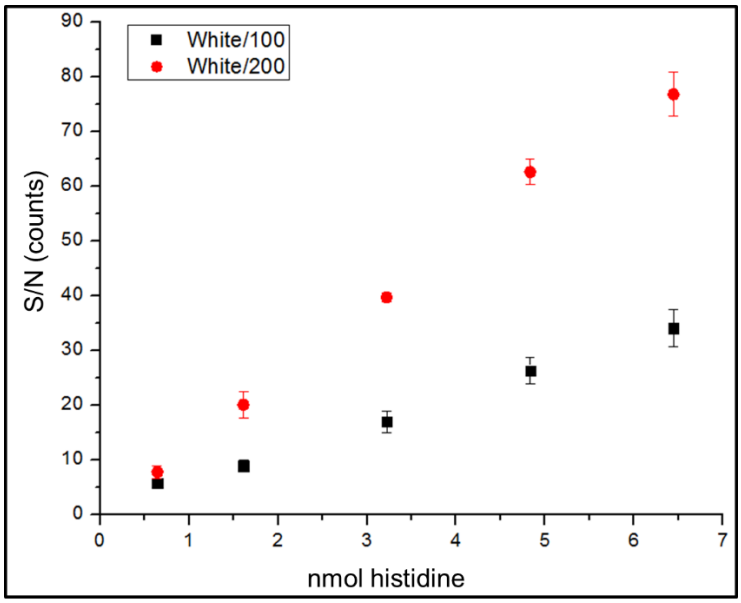

Figure 4-3. *Colorimetric calibration curves for histidine with white light.* S/N vs. nmol ninhydrin-labeled histidine with white light by ISO.

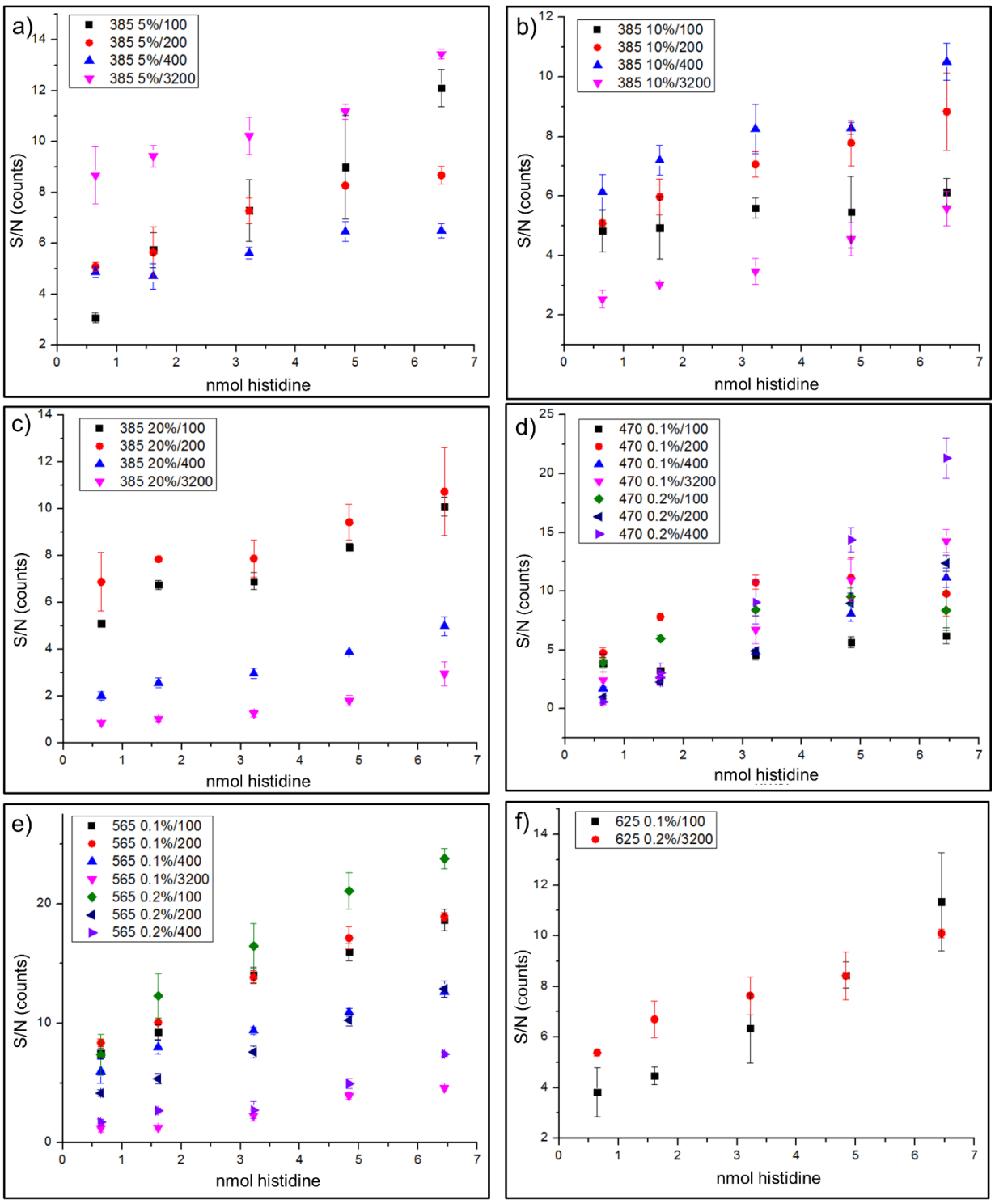

Figure 4-4. *Colorimetric calibration curves for histidine with monochromatic light.* a-f) S/N vs. nmol ninhydrin-labeled histidine. Legends show wavelength and intensity (%) of light followed by ISO.

Fluorometric detection & fluorescamine labeling. Fluorescamine-labeled amino acids were only visible under illumination with 385-nm light, as shown in figure 4-5. As with colorimetric detection, proline was not easily detected fluorometrically. While reaction with fluorescamine produces a fluorescent derivative for primary amino acids, the aminoenone produced by reaction of the secondary amino acid proline shows little to no fluorescence (18). Figure 4-6 shows calibration curves for histidine as a sample.

Indirect fluorescence detection. As shown in figure 4-7, only tryptophan was detectable at concentrations below 1 mg mL^{-1}; at concentrations up to 10 mg mL^{-1}, more amino acids were detected. Overall, indirect fluorescence was not sensitive for most amino acids, and no calibration curves for proline had positive slopes. Without elevating the UV lights, the TLC plate was overexposed at even the lowest sensitivity setting of the camera. Figure 4-8 shows calibration curves for histidine as a sample.

4.3.3 Detection optimization

Histidine is used as a sample here because it showed good linearity for all detection modes; figure 4-9 shows its colorimetric detection results, and 4-10 shows fluorometric and indirect fluorescence detection. The optimal ISO and light intensity for detection varied by illumination source, but lower ISO generally corresponded to more sensitive detection. For colorimetric detection, white light at 200 ISO was best for all twenty amino acids. For fluorometric detection, 5% 385-nm light at 100 ISO was most sensitive for eight amino acids, 10% at 100 ISO was best for five, 20% at 100 ISO was best for three, and no other condition was best for more than one amino acid. For indirect fluorescence detection, a 4" elevation of UV light at 200 ISO was most sensitive for twelve amino acids, 4" elevation at 100 ISO was best for five, and 10.5" elevation at 400 ISO was best for two. Even at higher concentrations, it performed so poorly for proline that no conditions gave a positive sensitivity. Proline was consistently difficult to detect, however, and commonly requires higher concentrations than other amino acids for sensitive detection (5).

Figure 4-11 shows the calibration curve in optimal conditions with each method for histidine as a sample, and figures 4-12 through 4-15 compare optimal conditions with each method for all amino acids. Fluorescamine was expected to be a more sensitive

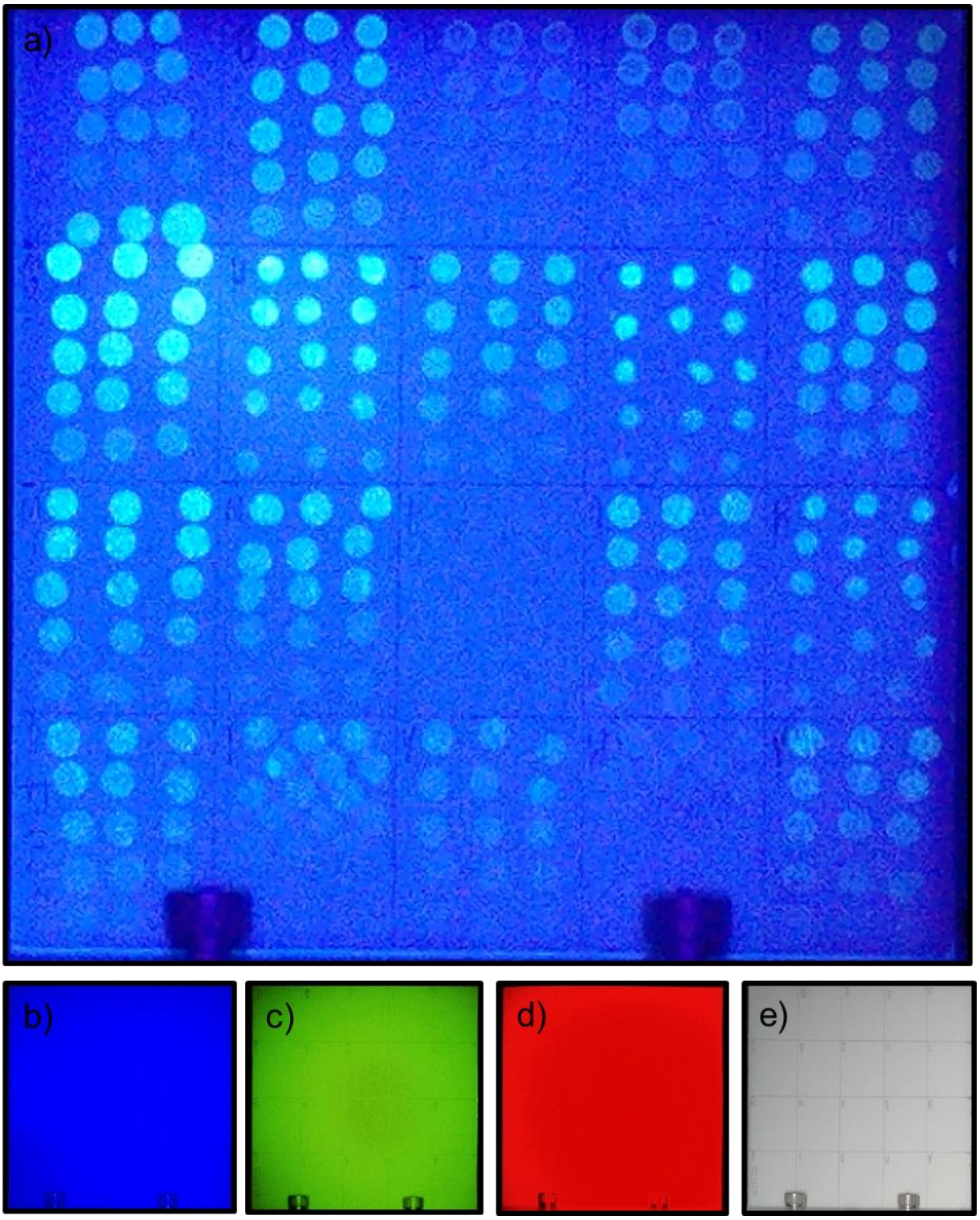

Figure 4-5. *Fluorometric amino acid detection.* Fluorescamine-labeled amino acids illuminated with a) 385-nm; b) 470-nm; c) 565-nm; d) 625-nm; and e) white light.

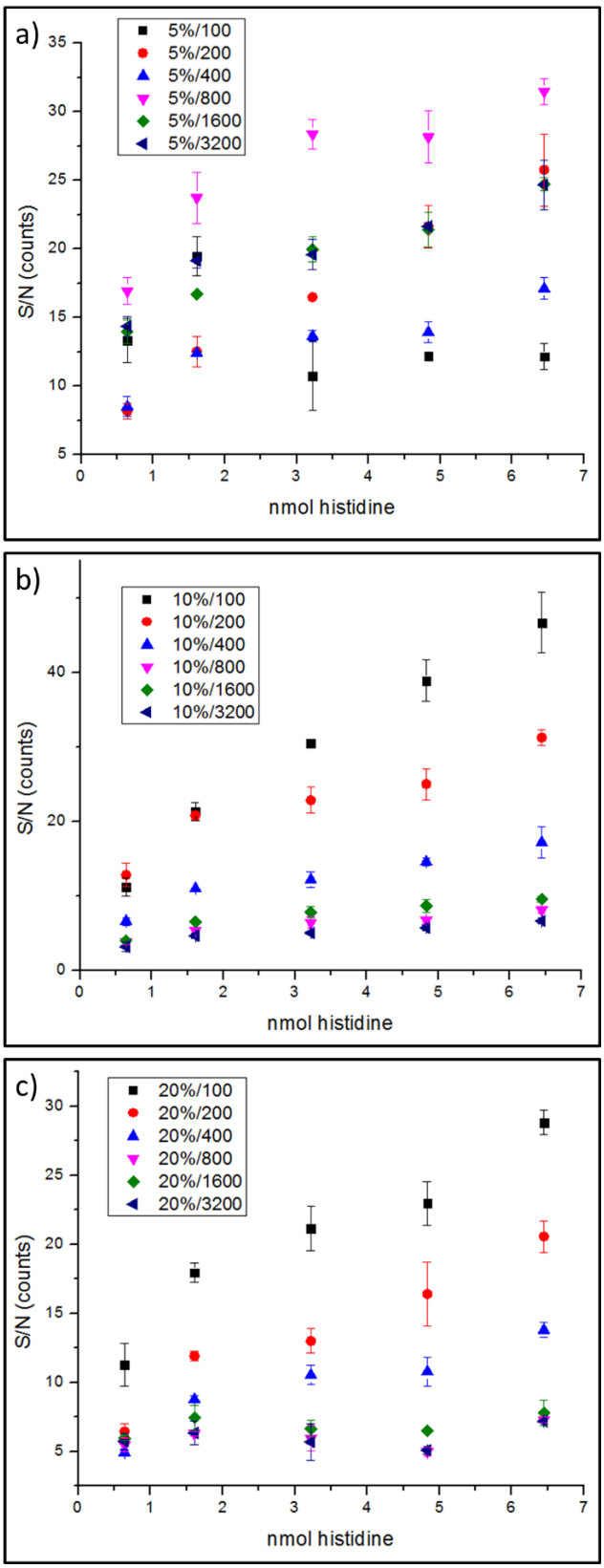

Figure 4-6. *Fluorometric calibration curves for histidine.* S/N vs. nmol fluorescamine-labeled histidine with 385-nm light. Legends show intensity (%) and ISO.

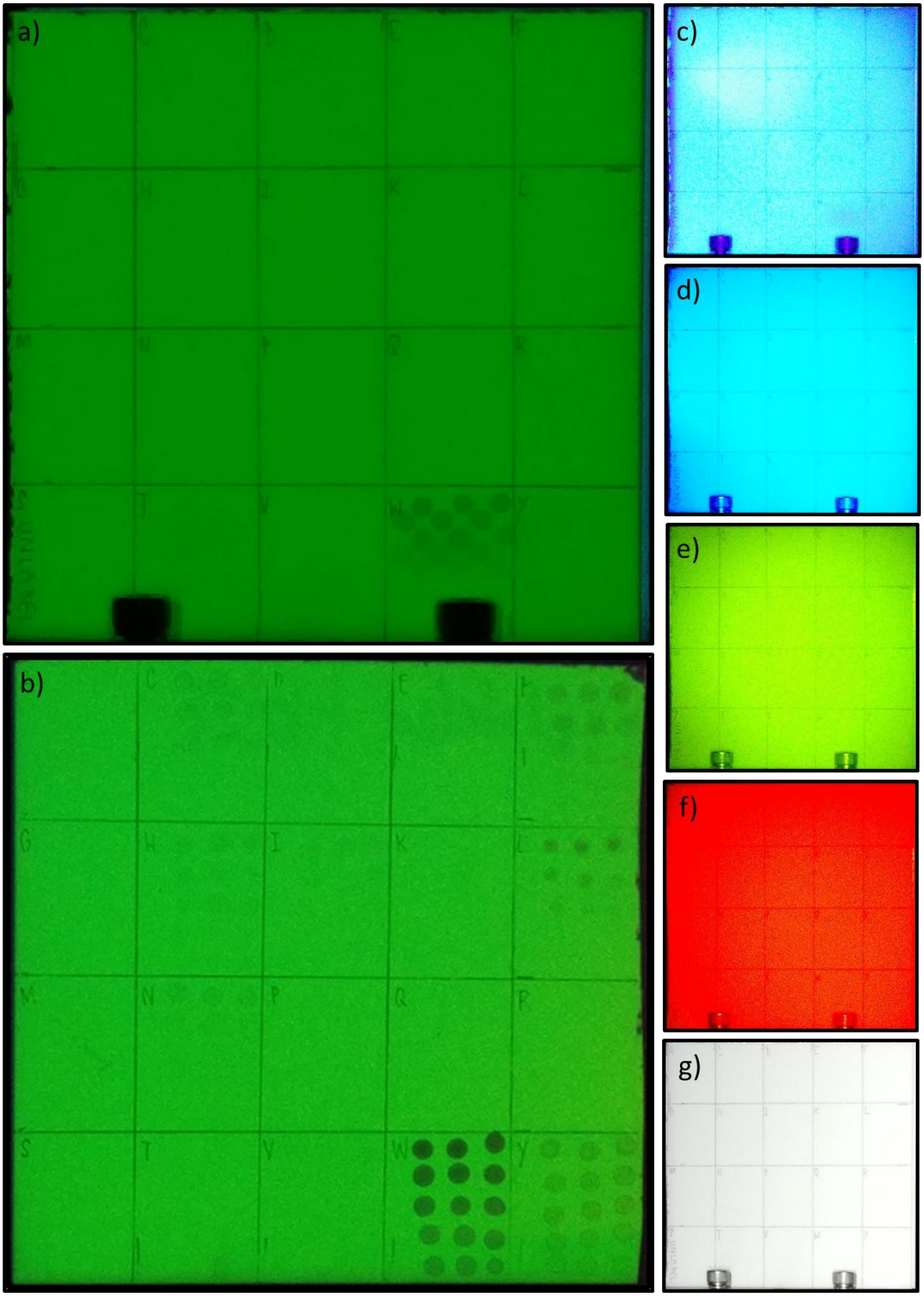

Figure 4-7. *Indirect fluorescence amino acid detection*. Illumination of unlabeled amino acids from 0.1-1 mg/mL with a) 254-nm UV; b) 385-nm; c) 470-nm; d) 565-nm; e) 625-nm; and f) white light; g) 254-nm illumination of 1.75-10 mg/mL amino acids.

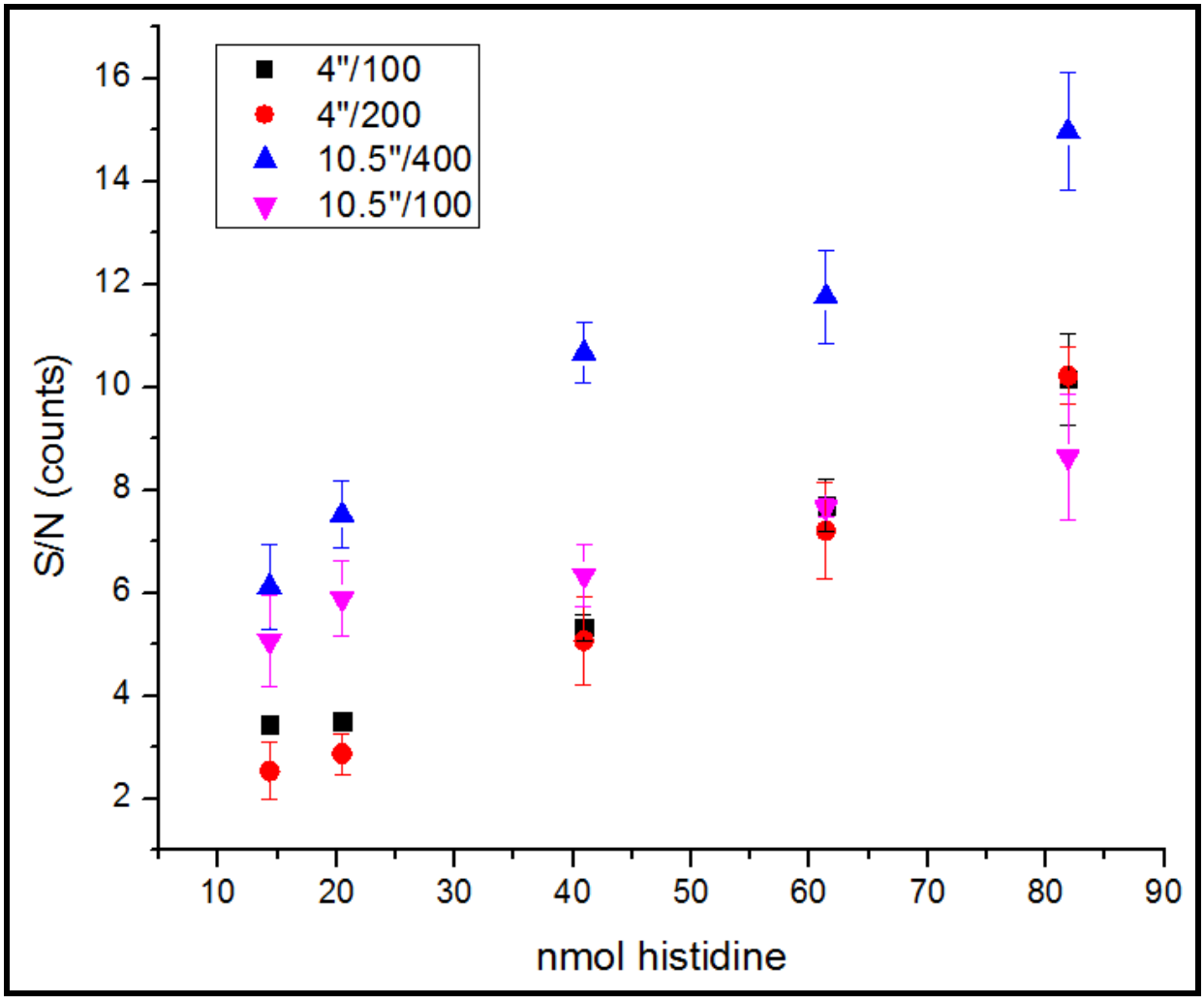

Figure 4-8. *Indirect fluorescence calibration curves for histidine.* S/N vs. nmol unlabeled histidine with 254-nm UV light. Legend shows elevation of light (inches) and ISO.

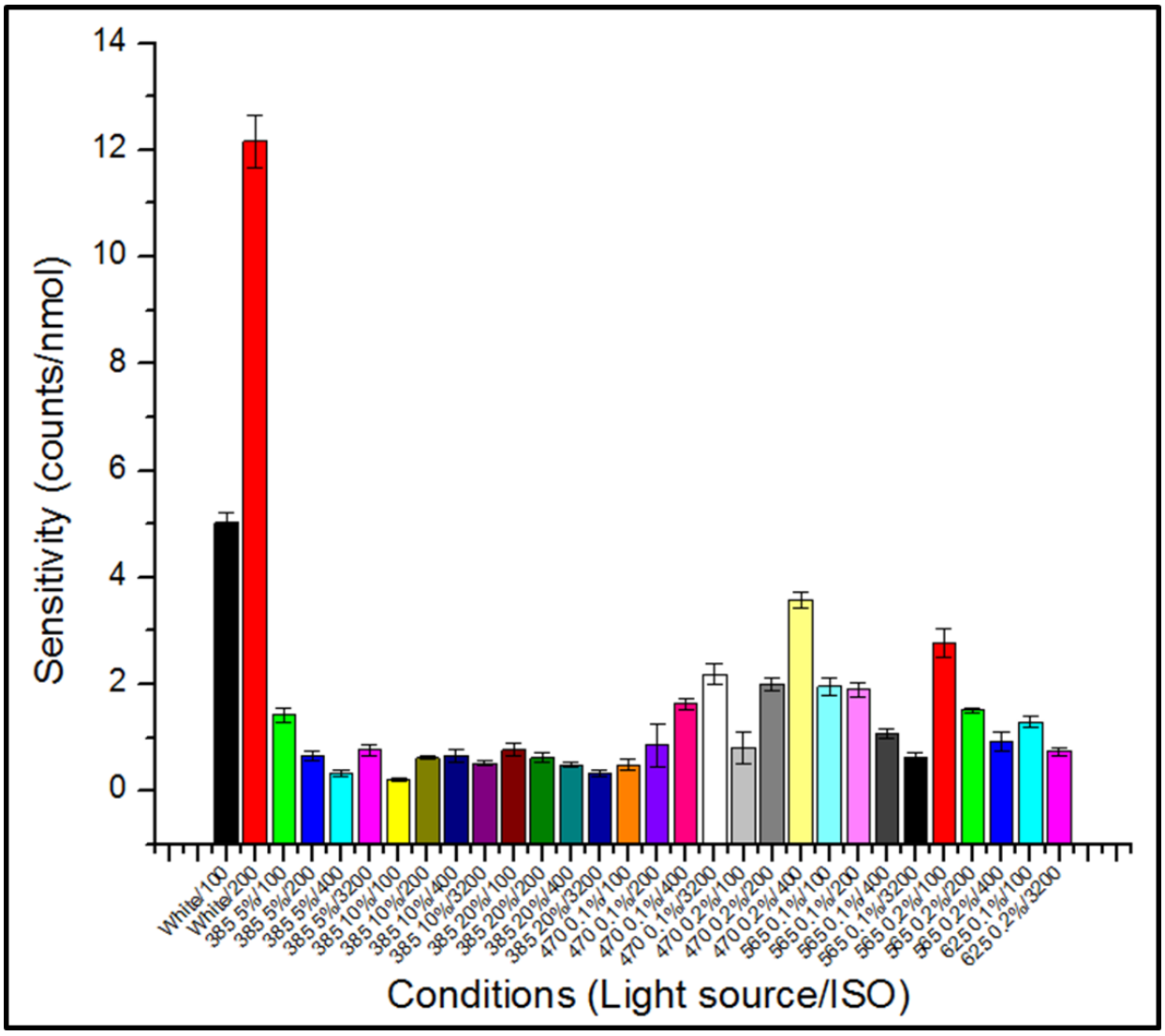

Figure 4-9. *Colorimetric detection sensitivities for histidine.* Sensitivity for all detection conditions of ninhydrin-labeled histidine.

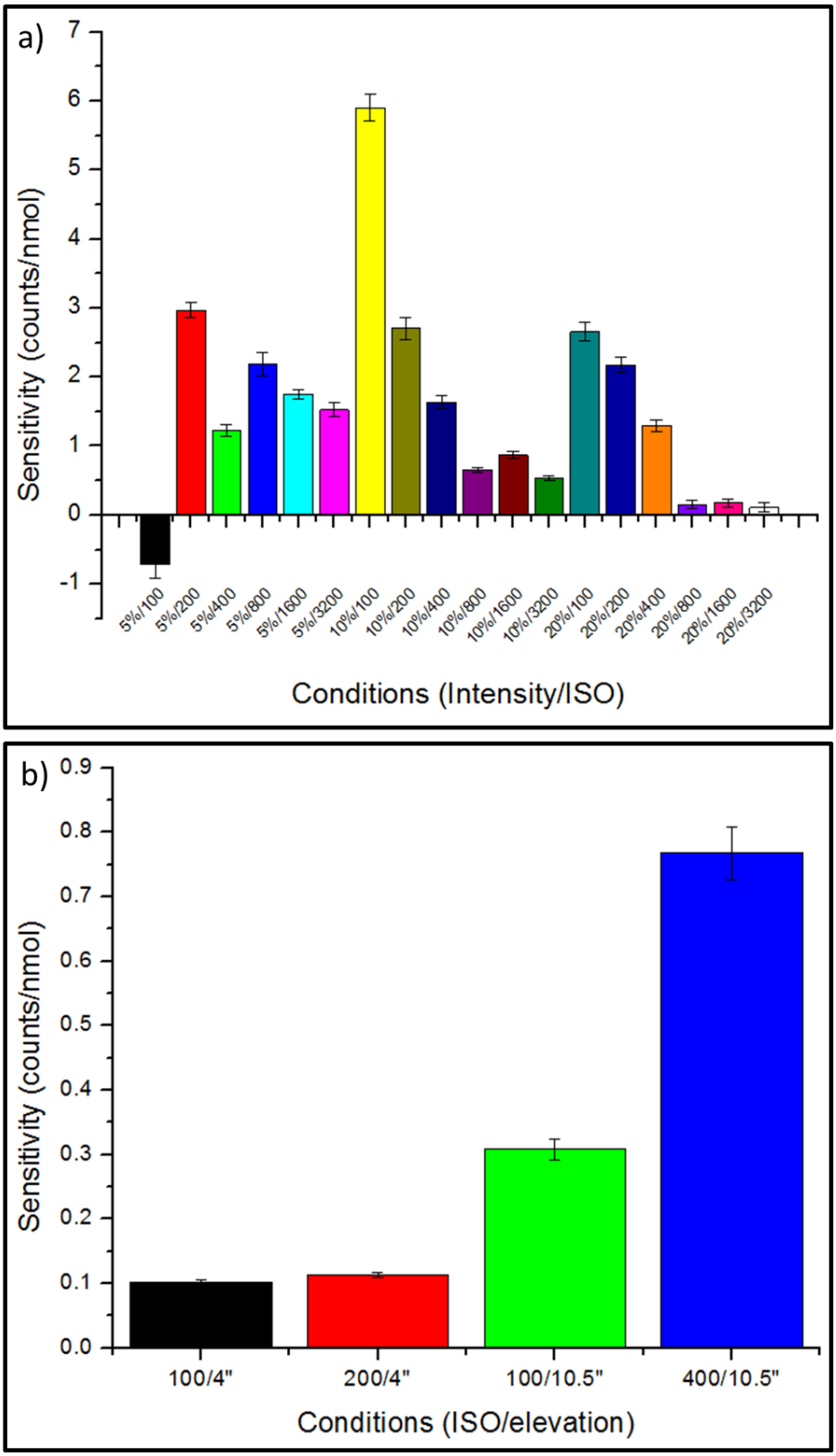

Figure 4-10. *Fluorometric and indirect fluorescence detection sensitivities for histidine.* Sensitivity for all detection conditions of a) fluorescamine-labeled histidine and b) unlabeled histidine.

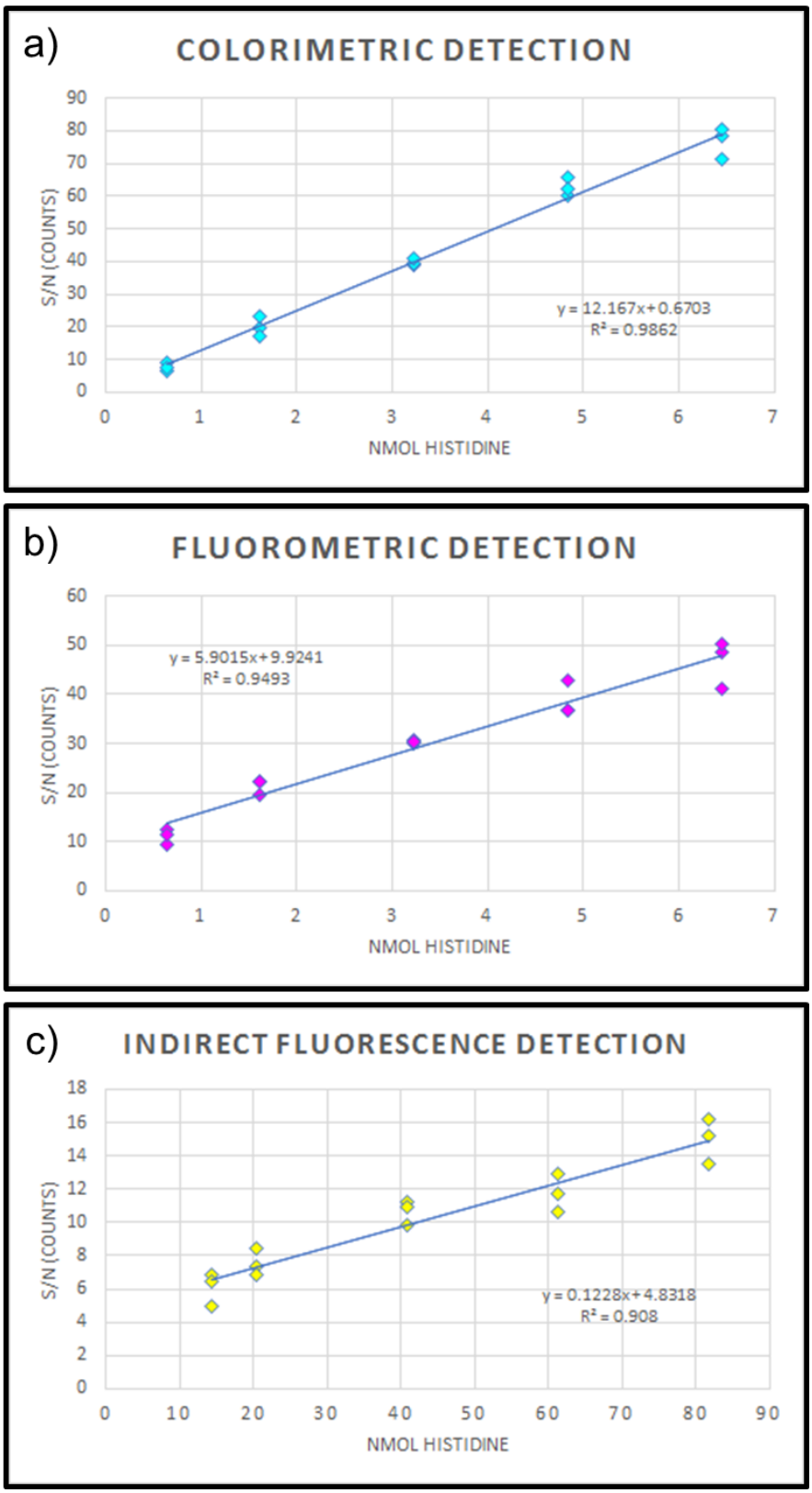

Figure 4-11. *Best calibration curves for histidine.* Calibration curves for most sensitive conditions with a) colorimetric, b) fluorometric, and c) indirect fluorescence detection of histidine.

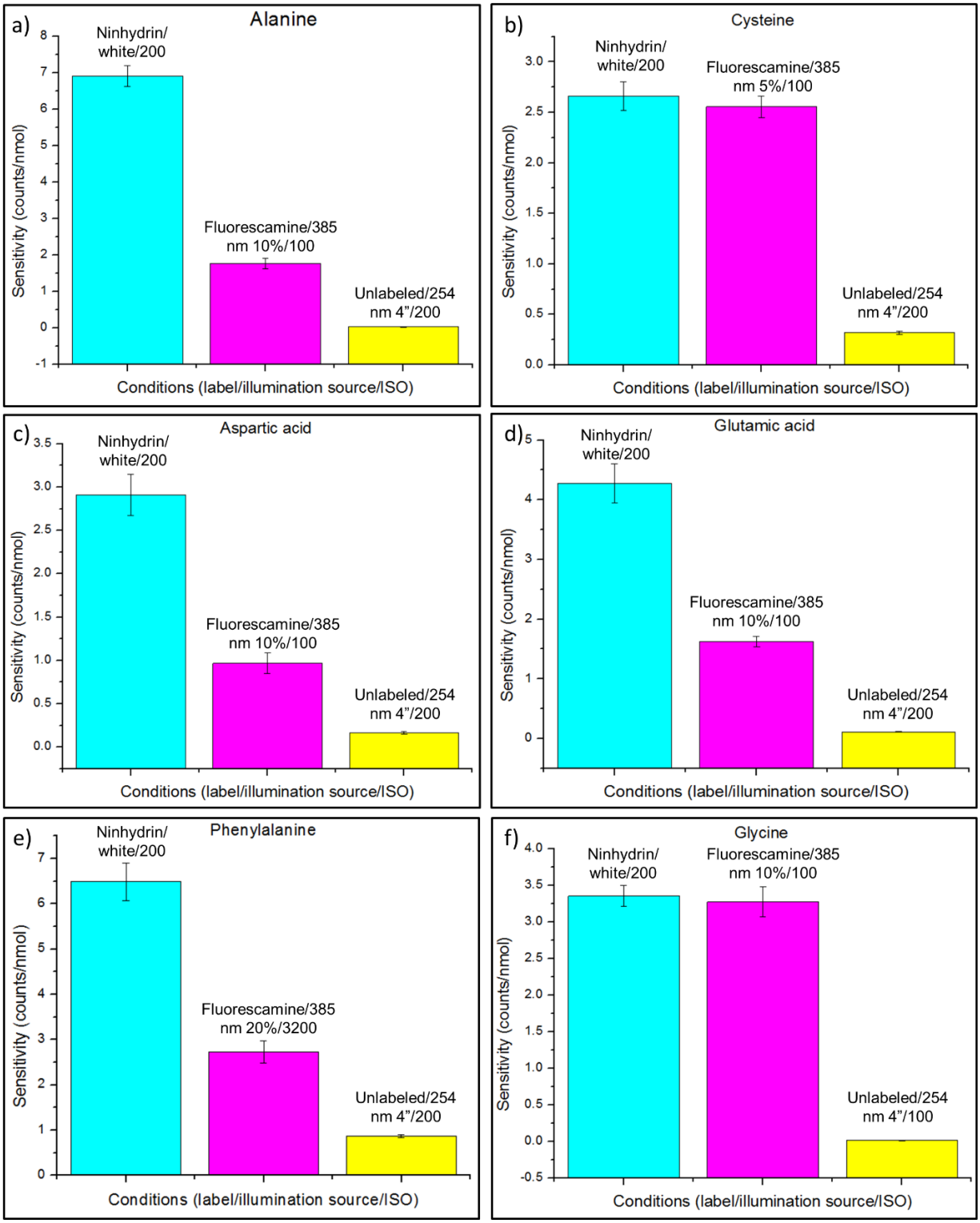

Figure 4-12. *Most sensitive conditions—alanine to glycine*. Most sensitive conditions in all detection modes for a) alanine, b) cysteine, c) aspartic acid, d) glutamic acid, e) phenylalanine, and f) glycine. Error bars represent 95% confidence interval.

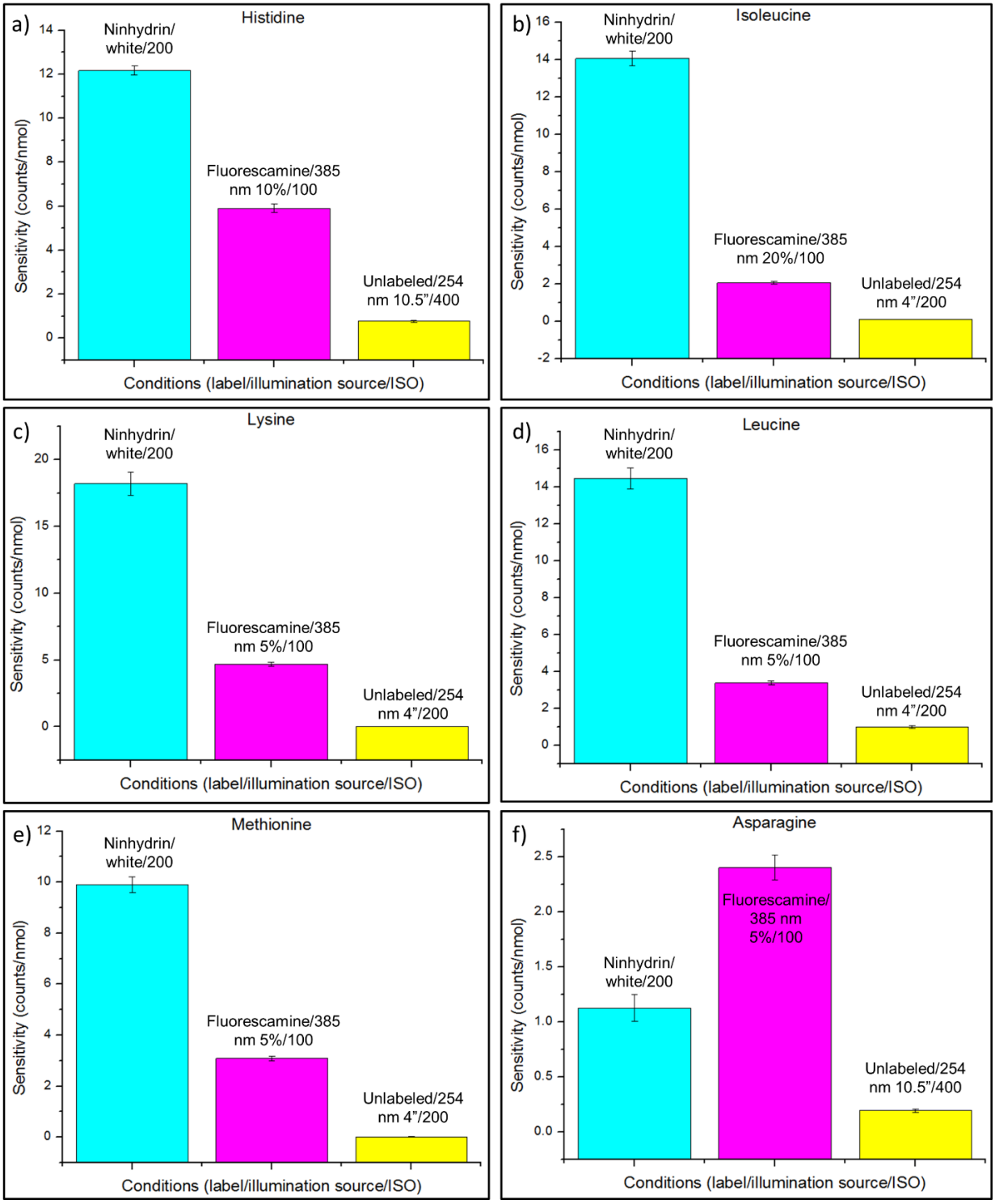

Figure 4-13. *Most sensitive conditions—histidine to asparagine.* Most sensitive conditions in all detection modes for a) histidine, b) isoleucine, c) lysine, d) leucine, e) methionine, and f) asparagine. Error bars represent 95% confidence interval.

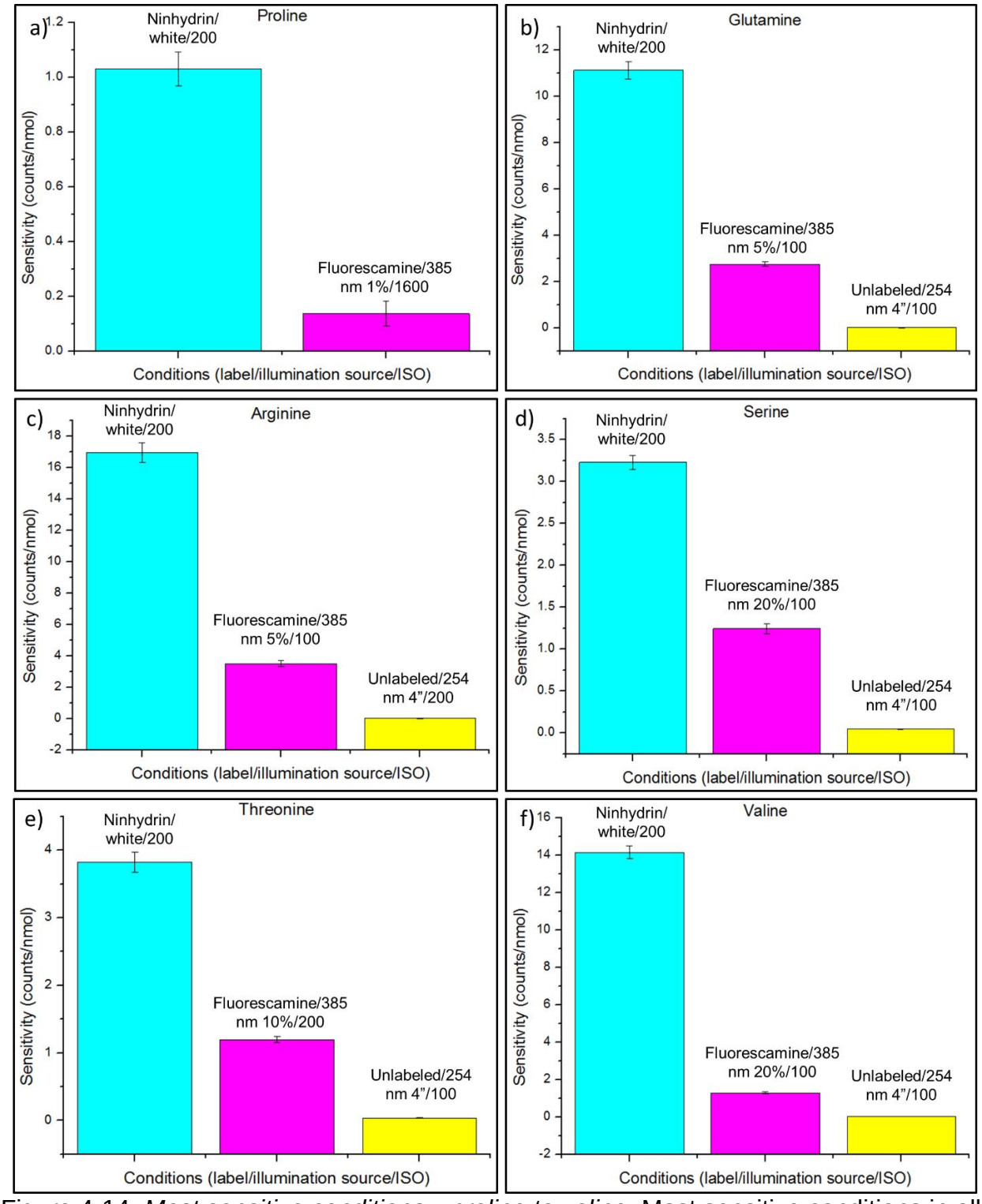

Figure 4-14. *Most sensitive conditions—proline to valine.* Most sensitive conditions in all detection modes for a) proline, b) glutamine, c) arginine, d) serine, e) threonine, and f) valine. Error bars represent 95% confidence interval.

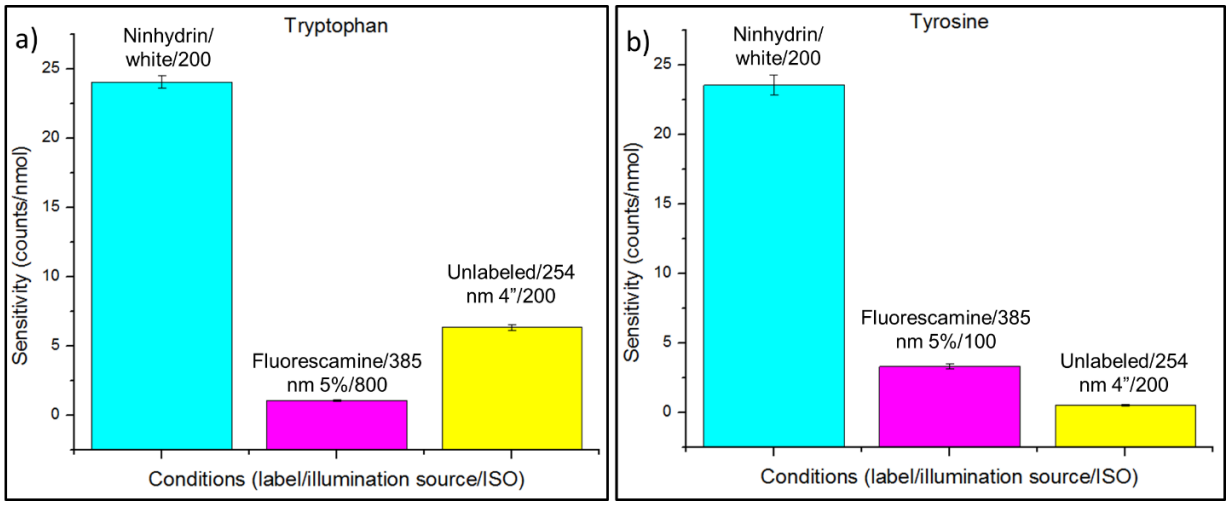

Figure 4-15. *Most sensitive conditions—tryptophan to tyrosine*. Most sensitive conditions in all detection modes for a) tryptophan and b) tyrosine. Error bars represent 95% confidence interval.

label than ninhydrin, but in this study, that was untrue for all amino acids but asparagine. Other than asparagine, colorimetric detection with white light illumination at 200 ISO was the most sensitive method overall. Indirect fluorescence detection had the lowest sensitivity of any method tested here for all amino acids except tryptophan.

4.3.4 Amino acid separation

As seen in figure 4-16, the retention factors for all pure amino acids were reproducible, though some results were surprising. Methionine had two component spots, one around the expected retention factor at 0.55 and one at 0.19; and cysteine had a retention factor of 0.13, which is much lower than expected. These amino acids have sulfur-containing side chains, which are susceptible to oxidation at pH 7 (19). Cysteine can be oxidized to its dimer cystine while methionine can be oxidized to methionine sulfoxide; both oxidized forms have lower retention factors around 0.13-0.14 in similar butanol/acetic acid/water systems (19-21). Based on observed retention factors, cysteine appears to in fact be cystine, and the methionine solution is most likely a mixture of its oxidized and reduced forms. Due to these and other slight aberrations in retention, the first separation attempt of five mixtures was unsuccessful, and not all amino acids were resolved (figure 4-17a and b). The second attempt rearranged the amino acids among six mixtures, and all were successfully resolved, with calculated resolutions of at least 1.2 between all amino acids (figure 4-17c and d). Interestingly, in

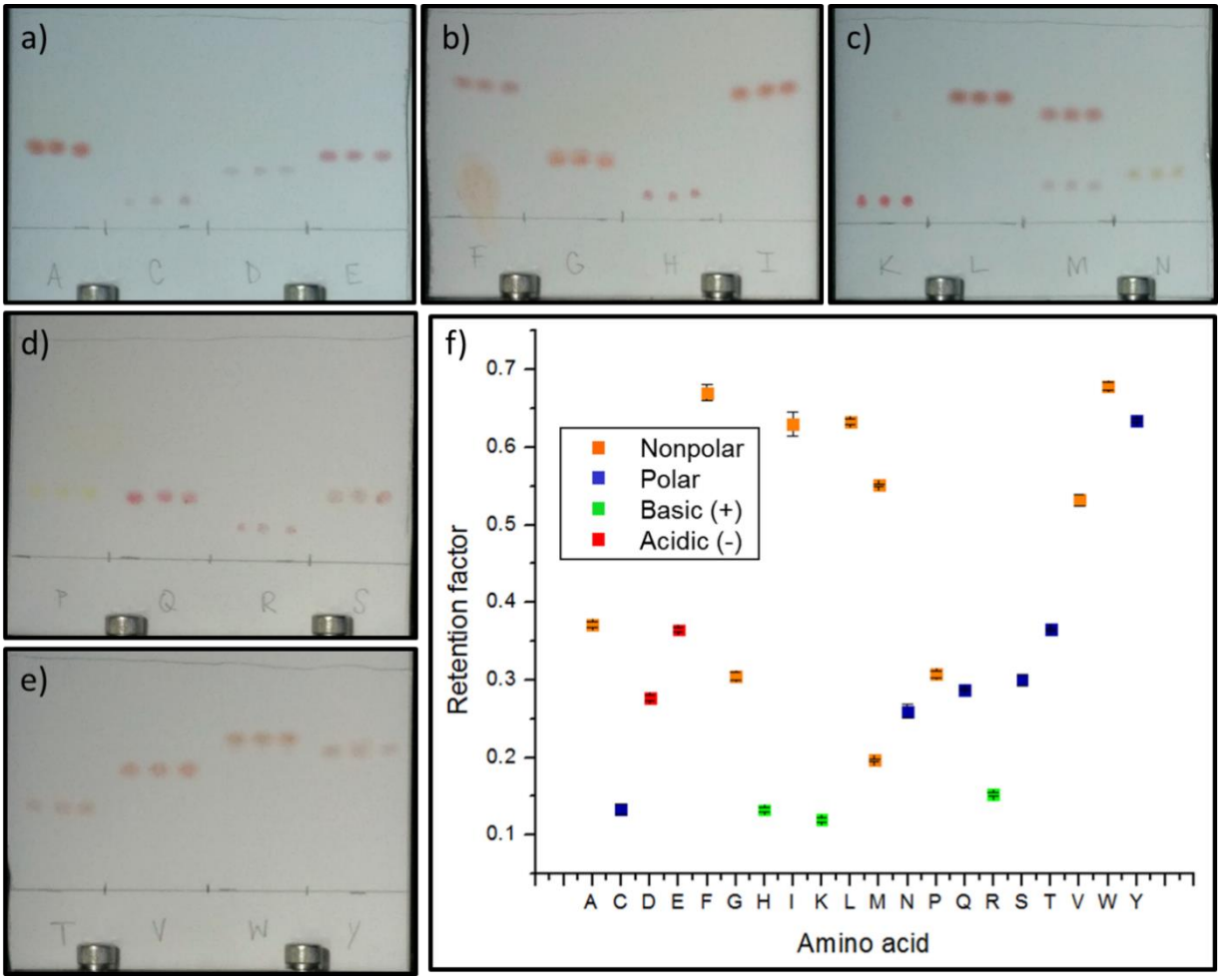

Figure 4-16. *TLC of pure amino acids.* a-e) Pure amino acids labeled by one-letter abbreviation; f) retention factors of pure amino acids by classification.

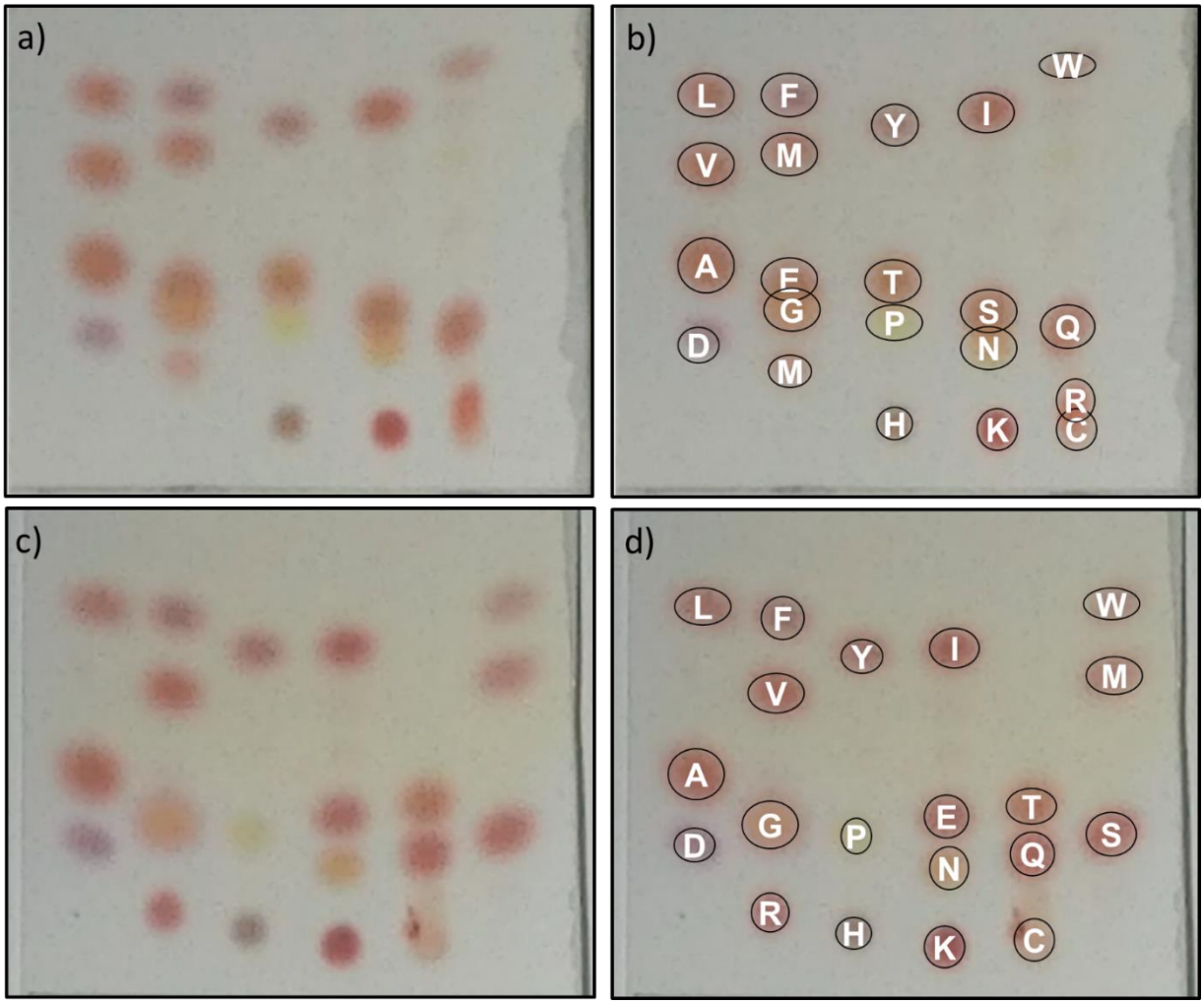

Figure 4-17. *Amino acid separations*. a) First separation attempt with five mixtures and b) labeled spots; c) second separation attempt with six mixtures and d) labeled spots.

its second mixture, methionine had only one component spot. It is possible but unlikely that methionine sulfoxide is combined with serine, as serine has a considerably higher retention factor.

4.3.5 Amino acid quantitation

All amino acids were successfully separated using the previously determined mixtures, allowing the construction of simultaneous calibration curves and minimizing the time spent developing plates for this experiment. However, as in other chromatography techniques, the spots experienced longitudinal diffusion during development. This decreased their intensity, making some amino acids more difficult to detect in previously optimized conditions. As shown in the middle rows of figure 4-18c and i, the yellow proline spots are more distinguishable from the background at 100 ISO than 200; the same can be said for asparagine (third row down in figure 4-18d, j) and cysteine (bottom row in figure 4-18e, k). As shown in figure 4-19a, 200 ISO had a negative sensitivity for cysteine. S/N should increase proportionally to the amount of amino acid present, with higher responses resulting in higher sensitivities; a negative sensitivity means this is not occurring, or at least that these imaging conditions are not optimal for detecting it. Detection at 200 ISO also had lower sensitivity than 100 ISO for asparagine, but for all other amino acids, 200 ISO was still more sensitive. For quantitation of 0.45 mg mL^{-1} spots, however, 100 ISO generally outperformed 200. At 100 ISO, over half of the amino acids were quantified within 25% error, while at 200 ISO nine were quantified with greater than 50% error. Twice as many amino acids were within 10% error at 100 ISO than at 200, including asparagine, which was insensitively detected and inaccurately quantified at 200 ISO.

4.4 Conclusions

In this work, three detection methods were investigated for the quantitation of all twenty standard amino acids. White light sources were found to be much more uniform than monochromatic for the illumination of TLC plates. Fluorometric and indirect fluorescence detection modes performed worse than expected, while colorimetric detection performed well for all amino acids. All ninhydrin-labeled amino acids at 0.1-1 mg mL^{-1} were sensitively detected under illumination with white light using a cellphone camera at

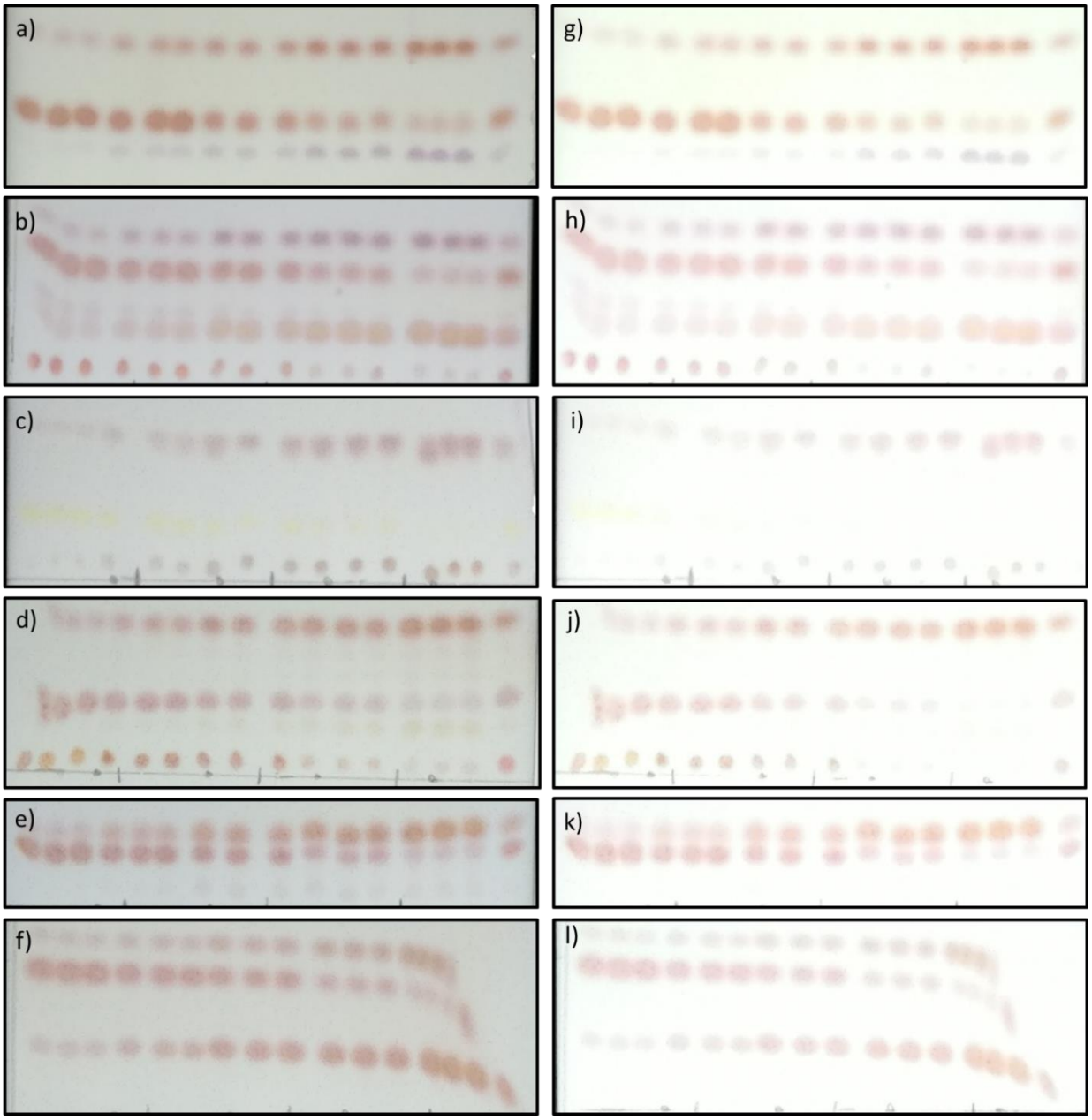

Figure 4-18. *Amino acid separations for calibration*. Separated amino acids from 0.1-1 mg/mL at a-f) 100 ISO and g-l) 200 ISO.

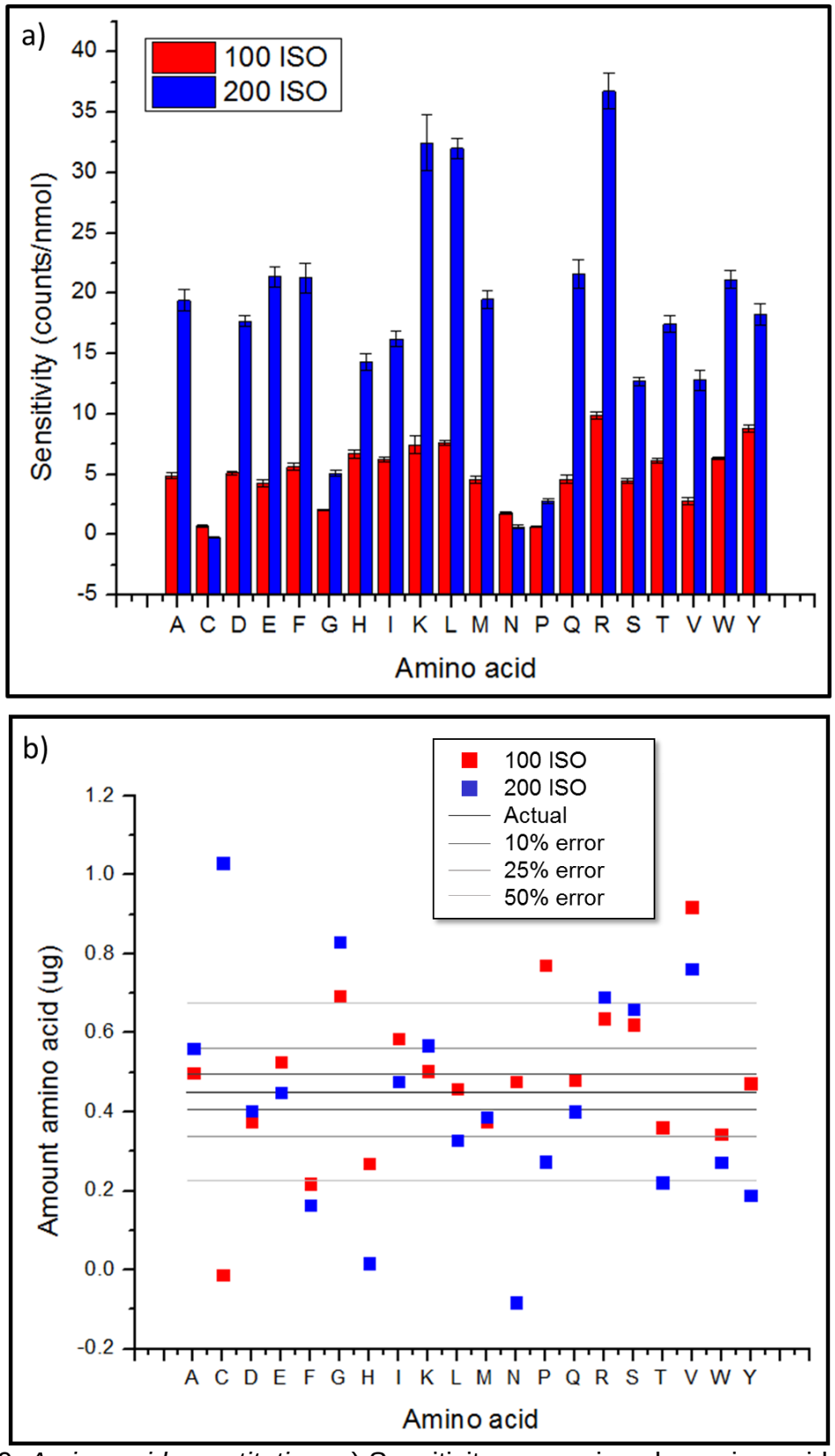

Figure 4-19. *Amino acid quantitation.* a) Sensitivity comparison by amino acid and ISO; b) results of amino acid quantitation by ISO.

200 ISO. Six mixtures of amino acids were successfully separated and detected under these optimized conditions, which were then used to construct simultaneous calibration curves. In an undergraduate lab, this will effectively minimize the class time devoted to the time-consuming separation process. Developing the mixtures decreased amino acid spot intensity due to diffusion, which made 100 ISO more sensitive for cysteine and asparagine, and more accurate overall for quantitation. Quantitation in optimized conditions could likely be improved for future use by using an internal standard in amino acid mixtures. The method developed here uses free software and a readily available cellphone camera, making it a simple and inexpensive option for pedagogical applications.

CHAPTER 5. FUTURE DIRECTIONS

Quantitative TLC detection of amino acids as developed in chapter 4 is a suitable analytical method for pedagogical applications. The method is fast and simple, and holds interest for students from preteens to college for many reasons. Amino acids as analytes are significant in medicine as biomarkers for metabolic illnesses, in nutrition as common elements of foods and supplements, and in forensics as trace evidence in fingerprints; the lab can easily be tailored to a specific subject, though all maintain relevance to the general population as well. Identification and quantitation of amino acids in blood samples or supplements can be done via TLC (1,2). Measuring retention factors and creating simultaneous calibration curves of a few amino acids will enable students to identify and quantify an unknown amino acid in a sample of choice. This information can be used for diagnosis of a metabolic illness or compared to the theoretical amount in the supplement. In our experience, students are particularly awed by forensic science; the ninhydrin reaction is used to label fingerprints at crime scenes, and a demonstration of this can easily be included in the lab to further interest students, as shown in figure 5-1 (3).

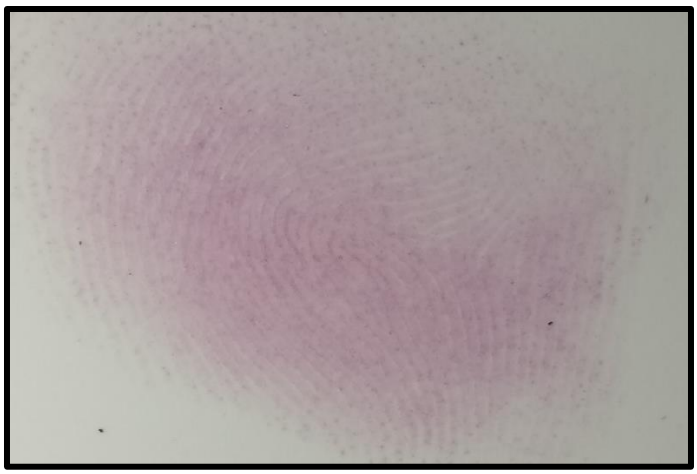

Figure 5-1. *Fingerprint detection.* Ninhydrin-labeled fingerprint imaged with cellphone.

Using cellphones to collect scientific data is also an engaging way to incorporate technology in the classroom. Students enjoy using cellphones for quizzes and other classroom activities, and using them in the laboratory setting will be an interesting and likely novel experience for them. The next step in the development of this lab is to

establish a new procedure to enable the entire TLC analysis to be done using a cellphone. With built-in cameras, light sources, and processors, cellphones have sufficient hardware to capture, process, and analyze images and resulting data, and existing software in the form of free applications can accomplish most necessary analytical functions. The first requirement is a manual camera, like Camera FV-5 Lite used in chapter 4, to allow user control of ISO, exposure time, focus, flash, and other camera settings to optimize imaging conditions (4). Once images are captured, they must be processed, and the application Photo Filter & Editor is one of many capable of grayscale conversion, inversion, and cropping, as shown in figure 5-2a (5). Most photo editing applications lack background subtraction like the rolling ball used in chapter 4, but more sophisticated imaging applications like eigenCAM feature alternatives like flat-field correction, which has been used with quantitative TLC previously (6,7). Once processed, spots should be analyzed similarly to bands in GelApp, a mobile gel electrophoresis analyzer (8). It detects bands of genetic material or protein, or, as shown in figure 5-2b, TLC component spots; where this application calculates band size, our procedure will require measurement of spot intensity. These measurements can then be plotted to construct a calibration curve and automatically quantify an unknown measurement, as with the graphing application StanXY (9). Figure 5-2c shows the calibration curve for glutamic acid at 200 ISO constructed using this application, with the same results as Excel used during method development in chapter 4. All applications mentioned above are free, and many use the same free open source software libraries to execute their desired functions (10,11). The future of this project will combine imaging, image processing and analysis, and data analysis on a cellphone for a novel, inexpensive, quantitative TLC experiment for students of many ages.

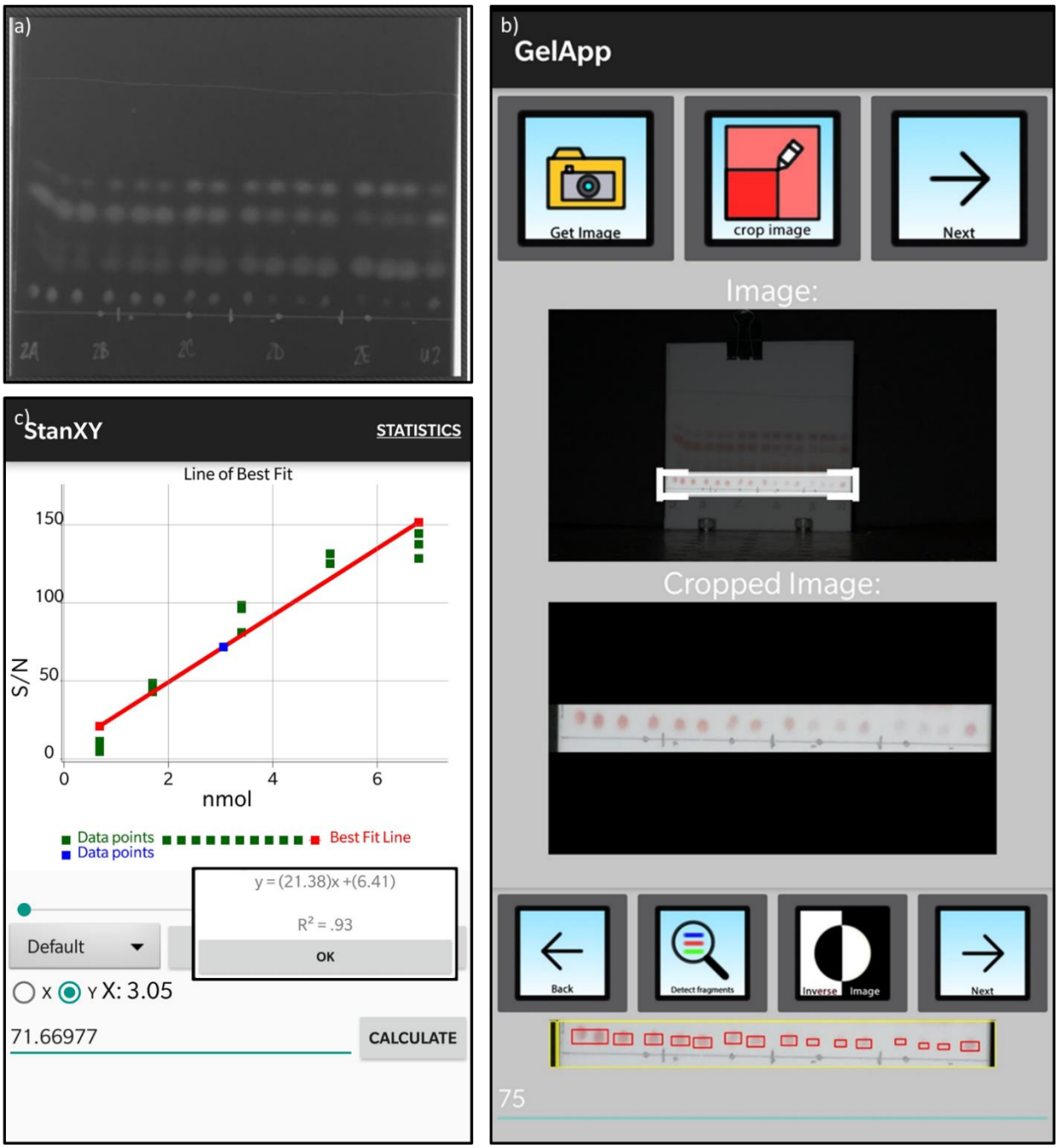

Figure 5-2. *Applications for image and data analysis.* a) TLC plate image edited with Photo Filter & Editor; b) TLC plate image with spots detected by GelApp; c) calibration curve and quantitation results for glutamic acid at 200 ISO using StanXY.

BIBLIOGRAPHY

Chapter 1

1. Chiu, D.T.; deMello, A.J.; Di Carlo, D.; Doyle, P.S.; Hansen, C.; Maceiczyk, R.M.; Wootton, R.C.R. Chem. 2017, 2, 2, 201-223.
2. Qi-Chen, Q.; Rui-Zhi, N.; Yuan, M.A.; Jin-Ming, L. Chin. J. Anal. Chem. 2016, 44, 4, 522-532.
3. Harris, D. Quantitative Chemical Analysis, Eighth Edition; W.H. Freeman and Company: New York, 2010; pp. 298-630.
4. Lopez, J.; Zheng, Y. J. Thromb. Haemost. 2013, 11 (SUPPL.1), 67–74.
5. Hasenberg, T.; Muhleder, S.; Dotzler, A.; Bauer, S.; Labuda, K.; Holnthoner, W.; Redl, H.; Lauster, R.; Marx, U. J. Biotechnol. 2015, 216, 1–10.
6. Bogorad, M. I.; DeStefano, J.; Karlsson, J.; Wong, A. D.; Gerecht, S.; Searson, P. C. Lab Chip 2015, 15 (22), 4242–4255.
7. Esch, M. B.; Post, D. J.; Shuler, M. L.; Stokol, T. Tissue Eng. Part A 2011, 17 (23–24), 2965–2971.
8. Bischel, L.; Young, E. W. K.; Mader, B.; Beebe, D. Biomaterials 2013, 16 (3), 387–393.
9. Chrobak, K. M.; Potter, D. R.; Tien, J. Microvasc. Res. 2006, 71 (3), 185–196.
10. Cucullo, L.; Rapp, E. 2005, No. FEBRUARY.
11. Jansen, J.; De Napoli, I. E.; Fedecostante, M.; Schophuizen, C. M. S.; Chevtchik, N. V.; Wilmer, M. J.; van Asbeck, A. H.; Croes, H. J.; Pertijs, J. C.; Wetzels, J. F. M.; Hilbrands, L. B.; van den Heuvel, L. P.; Hoenderop, J. G.; Stamatialis, D.; Masereeuw, R. Sci. Rep. 2015, 5 (October), 16702.
12. Lee, H.; Kim, S.; Chung, M.; Kim, J. H.; Jeon, N. L. Microvasc. Res. 2014, 91, 90–98.
13. Yuan, S. Y.; Rigor, R. R. 2010.
14. Luissint, A.-C.; Artus, C.; Glacial, F.; Ganeshamoorthy, K.; Couraud, P.-O. Fluids Barriers CNS 2012, 9 (1), 23.
15. Price, G. M.; Wong, K. H. K.; Truslow, J. G.; Leung, A. D.; Tien, J.; Acharya, C. Biomaterials 2010, 31 (24), 6182–6189.
16. Hasan, A.; Paul, A.; Memic, A.; Khademhosseini, A. Biomed. Microdevices 2015, 17 (5), 9993.

17. Grainger, S. J.; Putnam, A. J. PLoS One 2011, 6 (7).
18. Du, Y.; Ghodousi, M.; Qi, H.; Haas, N.; Xiao, W.; Khademhosseini, A. Biotechnol Bioeng. 2011, 108 (7), 1693–1703.
19. Jiang, L.-Y. Y.; Luo, Y. Soft Matter 2013, 9 (4), 1113–1121.
20. Golden, A. P.; Tien, J. Lab Chip 2007, 7 (6), 720–725.
21. Skoog, D.A.; West, D.M.; Holler, F.J. Analytical Chemistry: An Introduction, Sixth Edition; Saunders College Publishing: Philadelphia, 1994; pp. 490-528.
22. Hahn-Deinstrop, E. Applied Thin-Layer Chromatography: Best Practice and Avoidance of Mistakes; 1999.
23. Thin Layer Chromatography. https://chem.libretexts.org/Demos%2C_Techniques%2C_and_Experiments/General_Lab_Techniques/Thin_Layer_Chromatography (accessed March 23, 2018).
24. Manthorpe, D. P.; Lockley, W. J. S. J. Label. Compd. Radiopharm. 2013, 56, 544–552.
25. Sherma, J. Anal. Chem. 2008, 80 (12), 4253–4267.
26. Thin Layer Chromatography Stains. http://www.reachdevices.com/TLC_stains.html (accessed May 20, 2018).
27. Simon, R. E.; Walton, L. K.; Liang, Y.; Denton, M. B. Analyst 2001, 126, 446–450.
28. Stockert, J.C.; Blazquez, A.; Galaz, S.; Juarranz, A. Acta Histochemica. 2008, 110, 4, 333-340.
29. Pirrung, M.C. The Synthetic Organic Chemist's Companion [Online]; John Wiley & Sons: Hoboken, NJ, 2007; pp. 171-172. http://www.cchem.berkeley.edu/rsgrp/TLCStainRecipes.pdf (accessed May 2, 2018).
30. Friedman, M. J. Agric. Food Chem. 2004, 52, 385–406.
31. Wang, T.; Lee, M.; Tord, D. A. Jpn. J. Hum. Genet. 1983, 28, 273–284.
32. Pachuski, J.; Sherma, J. 2007, 6076.
33. Hess, B.; Sherma, J. Acta Chromatogr. 2004, No. 14, 60–69.
34. Felix, A. M. J. Chrom 1974, 89, 361–364.

35. What is High-Performance Thin Layer Chromatography? https://www.emdmillipore.com/US/en/analytics-sample-preparation/learning-center-thin-layer-chromatography/hptlc/NGub.qB.fCoAAAFVPmJDx07N,nav (accessed May 20, 2018).
36. Fisher Scientific Home Page. https://www.fishersci.com/us/en/home.html (accessed December 5, 2017).
37. Vovk, I.; Prosek, M. J. Chromatogr. A 1997, 768, 329–333.
38. Bhawani, S. A.; Ibrahim, M. N. M.; Sulaiman, O.; Hashim, R.; Hena, S. J. Liq. Chromatogr. Relat. Technol. 2012, 35, 1497–1516.
39. Tami, K.; Popova, A.; Proni, G. J. Chem. Educ. 2017, 94, 471–475.
40. Anwar, J.; Nagra, S. A.; Nagi, M. J. Chem. 1996, 73 (10), 977–979.
41. Cresswell, S. L.; Loughlin, W. A. J. Chem. Educ. 2015, 92, 1730–1735.
42. Fagundes, T. S. F.; Dutra, K. D. B.; Ribeiro, C. M. R.; Epifanio, D. A.; Valverde, A. L. 2016, 10–13.
43. Morra, B.; Dicks, A. P. 2016.
44. Morrill, L. A.; Kammeyer, J. K.; Garg, N. K. 2017, 1584–1586.
45. Hess, A.V.I. Digitally Enhanced Thin-Layer Chromatography: An Inexpensive, New Technique for Qualitative and Quantitative Analysis. J. Chem. Ed. 2007 84 (5), 842-847.
46. Johnson, M. E. J. Chem. Educ. 2000, 77 (3), 368–372.

Chapter 2

1. Ning R., Zhuang Q., Lin JM. (2018) Biomaterial-Based Microfluidics for Cell Culture and Analysis. In: Lin JM. (eds) Cell Analysis on Microfluidics. Integrated Analytical Systems. Springer, Singapore.
2. Lopez, J.; Zheng, Y. J. Thromb. Haemost. 2013, 11 (SUPPL.1), 67–74.
3. Cha, C.; Antoniadou, E.; Lee, M.; Jeong, J. H.; Ahmed, W. W.; Saif, T. A.; Boppart, S. A.; Kong, H. Angew. Chemie - Int. Ed. 2013, 52 (27), 6949–6952.
4. Chrobak, K. M.; Potter, D. R.; Tien, J. Microvasc. Res. 2006, 71 (3), 185–196.
5. Bischel, L.; Young, E. W. K.; Mader, B.; Beebe, D. Biomaterials 2013, 16 (3), 387–393.

6. Bogorad, M. I.; DeStefano, J.; Karlsson, J.; Wong, A. D.; Gerecht, S.; Searson, P. C. Lab Chip 2015, 15 (22), 4242–4255.
7. Cucullo, L.; Rapp, E. 2005, No. FEBRUARY.
8. Hasan, A.; Paul, A.; Memic, A.; Khademhosseini, A. Biomed. Microdevices 2015, 17 (5), 9993.
9. Grainger, S. J.; Putnam, A. J. PLoS One 2011, 6 (7).
10. Esch, M. B.; Post, D. J.; Shuler, M. L.; Stokol, T. Tissue Eng. Part A 2011, 17 (23–24), 2965–2971.
11. Griep, L. M.; Wolbers, F.; De Wagenaar, B.; Ter Braak, P. M.; Weksler, B. B.; Romero, I. A.; Couraud, P. O.; Vermes, I.; Van Der Meer, A. D.; Van Den Berg, A. Biomed. Microdevices 2013, 15 (1), 145–150.
12. Lin, K.; Hsu, P. P.; Chen, B. P.; Yuan, S.; Usami, S.; Shyy, J. Y.; Li, Y. S.; Chien, S. Proc. Natl. Acad. Sci. U. S. A. 2000, 97 (17), 9385–9389.
13. Papaioannou, T. G.; Stefanadis, C. Hell. J. Cardiol. 2005, 46 (1), 9–15.
14. Davies, P. F. Nat Clin Pr. Cardiovasc Med. 2009, 6 (1), 16–26.
15. Zhao, X.M.; Xia, Y.; Whitesides, G.M. J. Mater. Chem., 1997, 7, 1069-1074.
16. Xia, Y.N. Whitesides, G.M. Annu. Rev. Mater. Sci., 1998, 28, 153-184.
17. Suzuki, Y., Nishimura, Y., Tanihara, M. et al. J Artif Organs (1998) 1: 28. https://doi.org/10.1007/BF01340449
18. Armour Etch Safety Data Sheet. http://www.dick-blick.com/msds/DBH_SDS_609661004.pdf (accessed May 29, 2018).
19. Erlandsson, P.; Robinson, N.D.; Electrophoresis 2011, 32 (6-7), 784-790.
20. McDonell, M.W.; Simon, M.N.; Studier, F.W. J. Mol. Biol., 1977, 110, 119-146.

Chapter 3

1. Morrill, L. A.; Kammeyer, J. K.; Garg, N. K. 2017, 1584–1586.
2. Tami, K.; Popova, A.; Proni, G. J. Chem. Educ. 2017, 94, 471–475.
3. Anwar, J.; Nagra, S. A.; Nagi, M. J. Chem. 1996, 73 (10), 977–979.
4. Cresswell, S. L.; Loughlin, W. A. J. Chem. Educ. 2015, 92, 1730–1735.
5. Fagundes, T. S. F.; Dutra, K. D. B.; Ribeiro, C. M. R.; Epifanio, D. A.; Valverde, A. L. 2016, 10–13.

6. Morra, B.; Dicks, A. P. 2016.
7. Johnson, M. E. J. Chem. Educ. 2000, 77 (3), 368–372.
8. Product prices. https://www.wavemetrics.com/order/order_prices.htm (accessed May 28, 2018).
9. Buying Photoshop. https://www.gcflearnfree.org/photoshopbasics/buying-photoshop/1/ (accessed May 28, 2018).
10. Hess, A.V.I. Digitally Enhanced Thin-Layer Chromatography: An Inexpensive, New Technique for Qualitative and Quantitative Analysis. J. Chem. Ed. 2007 84 (5), 842-847.

Chapter 4

1. Thin Layer Chromatography Stains. http://www.reachdevices.com/TLC_stains.html (accessed May 20, 2018).
2. Bhawani, S. A.; Ibrahim, M. N. M.; Sulaiman, O.; Hashim, R.; Hena, S. J. Liq. Chromatogr. Relat. Technol. 2012, 35, 1497–1516.
3. Friedman, M. J. Agric. Food Chem. 2004, 52, 385–406.
4. Johnson, M. E. J. Chem. Educ. 2000, 77 (3), 368–372.
5. Wang, T.; Lee, M.; Tord, D. A. Jpn. J. Hum. Genet. 1983, 28, 273–284.
6. Felix, A. M. J. Chrom 1974, 89, 361–364.
7. Teens, social media, & technology overview 2018. Pew Research Center. http://www.pewinternet.org/2018/05/31/teens-social-media-technology-2018/ (accessed June 1, 2018).
8. Mobile Fact Sheet. Pew Research Center. http://www.pewinternet.org/fact-sheet/mobile/ (accessed June 1, 2018).
9. Compare iPhone Models. Apple. https://www.apple.com/iphone/compare/ (accessed May 5, 2018).
10. Apple Passes Samsung to Capture the Top Position in the Worldwide Smartphone Market While Overall Shipments Decline 6.3% in the Fourth Quarter, According to IDC. https://www.idc.com/getdoc.jsp?containerId=prUS43548018 (accessed June 11, 2018).

11. Camera FV-5: professional camera application for Android. https://www.camerafv5.com/ (accessed June 1, 2018).
12. What is ISO speed? https://electronics.howstuffworks.com/what-is-iso-speed.htm (accessed March 3, 2018).
13. Sherma, J. Anal. Chem. 2008, 80 (12), 4253–4267.
14. Manthorpe, D. P.; Lockley, W. J. S. J. Label. Compd. Radiopharm. 2013, 56, 544–552.
15. Vovk, I.; Prosek, M. J. Chromatogr. A 1997, 768, 329–333.
16. Simon, R. E.; Walton, L. K.; Liang, Y.; Denton, M. B. Analyst 2001, 126, 446–450.
17. Petrovic, M. 2000, No. November 2014.
18. Felix, A.M.; Toome, V.; DeBernardo, S.; Weigele, M. Archives of Biochem. And Biophysics, 1975, 168, 601-608.
19. Enache, T.A.; Oliveira-Brett, A.M. Bioelectrochemistry. 2011, 81 (1), 46-52.
20. Takizawa, Y.; Fukushima, H.; Usui, T. J. Oleo Sci. 1992, 41 (5), 54-56.
21. Thin layer chromatography of amino acids and short peptides. Reach Devices. http://www.reachdevices.com/TLC_aminoacids.html (accessed January 31, 2018).

Chapter 5

1. Hess, B.; Sherma, J. Acta Chromatogr. 2004, No. 14, 60–69.
2. Pachuski, J.; Sherma, J. 2007, 6076.
3. Amino acid fingerprints. Flinn Scientific. https://www.flinnsci.com/api/library/Download/a71f79d2e9434d53b0aeb9863e2928d4 (accessed June 15, 2018).
4. Camera FV-5: professional camera application for Android. https://www.camerafv5.com/ (accessed June 1, 2018).
5. Photo Filter & Editor. KXAppCenter.Inc. https://play.google.com/store/apps/details?id=coocent.app.photo.editor.filter.effect&hl=en_US (accessed July 11, 2018).

6. eigenCAM App. Eigen Imaging. https://www.eigenimaging.com/pages/eigencam-app (accessed July 11, 2018).
7. Simon, R. E.; Walton, L. K.; Liang, Y.; Denton, M. B. Analyst 2001, 126, 446–450.
8. Sim, J.Z.; Nguyen, P.V.; Lee, H.K.; Gan, S.K.E. Nature Methods, 2015, 1-2.
9. Budianto, I.H.; Wong, C.F.; Nguyen, P.V.; Gan, S.K.E. Scientific Phone Apps and Mobile Devices, 2015, 1-3. DOI 10.1186/s41070-015-0003-0
10. AChartEngine. http://www.achartengine.org/ (accessed July 11, 2018).
11. Open Source Computer Vision Library. https://opencv.org/about.html (accessed July 11, 2018).

VITA

Alexandra Marie Anderson grew up in the small town of Elkhorn City, Kentucky, and attended college at Eastern Kentucky University. With the Crime and Chemistry Club there, she participated in chemistry demonstrations and STEM fairs on the way to earning her B.A. in chemistry in May of 2015. While in graduate school at the University of Tennessee, Knoxville, Alex discovered a love of teaching chemistry at the college level, and has developed experiments now taught in undergraduate laboratories there. In her free time, Alex enjoys working with her hands and spending time outdoors with her husband, Brandon. She will earn her M.S. in analytical chemistry in fall 2018.